AFGL-TR-84-0224

BACKGROUND EQUATORIAL ASTRONOMICAL MEASUREMENTS FOCAL PLANE ASSEMBLY

(REFURBISHED HI STAR SOUTH)

R. O. Davis, C. B. Tacelli
Santa Barbara Research Center
75 Coromar Drive
Goleta, CA 93117

SEPTEMBER 1984

FINAL TECHNICAL REPORT

February 1983 - September 1984

Prepared for
Air Force Geophysics Laboratory
Air Force Systems Command
Hanscom Air Force Base, Massachusetts 01731

This report has been reviewed by the ESD Public Affairs Office (PA) and is releasable to the National Technical Information Service (NTIS)

"This technical report has been reviewed and is approved for publication"

FOR THE COMMANDER

BERTRAM D. SCHURIN, Chief
Infrared Physics Branch

JOHN S. GARING, Director
Optical Physics Division

Qualified requestors may obtain additional copies from the Defense Technical Information Center. All others should apply to the National Technical Information Service.

If your address has changed, or if you wish to be removed from the mailing list, or if the addressee is no longer employed by your organization, please notify AFGL/DAA, Hanscom AFB, MA 01731. This will assist us in maintaining a current mailing list.

Do not return copies of this report unless contractual obligations or notices on a specific document requires that it be returned.

Unclassified

SECURITY CLASSIFICATION OF THIS PAGE (When Data Entered)

REPORT DOCUMENTATION PAGE		READ INSTRUCTIONS BEFORE COMPLETING FORM
1. REPORT NUMBER AFGL-TR-84-0224	2. GOVT ACCESSION NO. AD-A155 215	3. RECIPIENT'S CATALOG NUMBER
4. TITLE (and Subtitle) Background Equatorial Astronomical Measurements Focal Plane Assembly (Refurbished HI STAR SOUTH)		5. TYPE OF REPORT & PERIOD COVERED Final Technical Report February 1983 - September 1984 6. PERFORMING ORG. REPORT NUMBER 41413
7. AUTHOR(s) R.O. Davis, C.B. Tacelli		8. CONTRACT OR GRANT NUMBER(s) F19628-83-C-0062
9. PERFORMING ORGANIZATION NAME AND ADDRESS Santa Barbara Research Center 75 Coromar Dr. Goleta, CA 93117		10. PROGRAM ELEMENT, PROJECT, TASK AREA & WORK UNIT NUMBERS DI-A-3591/A/M
11. CONTROLLING OFFICE NAME AND ADDRESS Air Force Geophysics Laboratory Hanscom AFG, Massachusetts 01731 Monitor/ Paul D. LeVan/OPI		12. REPORT DATE September 1984 13. NUMBER OF PAGES 115
14. MONITORING AGENCY NAME & ADDRESS(if different from Controlling Office)		15. SECURITY CLASS. (of this report) Unclassified 15a. DECLASSIFICATION/DOWNGRADING SCHEDULE

16. DISTRIBUTION STATEMENT (of this Report)

Approved for public release; distribution unlimited

17. DISTRIBUTION STATEMENT (of the abstract entered in Block 20, if different from Report)

18. SUPPLEMENTARY NOTES

19. KEY WORDS (Continue on reverse side if necessary and identify by block number)

Focal Plane Assembly, HI STAR SOUTH

20. ABSTRACT (Continue on reverse side if necessary and identify by block number)

A customer-furnished HI STAR SOUTH FPA was modified for use on the BEAM Program. This report details the modification and presents the final performance and environmental test data. Test setups and methods are also covered. The BEAM FPA met all specifications as listed in the contract.

DD FORM 1 JAN 73 1473 EDITION OF 1 NOV 65 IS OBSOLETE

Unclassified

SECURITY CLASSIFICATION OF THIS PAGE (When Data Entered)

CONTENTS

TABLES

ILLUSTRATIONS

ILLUSTRATIONS (cont'd)

ILLUSTRATIONS (cont'd)

TABLES

Section 1
INTRODUCTION

This report covers the work performed under contract No. F19628-83-C-0062 for the Air Force Geophysics Laboratory, Hanscom AFB, Massachusetts. The objective of the contract was to revise the existing design and to disassemble, modify, reassemble, test, and deliver one customer-furnished HI STAR SOUTH Focal Plane Assembly (FPA) for use on the Background Equatorial Astronomical Measurements (BEAM) program. A second FPA was furnished by the customer for parts.

The first part of this report discusses the changes made in the design and provides photographs and drawings showing the various stages of modification and assembly of the focal plane. The major portion of the report presents the final performance and environmental test data taken on the modified FPA. A brief description of the test setups used for each test is provided, with a summary of the method of measurement and the resultant data. The data taken on the spectral filters (transmission vs wavelength) are included in Appendix A. Appendix B gives the temperature sensor calibration curves.

Section 2

FOCAL PLANE DESIGN

2.1 FOCAL PLANE CONFIGURATION

The HI STAR SOUTH FPA (Figures 1 and 2) consists of three frame subassemblies containing eight detectors each, clamped to the focal plane base. Spectral filters and an aperture plate are mounted over the detectors and the assembly is enclosed by a case which also supports two Internal Calibration Source (ICS) units.

The three identical frame subassemblies each consists of a gold plated OFH copper frame which supports eight discrete Si:Ga detectors, an alumina preamp board and a nano-pin connector. The detectors are bonded into slots along the top edge with four on each side of the band frame. Gold wirebonds routed through notches in the frame are used to connect the detectors to the preamp board.

84-4-97

Figure 1. BEAM Focal Plane Assembly

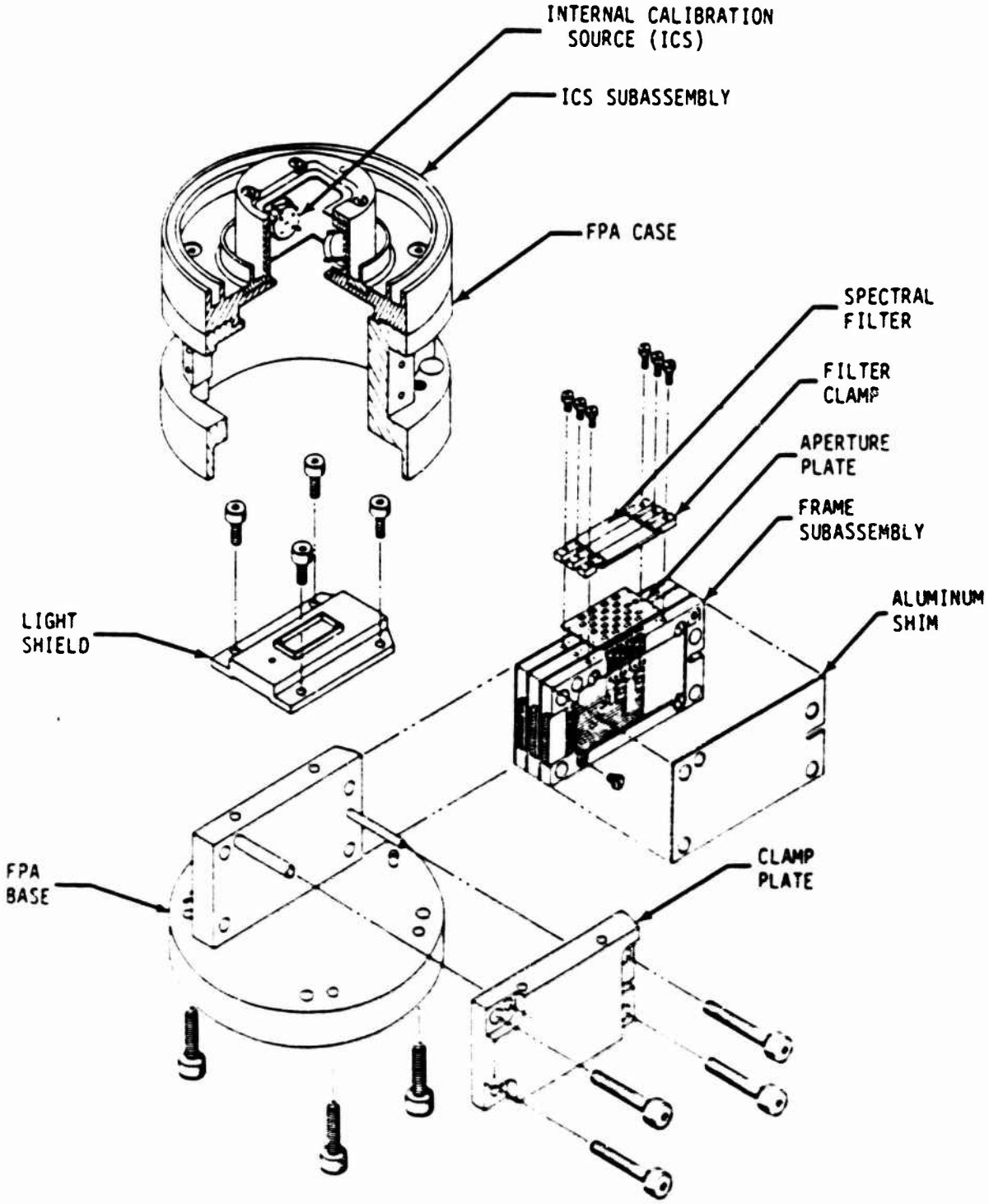

Figure 2. BEAM FPA - Exploded View

The alumina preamp board is attached to the frame by four screws, and mounts two 6-channel FETs on one side and eight feedback resistors on the other. Interconnections between components are provided by titanium-gold traces on each side of the board. Gold wirebonds connect the traces to the resistors and FETs, and the fourteen leads of the nano-pin connector are wire bonded to pads on the board.

The three frame subassemblies are clamped to the focal plane base by a clamp plate and four screws. Aluminum shims are placed between the frames to achieve proper band-to-band detector spacing. The thermal path for cooling the detectors is through the copper frames, across the clamped frame/frame and frame/base interfaces, and through the copper base to the coldfinger. The aperture plate and the three spectral filter sets (two doublets and one singlet) are attached to the top edges of the frames by clamps and screws (Figure 3).

The focal plane is enclosed by an aluminum case and an aluminum cover which mounts two alumina-diaphragm ICS units above the plane of the detectors (one on each side of the bezel opening), which allows radiation to enter the focal plane assembly (Figure 4).

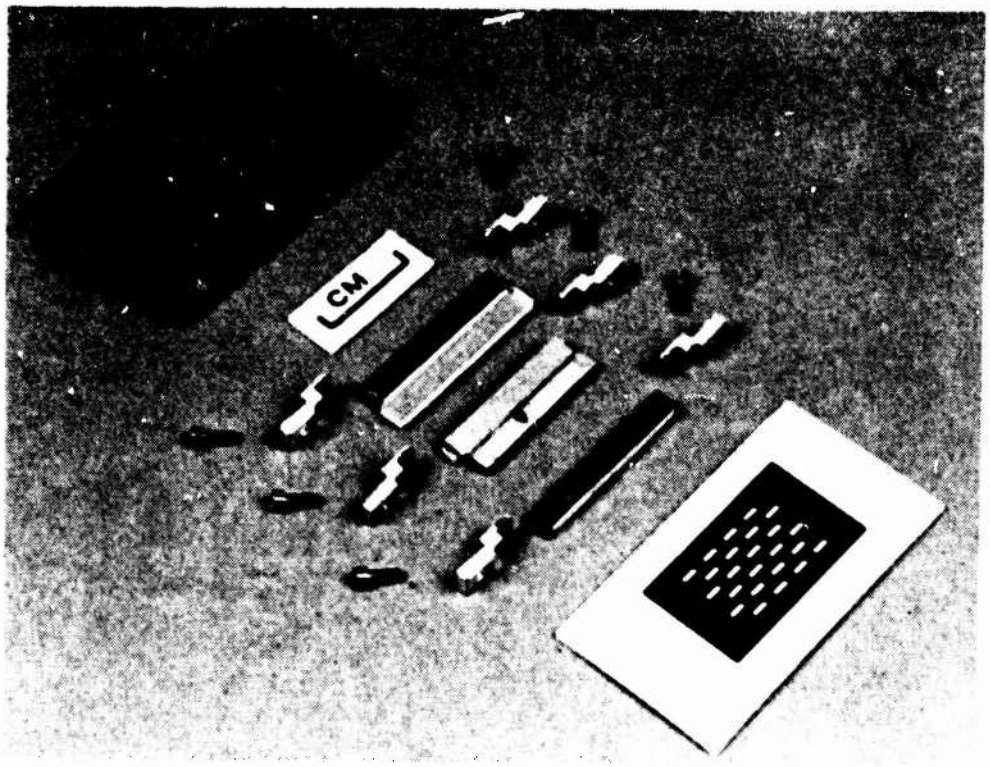

84-4-95

Figure 3. Spectral Filters and Aperture Plate

84-4-96

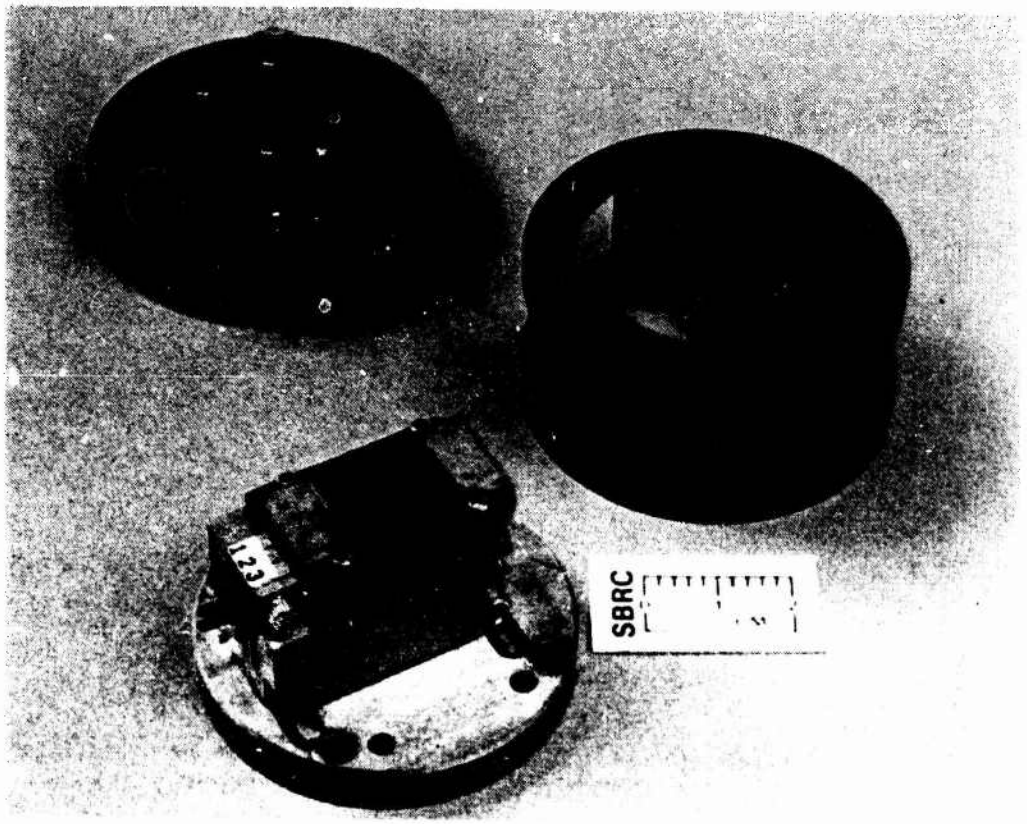

Figure 4. FPA Case and ICS Subassembly With Partial FPA

Kapton insulated ribbon cables and stacked epoxy glass paddleboards interconnect the instrument bulkhead connectors with the band frames (Figure 5) and the ICS subassembly (Figure 6).

2.2 FOCAL PLANE MODIFICATIONS

In the original HI STAR SOUTH focal plane circuit design the copper frame was used as the common detector bias for each band. This required that the band frames be electrically isolated from each other and from the focal plane base by mylar shims since the detector bias level was different for each band.

One requirement in refurbishing the HI STAR SOUTH FPA for use on the BEAM program was to redesign the detector mounting to isolate the detector bias from the frame. This allowed the removal of the mylar shims connecting the frames to shield ground, which in turn increased overall shielding of high-impedance circuits, improved thermal conductivity across the clamped interfaces, and reduced the chance of accidental static discharge damage to the

84-4-94

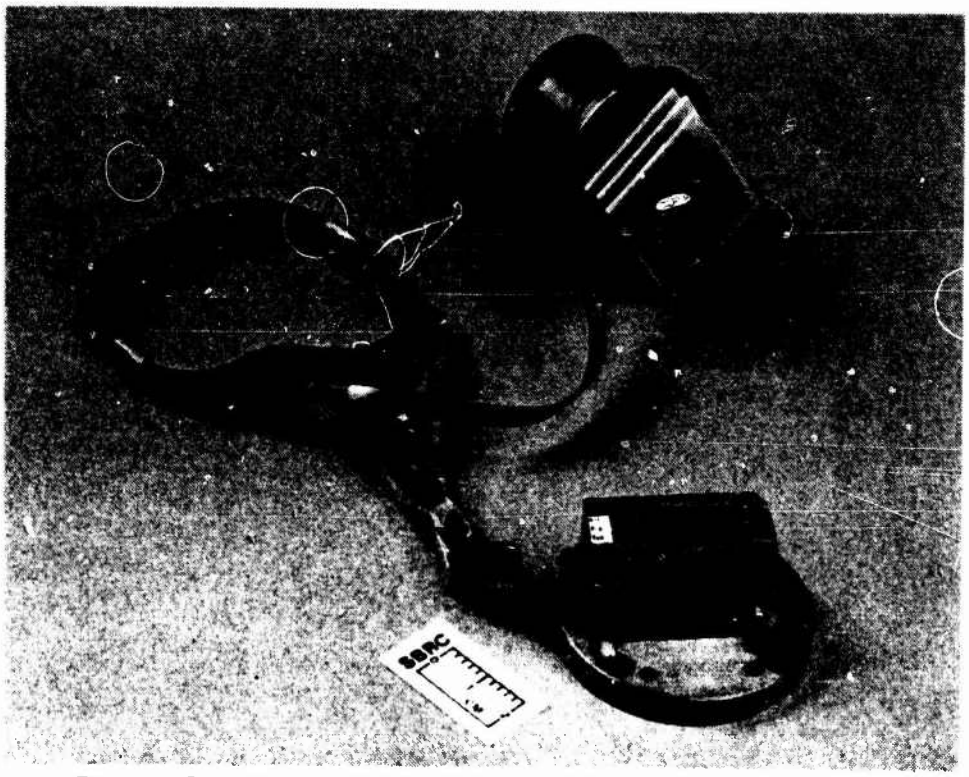

Figure 5. Signal Cable Subassembly with Partial FPA

84-4-93

Figure 6. ICS Cable and Connector with ICS Subassembly

MOSFETs during assembly and test. The old and new designs are shown in Figure 7. The copper webs between the first and second and between the third and fourth recesses on each side of the frame were cut away and thin sapphire detector boards were installed to insulate the detectors from the frame. The new detectors were bonded to the detector boards with additional support provided by sapphire blocks bonded to the rear surface of the detectors and to the detector board. The detector bias connection is made by aluminum wirebonds from the transparent contact on the front surface of each of the new detectors to a titanium-gold circuit trace on the detector boards. Insulated gold wirebonds are passed through notches machined in the remaining webs between the detector recesses and through a small hole drilled through the frame to connect the traces of all four detector boards in each frame together. The resulting common band detector bias was attached to the detector bias connector lead by an insulated gold wirebond routed through a notch machined in the frame web between one of the detector recesses and the board recess. The sapphire support blocks were made narrower than the detectors, which allowed the detector output connections to be made by insulated gold wirebonds from the exposed area of the rear surface of each detector routed through existing notches in the frame to existing pads on the circuit board. Figure 8 shows an unmodified frame with the new parts required for refurbishment. Figures 9 through 11 show both sides of refurbished frame assemblies 1, 2 and 3.

2.3 DETECTOR BOARD

A new detector board which allowed isolation of the detectors was incorporated into the modification design. This detector board was fabricated from 0.010-in. thick sapphire and cut to an appropriate dimension to fit into a two-detector wide slot with allowable tolerances for thermal expansion and contraction. Sapphire was chosen for its close coefficient of expansion relationship with the copper frame housing.

A titanium-gold deposition provided the bias trace necessary to weld the aluminum top contact detector lead onto. Ablestick 7216 epoxy adhered the detector board to the frame, and the detectors and sapphire blocks to the detector board. Figure 12 shows an exploded view of one detector board assembly.

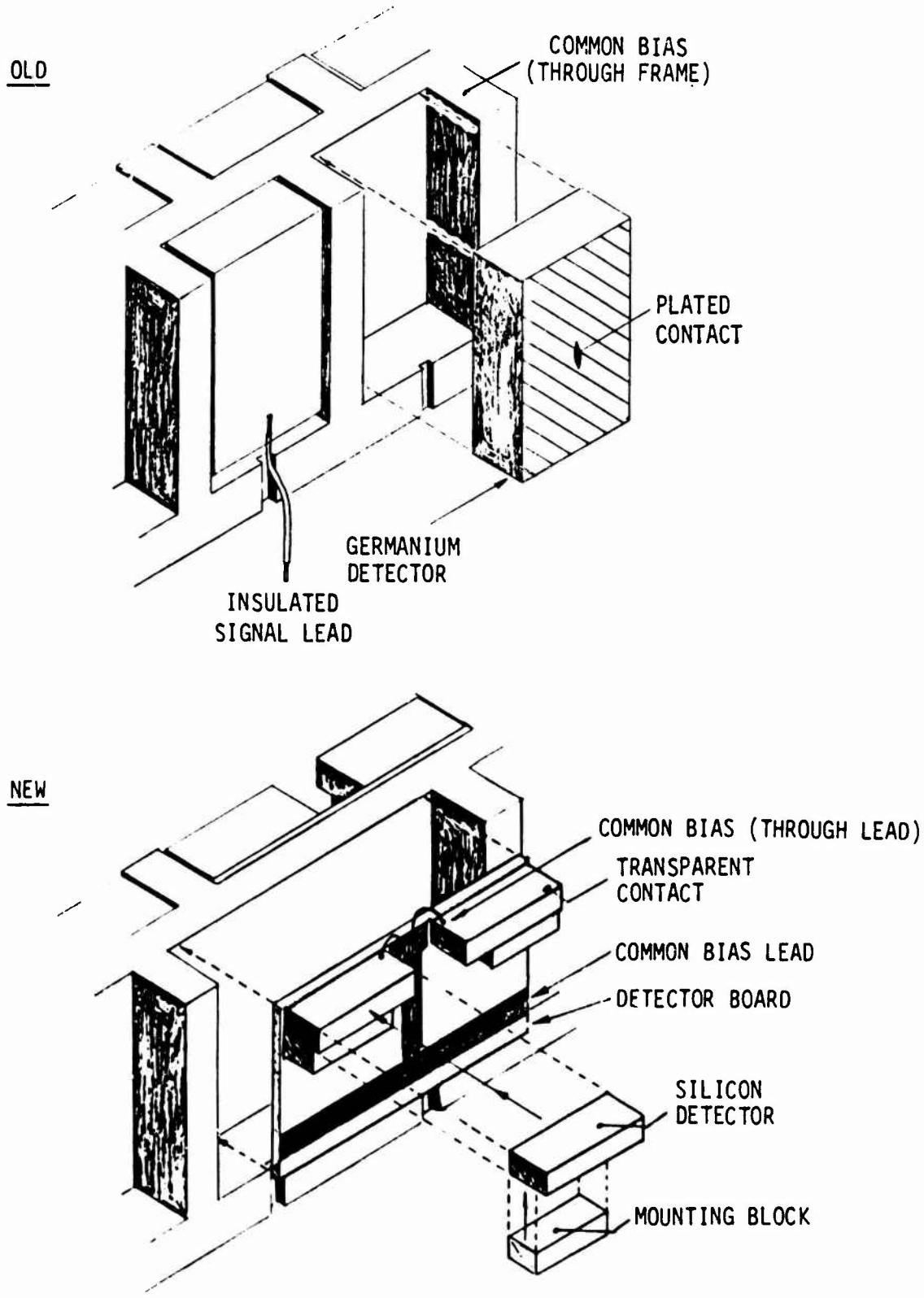

Figure 7. Detector Mounting - Old and New

84-4-92

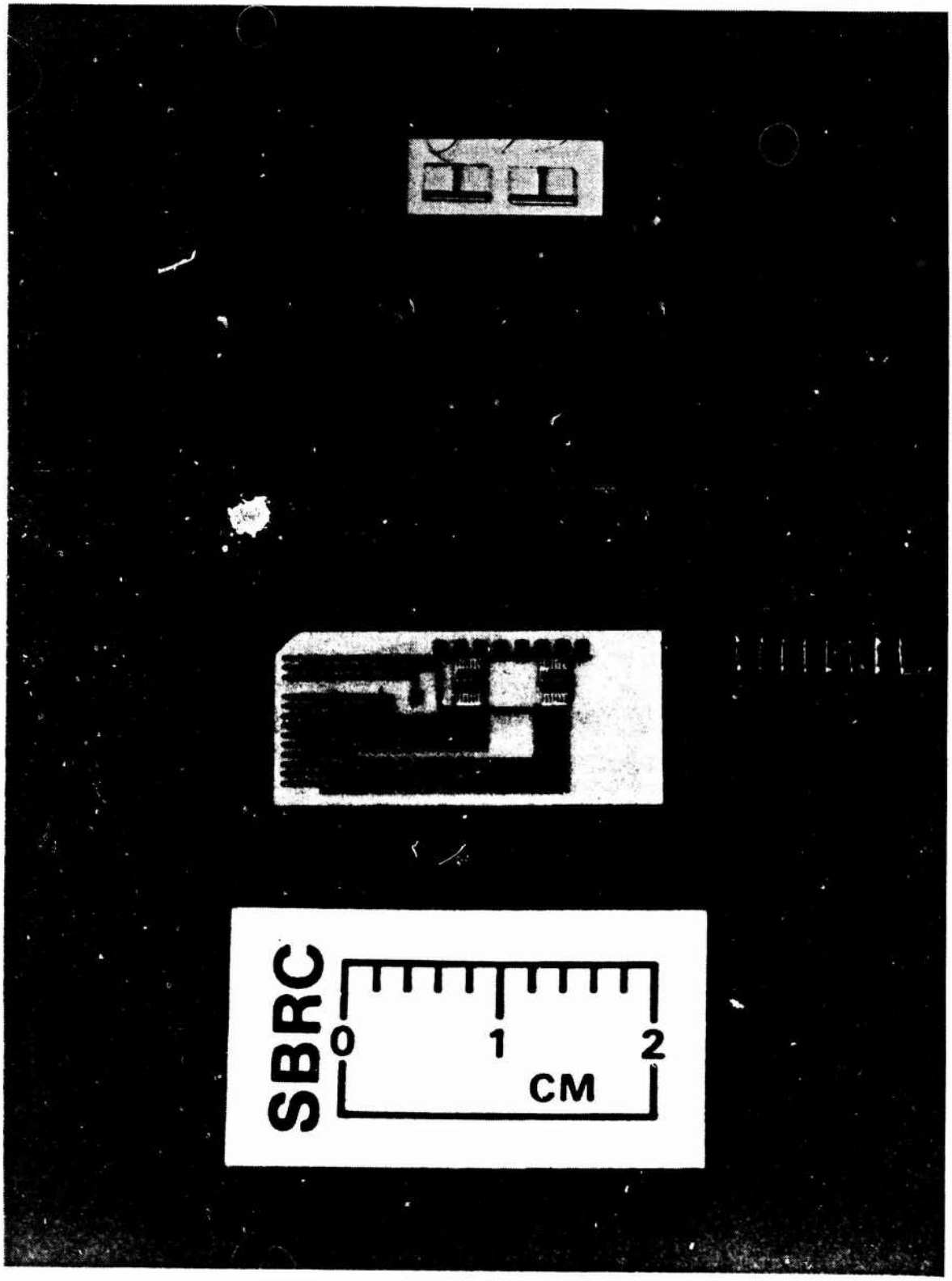

Figure 8. Unmodified Frame with New Parts for Refurbishment

83-8-10

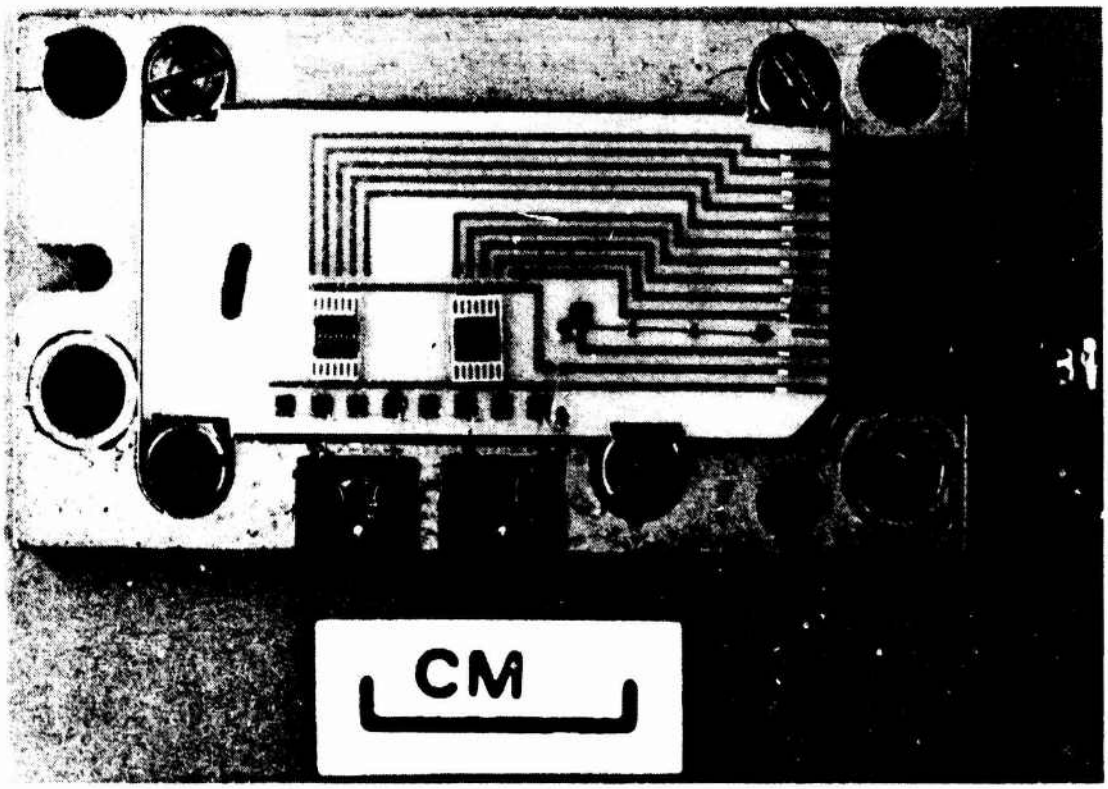

FRONT

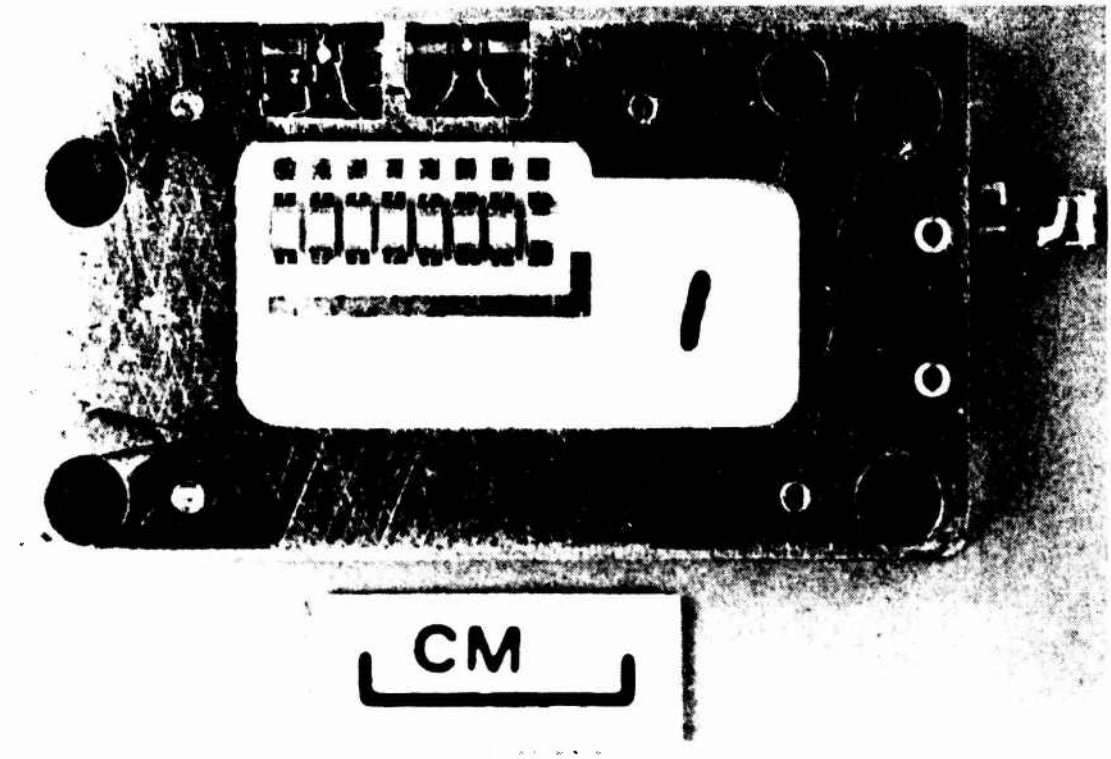

83-8-11

REAR

Figure 9. Frame 1 Assembly - Refurbished

83-8-14

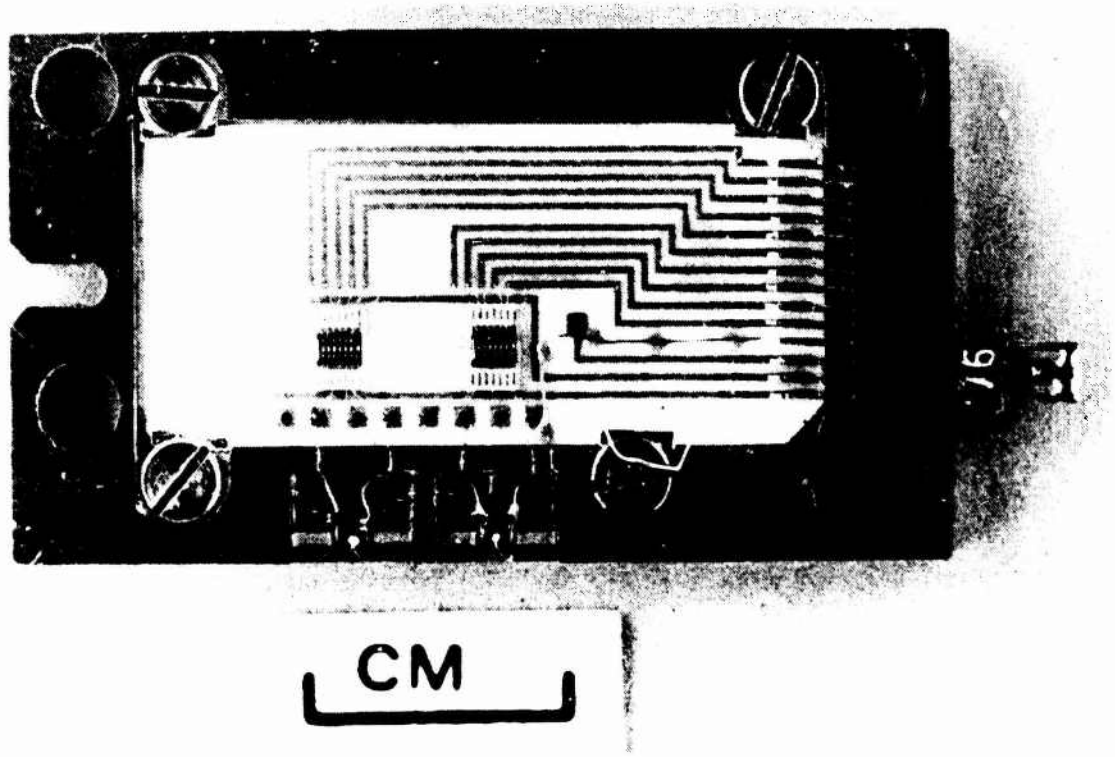

FRONT

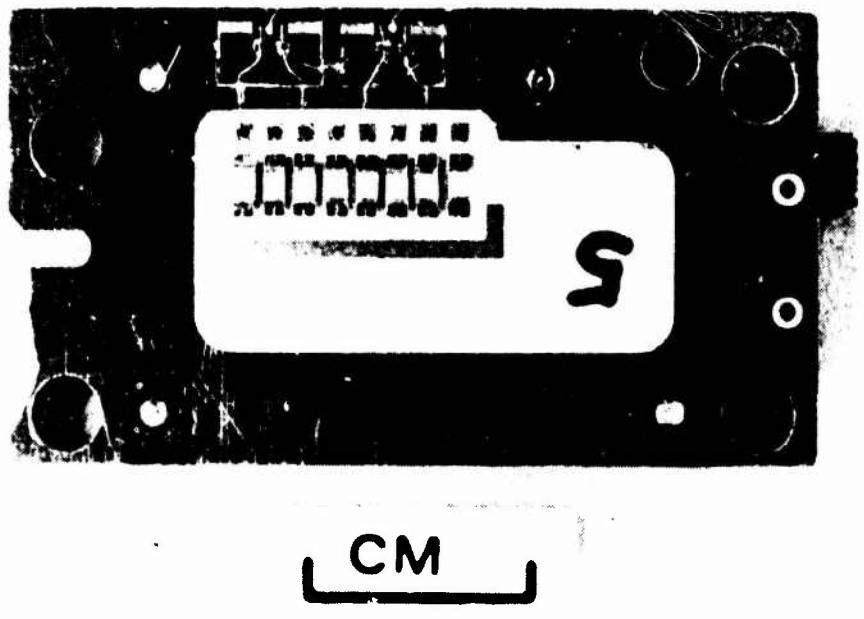

REAR

83-8-15

Figure 10. Frame 2 Assembly - Refurbished

83-8-12

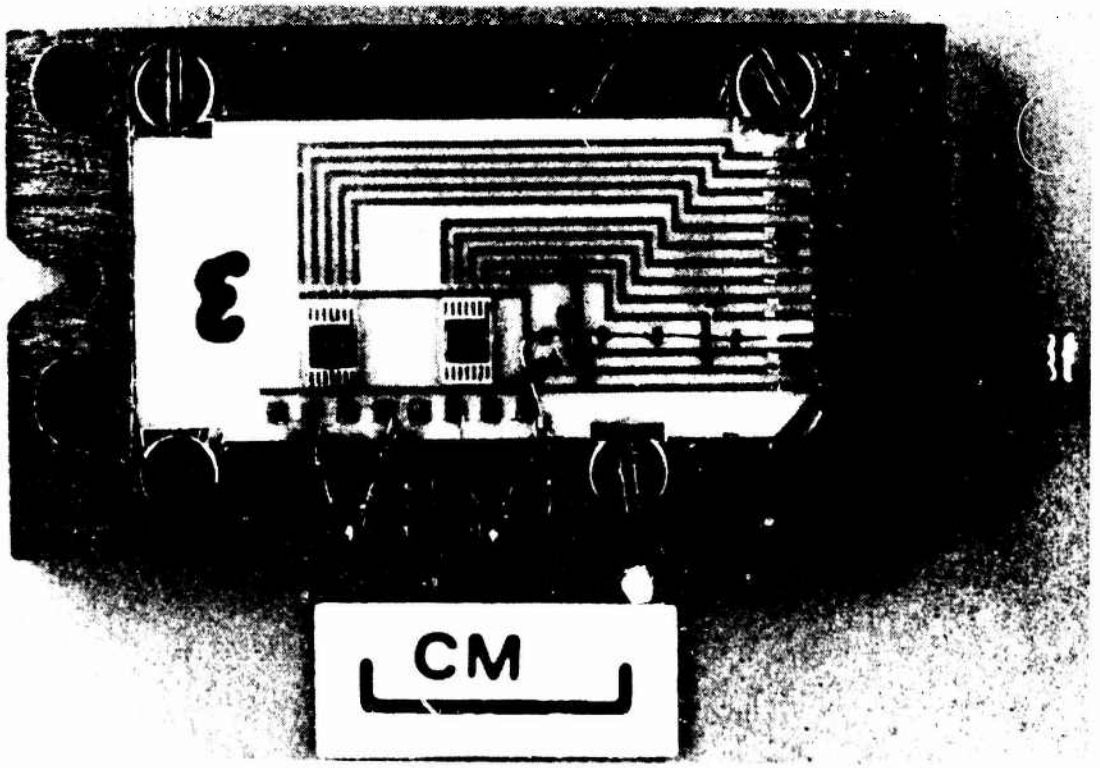

FRONT

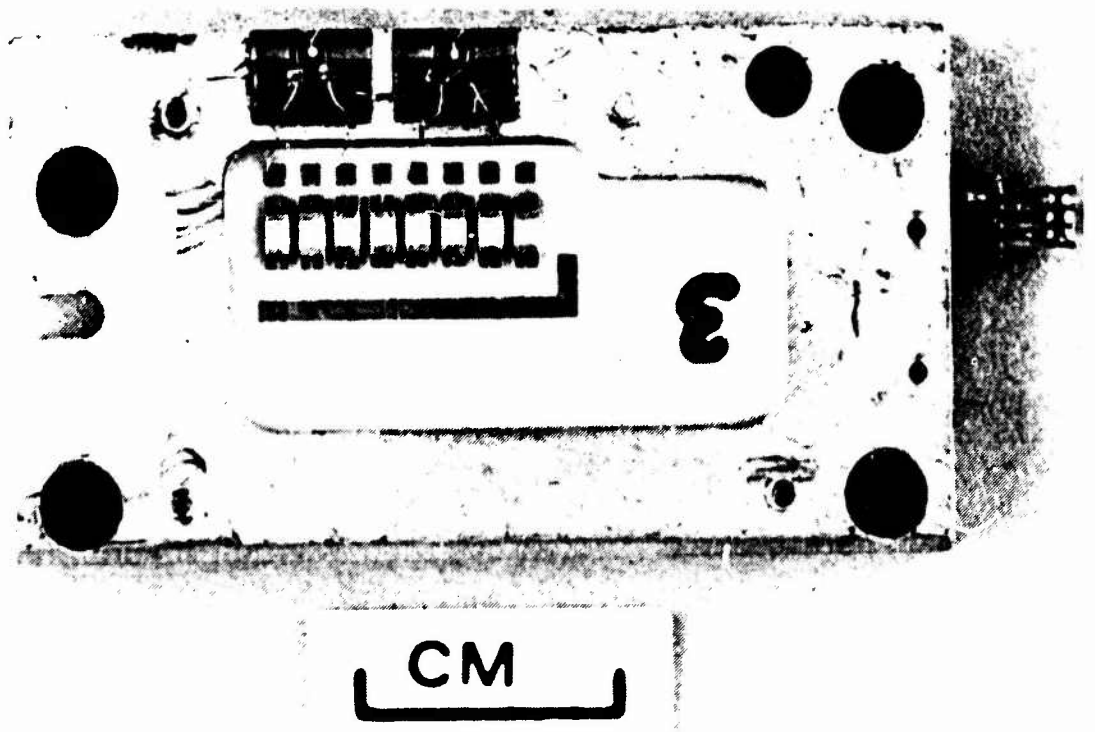

83-8-13

REAR

Figure 11. Frame 3 Assembly - Refurbished

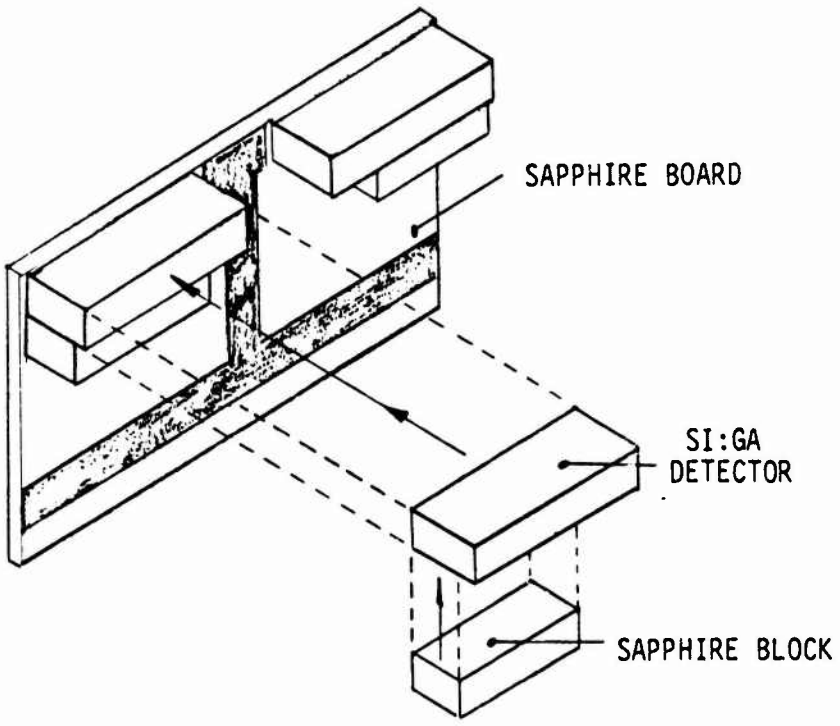

Figure 12. BEAM Detector Board Assembly

2.4 ARRAY LAYOUT

The frame subassemblies are numbered in accordance with the band numbers:

Band 1 = Frame 1 (3 to 5 μm Filter Combination)
Band 2 = Frame 2 (5 to 7 μm Filter Combination)
Band 3 = Frame 3 (8 to 14 μm Filter)

The aperture mask is positioned directly over the detector elements and defines both the detector positions and element sizes. Each detector has a defined area of:

$$0.0625 \text{ in.} \times 0.0200 \text{ in.} = 1.25 \times 10^{-3} \text{ in.}^2$$

$$(1.25 \times 10^{-3} \text{ in.}^2 \times (2.54 \text{ cm/in.})^2 = \underline{8.065 \times 10^{-3} \text{ cm}^2})$$

Figure 13 depicts the aperture geometric configuration, showing element sizes and spacing between elements. Figure 14 shows the positions of the detectors as designated by detector numbers, as well as the band positions and relative spectral range for each band.

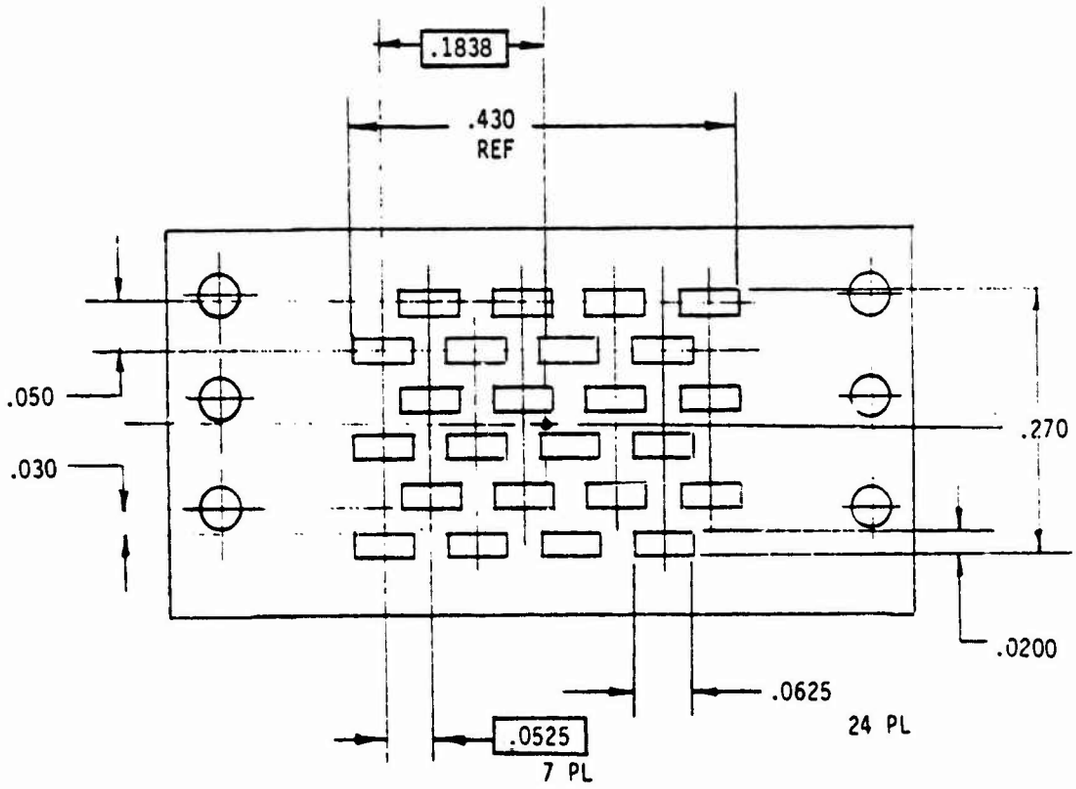

Figure 13. Aperture Mask Dimensions

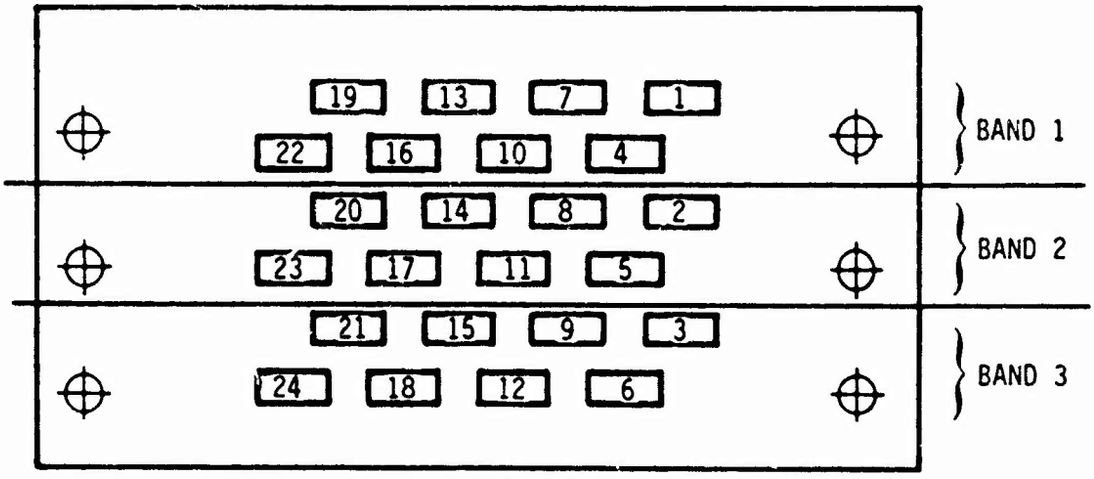

Figure 14. Detector Positions

2.5 CIRCUIT LAYOUT AND INTERCONNECTIONS

This section deals with the information primarily through figures and tables, necessary to trace the individual components to their origin. Figure 15 shows a top view of the HIGH STAR/BEAM FPA and the relative positions of the color bands. Figure 16 shows the electrical functions of the potted connector in the frame module. Table 1 cross references the various designation systems used for the focal plane. Table 2 is a signal function pin assignment list for the band frame nano-connectors, the paddle board and the dewar housing connector.

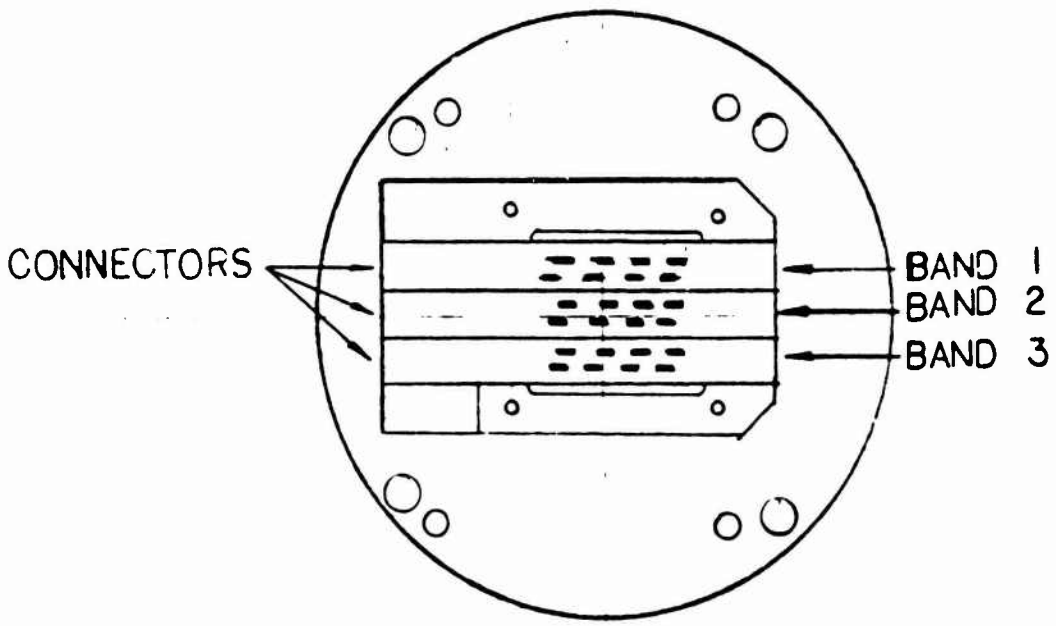

Figure 15. FPA Top View - Band Positions

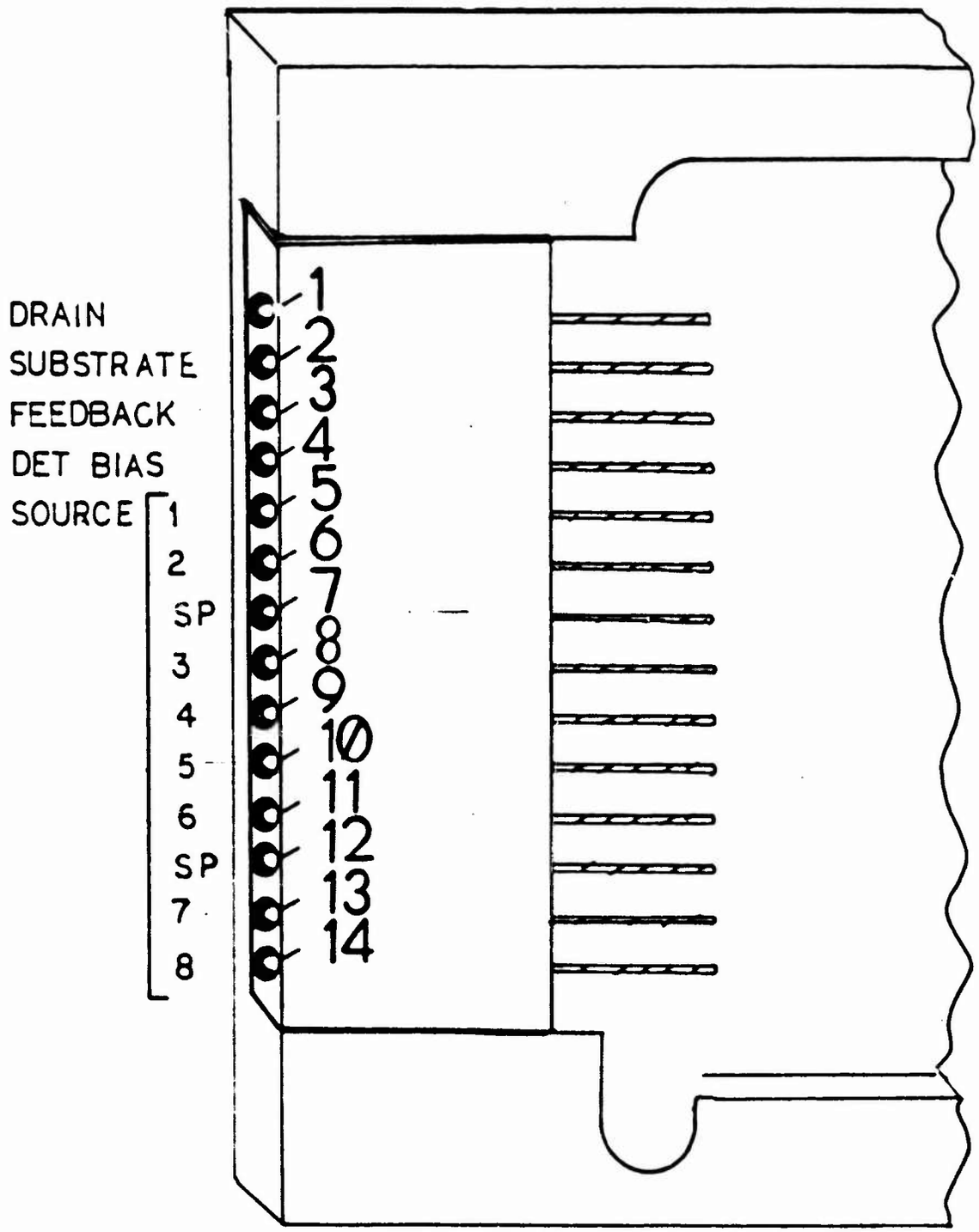

Figure 16. Electrical Functions of Potted Connector in Frame Module

Table 1. Cross Reference Sheet

BENDIX	AFGL DETECTOR DESIGNATION	FRAME OR BAND NO.	SBRC BREAKOUT BOX	SBRC FRAME-DET. NO.	FRAME PIN NO.
A	22	1	1-1	1-1	5
B	7	1	4-4	1-6	11
C	4	1	5-3	1-7	13
D	1	1	6-2	1-8	14
E	6	3	6-1	3-7	13
F	12	3	4-3	3-5	10
G	21	3	2-2	3-2	6
H	Bias	1,2,3	-	-	3
J	Drain	1,2,3	-	-	1
K	Subst	1,2,3	-	-	2
L	24	3	1-3	3-1	5
M	3	3	6-4	3-8	14
N	9	3	5-2	3-6	11
P	23	2	1-2	2-1	5
R	14	2	3-3	2-4	9
S	2	2	6-3	2-8	14
T	5	2	5-4	2-7	13
U	8	2	5-1	2-6	11
V	16	1	2-3	1-3	8
W	10	1	4-1	1-5	10
X	13	1	3-2	1-4	9
Y	18	3	3-1	3-3	8
Z	Spare	2	-	S	7
a	FB	1,2,3	-	-	4
b	15	3	3-4	3-4	9
c	20	2	2-1	2-2	6
d	17	2	2-4	2-3	8
e	11	2	4-2	2-5	10
f	19	1	1-4	1-2	6
g	Spare	1	-	S	7
h	Spare	3	-	S	7
j	Shield	1,2,3	-	-	-
-	Spare	1,2,3	-	S	12

Table 2. Cable/Connector Function Sheet

PADDLE BOARD TRACE NO.	NANO CONNECTOR NO.	FUNCTION	J-39 CONNECTOR		
			BAND 1	BAND 2	BAND 3
1	1	DRAIN	J	J	J
2	2	SUBSTRATE	K	K	K
3	3	FEEDBACK	H	H	H
4	4	DETECTOR BIAS	a	a	a
5	5	SOURCE NO. 1	A	P	L
6	6	SOURCE NO. 2	f	c	G
7	7	SPARE	g	Z	h
8	8	SOURCE NO. 3	V	d	Y
9	9	SOURCE NO. 4	X	R	b
10	10	SOURCE NO. 5	W	e	F
11	11	SOURCE NO. 6	B	U	N
12	12	SPARE	---	---	---
13	13	SOURCE NO. 7	C	T	E
14	14	SOURCE NO. 8	D	S	M

NOTE: J-39 Connector is a 35-pin Bendix (Dewar housing)

2.6 CABLE ASSEMBLIES

There were two cable assemblies built for the BEAM FPA. One is for the ICS and temperature sensors only while the other is the interface for the detector circuitry.

The ICS cable assembly (Figure 17) consists of a nine conductor flat ribbon cable with 8-pin band connectors on each end. The end which mates to the ICS assembly is female or contains the socket connector. Only six of the conductors are used while the remainder are for spares.

Pin Assignments

1.1 KΩ	1.	Temp Sensor (ICS)
	2.	Temp Sensor (ICS)
6.6 KΩ	3.	ICS
	4.	ICs
1.1 KΩ	5.	Temp. Sensor (Base)
	6.	Temp. Sensor (Base)

Figure 17. ICS Cable Assembly Pin Assignments

The FPA main cable assembly consists of three individual and identically wired ribbon cables which come together at a 35-pin Bendix connector. At this Bendix connector a three stage paddle board configuration interconnects the cable elements to the appropriate connector pin. The opposite end terminates with three individual 14-pin band connectors, one per band. Figure 18 shows the paddle board layout. Figure 5 is a photo of this assembly.

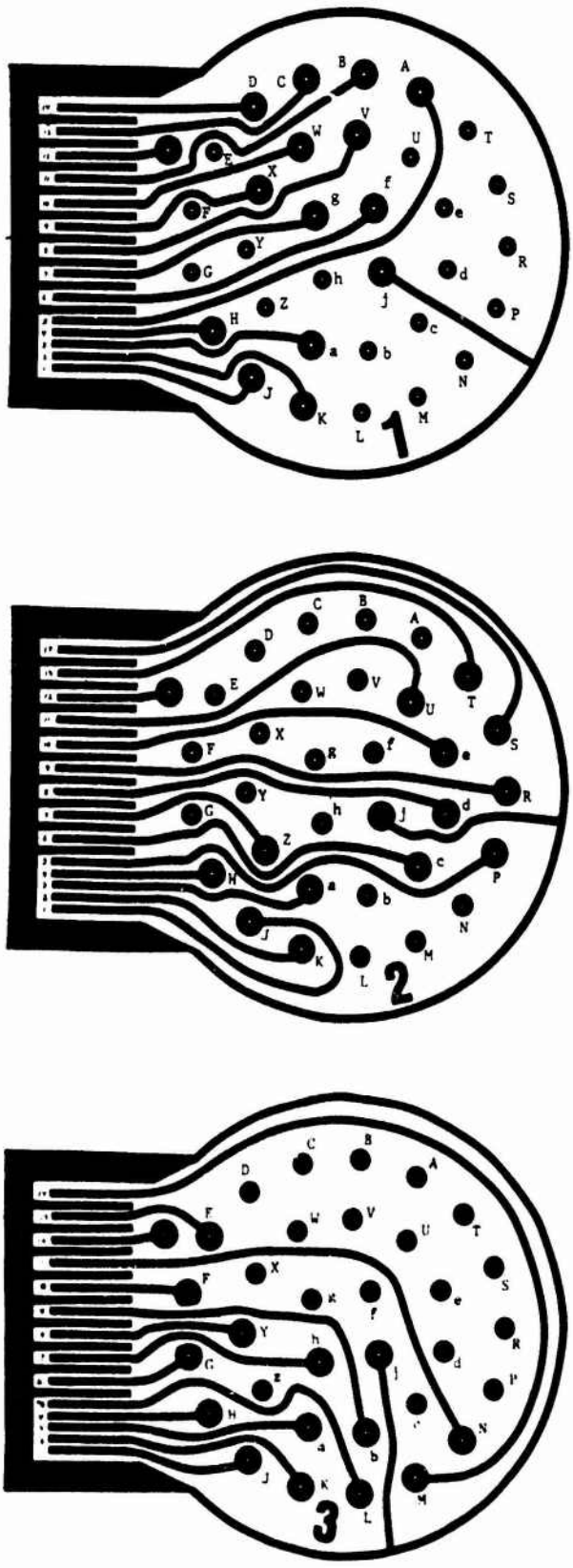

Figure 18. Paddleboard Layout

Section 3
FPA PERFORMANCE CHARACTERIZATION TESTS

3.1 DESCRIPTION

The HI-STAR array consists of three independent and identical frame subassemblies, hereafter called 'frames'. Radiometric tests were performed on all three frame subassemblies to form a complete set of baseline measurements. Randomly selected individual detector circuits were chosen to undergo tests under varied conditions to determine overall performance of the FPA to changes in its environment. All of the required NEP and responsivity specifications in the contract were met.

The 24 discrete IR detectors are all gallium doped silicon (Si:Ga) made from Crystal No. Z027, which covers the spectral region from 2 to 18 $\times 10^{-6}$ meters. These are extrinsic photoconductors, manufactured by Hughes Aircraft Company (HAC), Carlsbad, CA.

The three cooled preamplifier circuit boards consist of two tandem multiple-channel MOSFETs and eight high-impedance feedback resistors per frame assembly. The detector temperatures and preamp temperatures are considered to be the same. The MOSFETs are 6-channel Hughes W-164 low noise devices and the feedback resistors are ELTEC Model 112 with nominal values of 4 $\times 10^{9}\,\Omega$ ambient.

Temperature values were determined from three strategically located sensors on the FPA and dewar cold head. All sensors were 1/4-watt carbon 1 kΩ resistors with calibrations done prior to installation.

3.2 SETUP

Initial radiometric measurements were taken to determine detector/preamp operation characteristics independent of bandpass filtering at a known background level. A Janis dewar specially modified for low-background detector/FPA testing was used. This allowed the FPA to be run with its four flight cables and external connector as a means of outputting signals and inputting bias voltages.

The internal dewar environment utilized a large distance from aperture to FPA in order to achieve a uniform and predictable background photon level.

Figure 19 shows this setup graphically. Neutral density attenuating filters and a pinhole aperture were placed a long distance away from the detector plane and cooled to near liquid helium temperatures to achieve the desired background flux. A 500K blackbody with integral variable speed chopper and a controllable shutter provided the optical signal necessary for responsivity and NEP measurements.

Four metallized ribbon cables weave through the dewar from the focal plane assembly to the 35-pin Bendix connector on the outside dewar housing. One cable is used for powering the internal calibration sources along with the two temperature sensors, while the remaining three cables interface each of the three frame subassemblies.

For accessing the FPA from the dewar output connector, SBRC built a complete cable assembly made of shielded coax cable which mates to a test box. The test box also regulates the power supplies to provide for all 24 detector and MOSFET bias voltages.

3.3 MEASUREMENT METHOD

The detector signal and noise output voltages were fed through an AFGL-supplied amplifier, and then into a Hewlett Packard wave analyzer, a Tektronix oscilloscope, and a Fluke dc voltmeter. Figure 20 shows the experimental setup used in the responsivity and NEP measurements. Figure 21 shows the schematic of the AFGL-supplied amplifier that was also used.

The amplifier increased the upper frequency response of the detector circuit, which was nominally flat to less than 6 Hz, to better than 200 Hz. The common feedback configuration, which was part of the original FPA design, forced testing in the source follower mode rather than the usual TIA mode. This meant an early rolloff as a function of frequency and limited the extent of testing to very low frequencies which would uncharacteristically represent the performance of the FPA. A frequency response curve for this amplifier gain is shown in Figure 22.

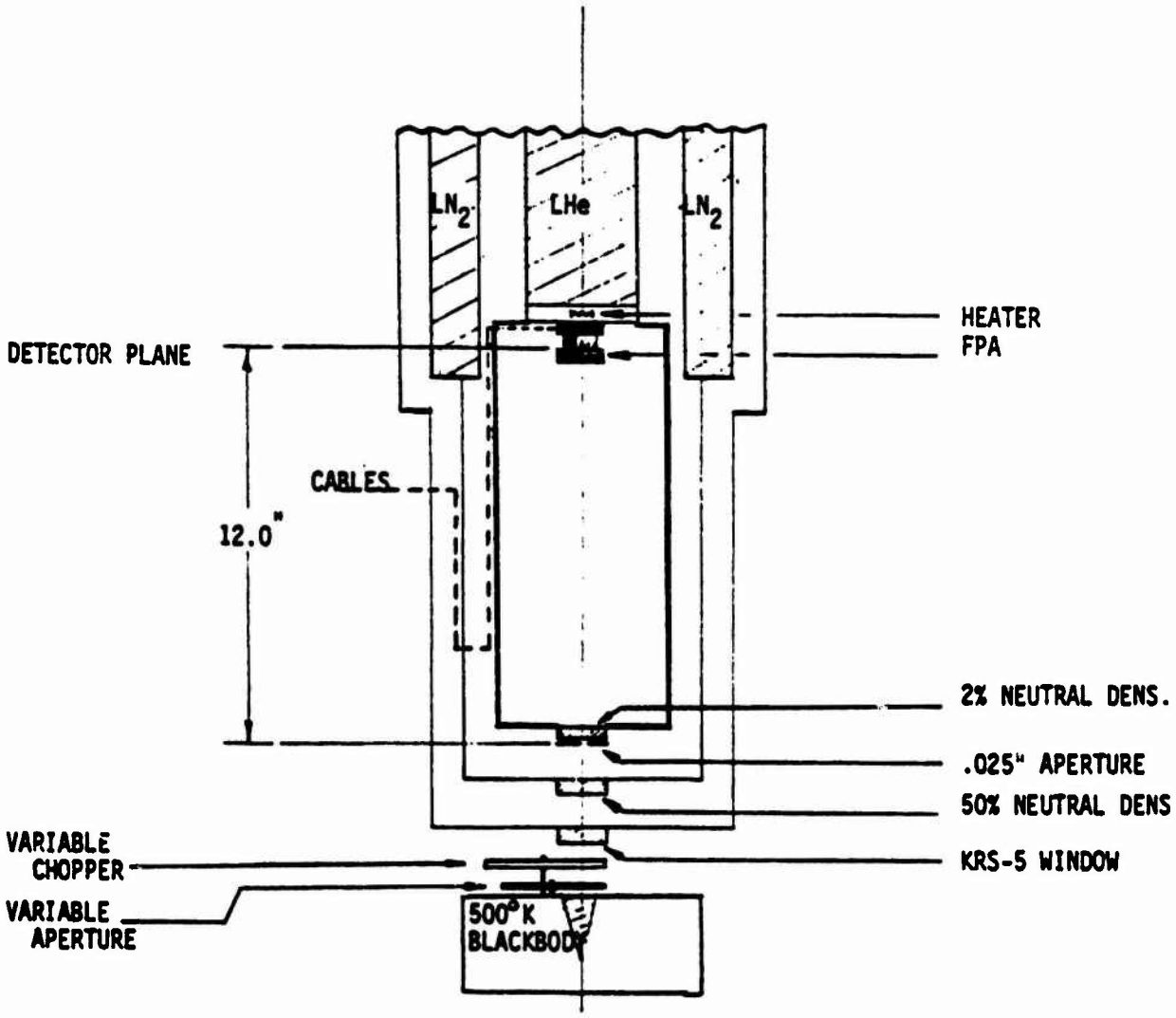

Figure 19. Dewar Setup for NEP and Responsivity Measurements

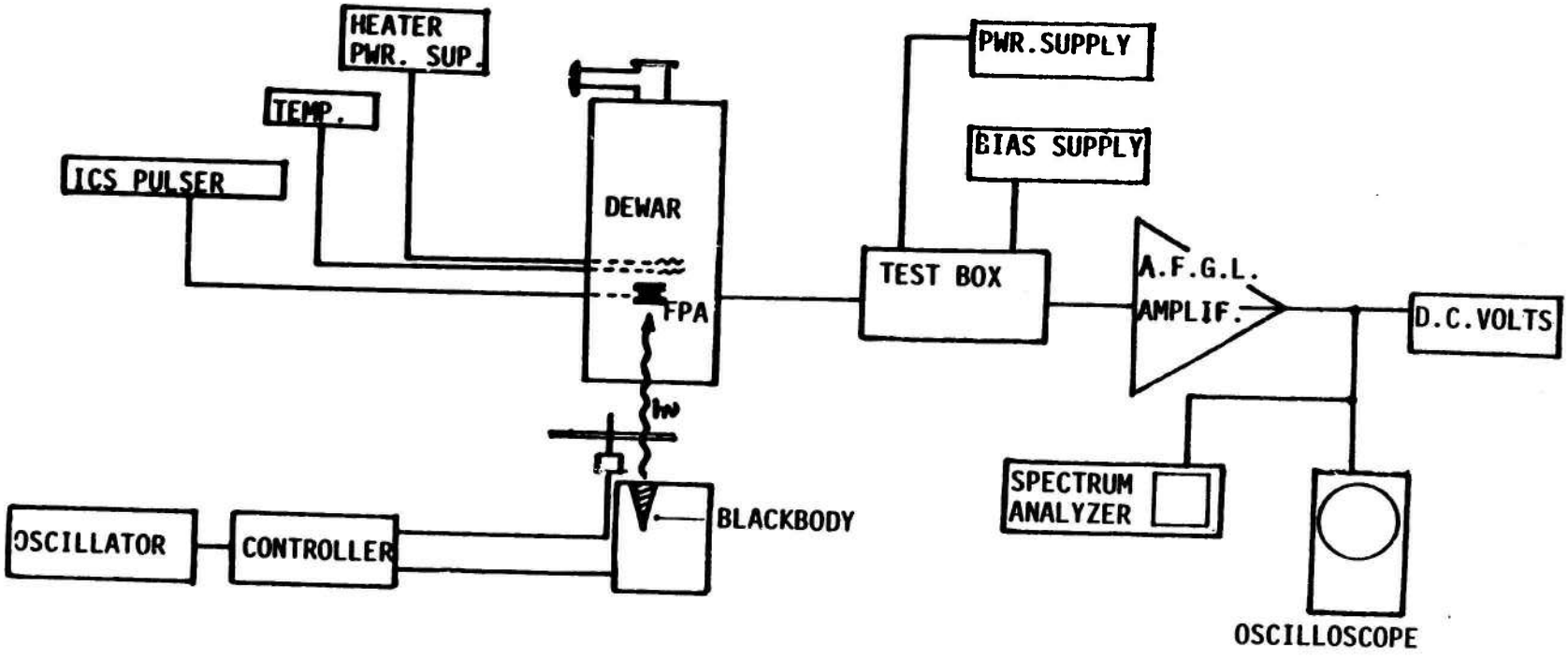

Figure 20. Experimental Set-up

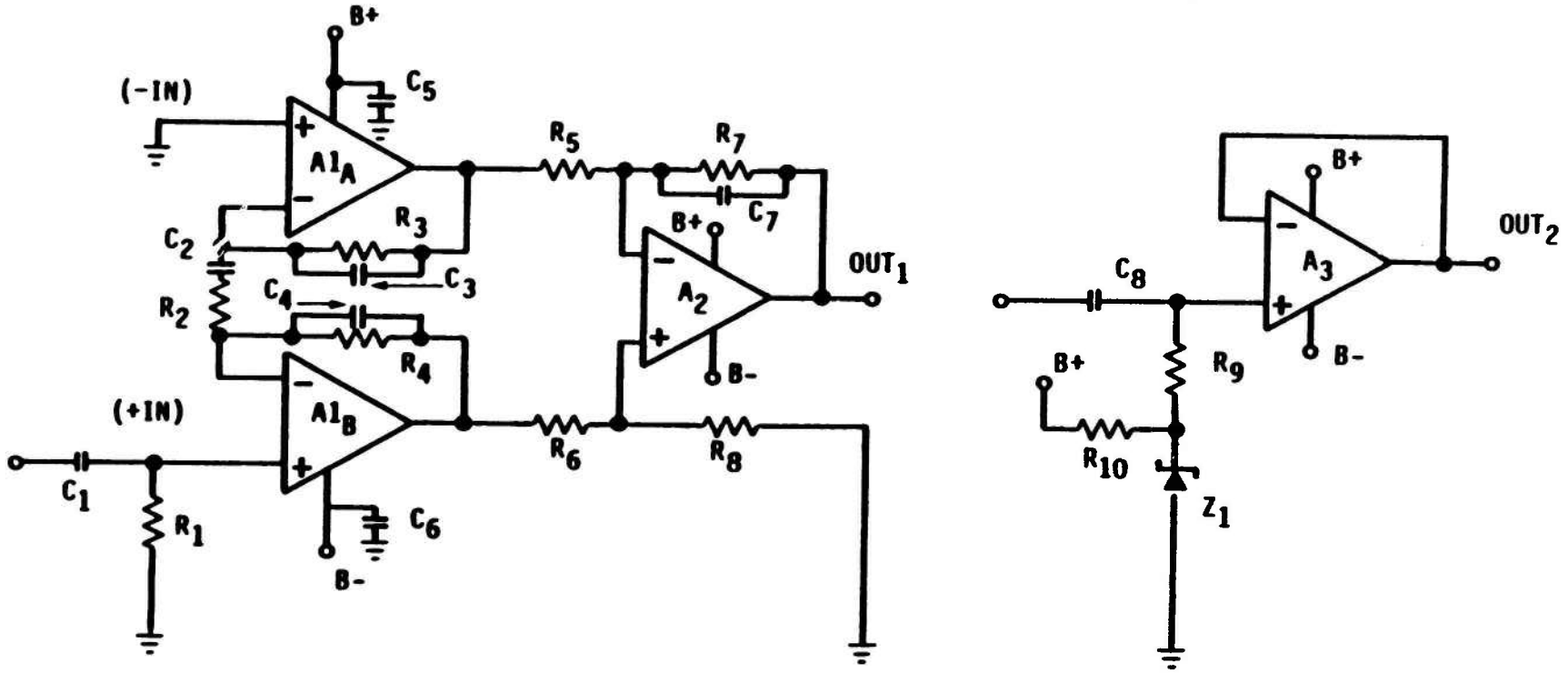

Figure 21. AFGL-Supplied Amplifier

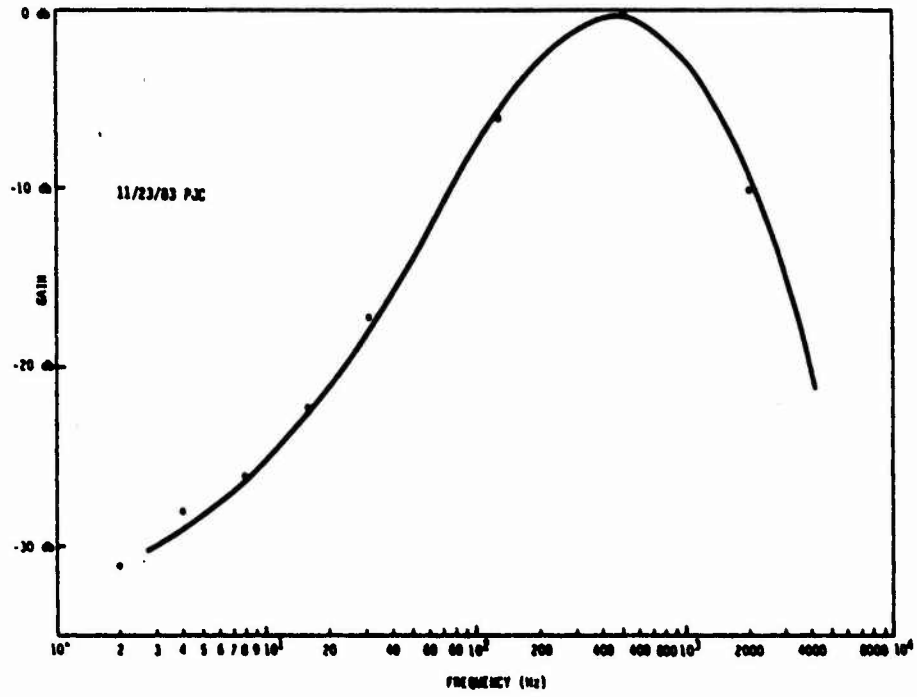

Figure 22. Frequency Response Curve

3.4 NEP AND RESPONSIVITY SPECIFICATIONS

In compliance with the requirements set forth, all detectors used in the FPA must match or better the noise equivalent power and responsivity specifications as called out in the contract. They are:

	NEP AVERAGE	NEP WORST	UNITS
Array No. 1 (3 to 5 μm)	5×10^{-16}	1×10^{-15}	$(W/Hz^{1/2})$
Array No. 2 (5 to 7 μm)	3×10^{-16}	8×10^{-16}	$(W/Hz^{1/2})$
Array No. 3 (8 to 14 μm)	2×10^{-16}	4×10^{-16}	$(W/Hz^{1/2})$

NEP values are obtained by:

$$NEP = \frac{V_N}{V_S} \cdot \frac{H_{EFF}\, A_D}{\sqrt{BW}} \quad [watts/Hz^{1/2}]$$

where

H_{EFF} = Effective blackbody radiant power density in $watts/cm^2$

A_D = Detector area in cm^2

BW = Noise bandwidth of the measurement system in Hz

V_N = Noise in volts (rms)

V_S = Signal in volts.

Responsivity is calculated by:

$R_{(I)pk}$ = Peak current responsivity =

$$\frac{V_S}{G} \cdot \frac{1}{H_{EFF} \cdot A_D \cdot R_{FB}}$$

where

R_{FB} = Feedback resistor value at 5K in ohms

G = Voltage gain (no units)

These tests were conducted prior to bandpass filter installation. After filters were installed, these tests were again run at single bias and frequency levels. Results of measurements taken once the filters were installed and again after shock and vibration tests proved repeatability and reliability of the instrument. The data are given in Section 3.7.

3.5 SPECTRAL RESPONSE

Spectral response measurements of the detectors were performed to provide the blackbody flux density used in the responsivity and noise equivalent power equations as well as to provide response profiles of the detector-filter combinations. SBRC used a similar detector from the same area of the silicon wafer as those used in the HI-STAR South Array to determine the relative response of this "sister" detector. Appendix A shows this curve for the Si:Ga detectors from Lot 2027. This appendix also includes spectral measurement data for the bandpass filters and blockers used for each of the three bands.

3.6 BASELINE MEASUREMENTS

3.6.1 Source Voltages

The preamp configuration consists of the cooled MOSFETS and warm external electronics as per Figure 23. The FETs are powered by using a +10V supply and an 82 KΩ resistor tied to the source, a 5V supply at the substrate, and a grounded drain. The gate is grounded via the detector. The FET current for each of the 24 channels is, therefore, calculated by:

$$I_{FET} = \frac{10V - Vs}{82{,}000\Omega} \text{ where } Vs = \text{source voltage}$$

$$I_{TOTAL} = (24)\ I_{FET} = 2.0 \times 10^{-3} \text{ amps}$$

And the MOSFET impedance is given by:

$$R_{FET} = \frac{Vs}{I_{FET}} = 34\text{-}40\ K\Omega$$

A bar chart for each of the channels' source voltages is given in Figure 24.

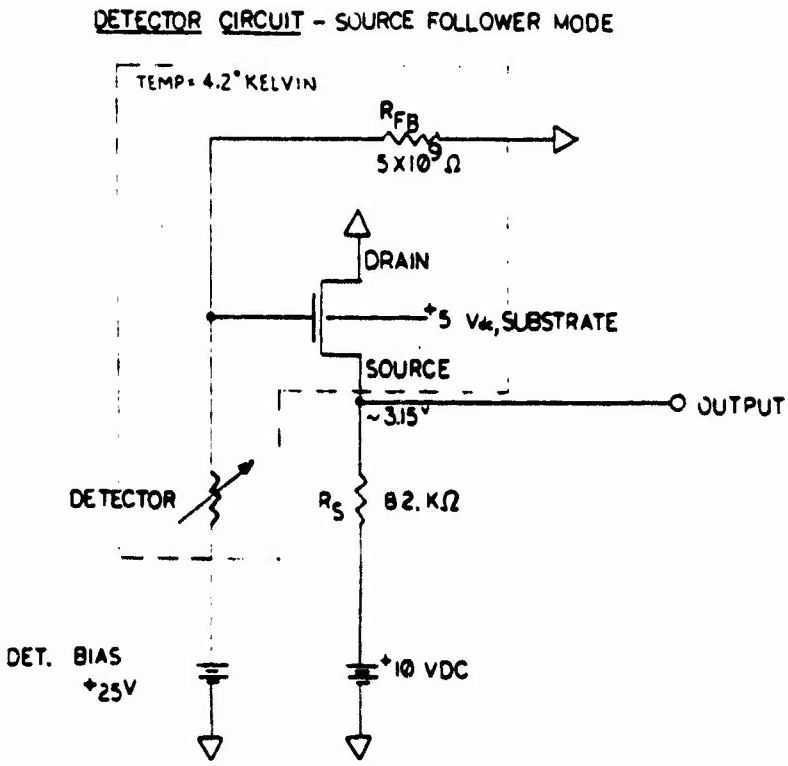

Figure 23. Preamp Schematic

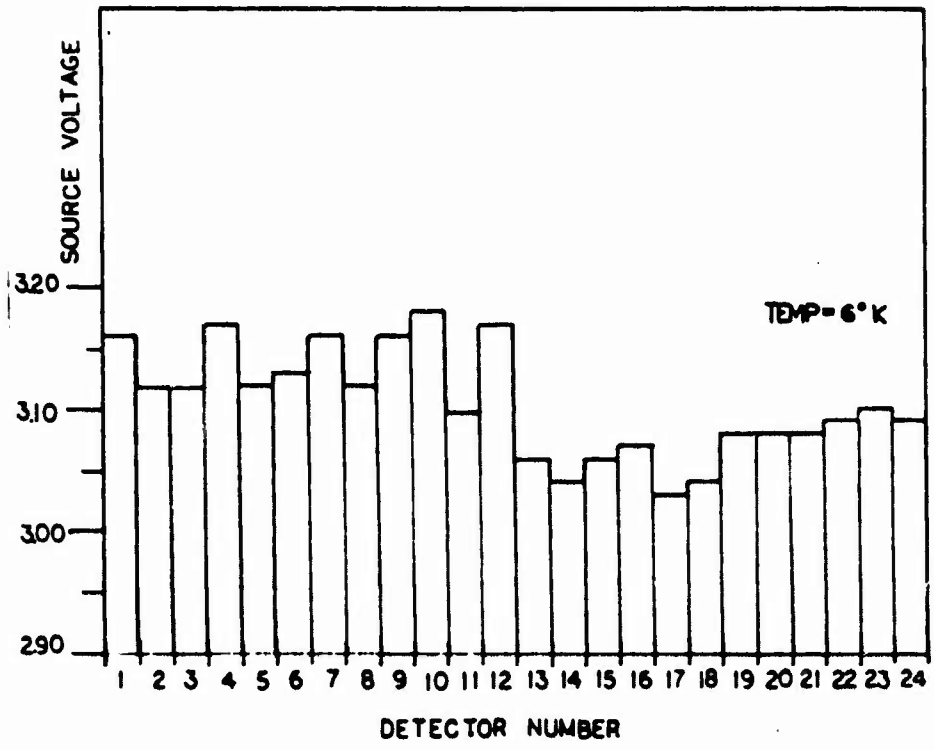

Figure 24. Source Voltages

3.6.2 Zero Bias Noise

All 24 detector channels were measured for noise with the detector bias supply off. The measurements were taken as a function of frequency both with and without the customer supplied amplifier. Figures 25-1, 25-2, and 25-3 show the frequency response profile for a typical detector channel. A bar chart (Figure 25-4) is used to list the remaining channels, which were measured using the amplifier. This bar chart is for comparative purposes as it does contain amplifier noise components.

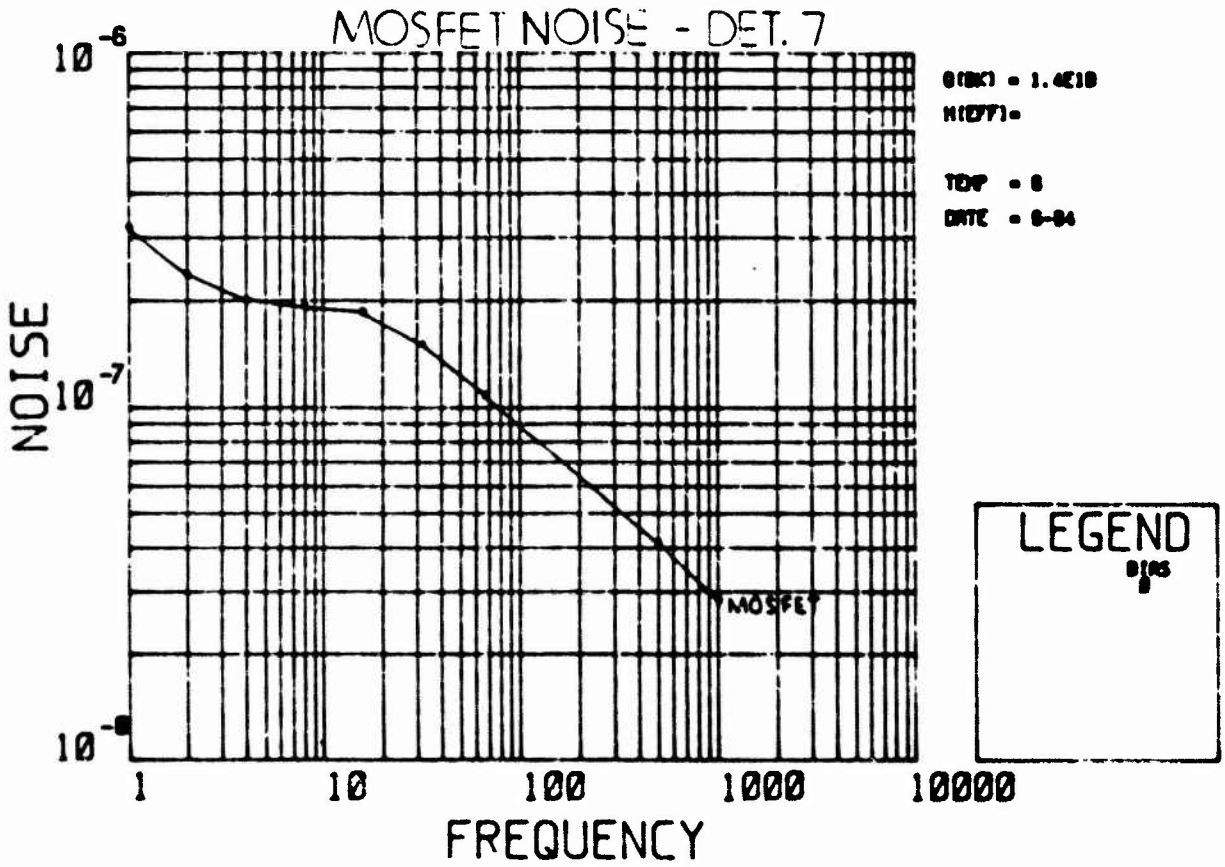

Figure 25-1. MOSFET Noise vs. Frequency

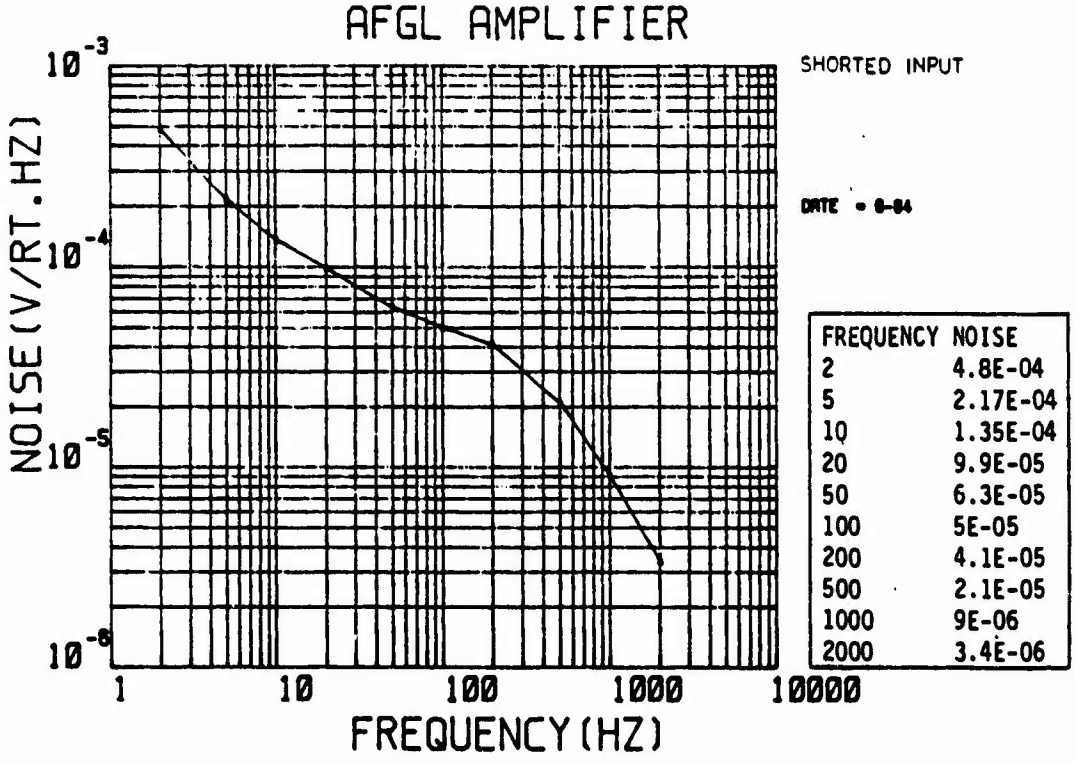

Figure 25-2. AFGL Amplifier Noise vs. Frequency

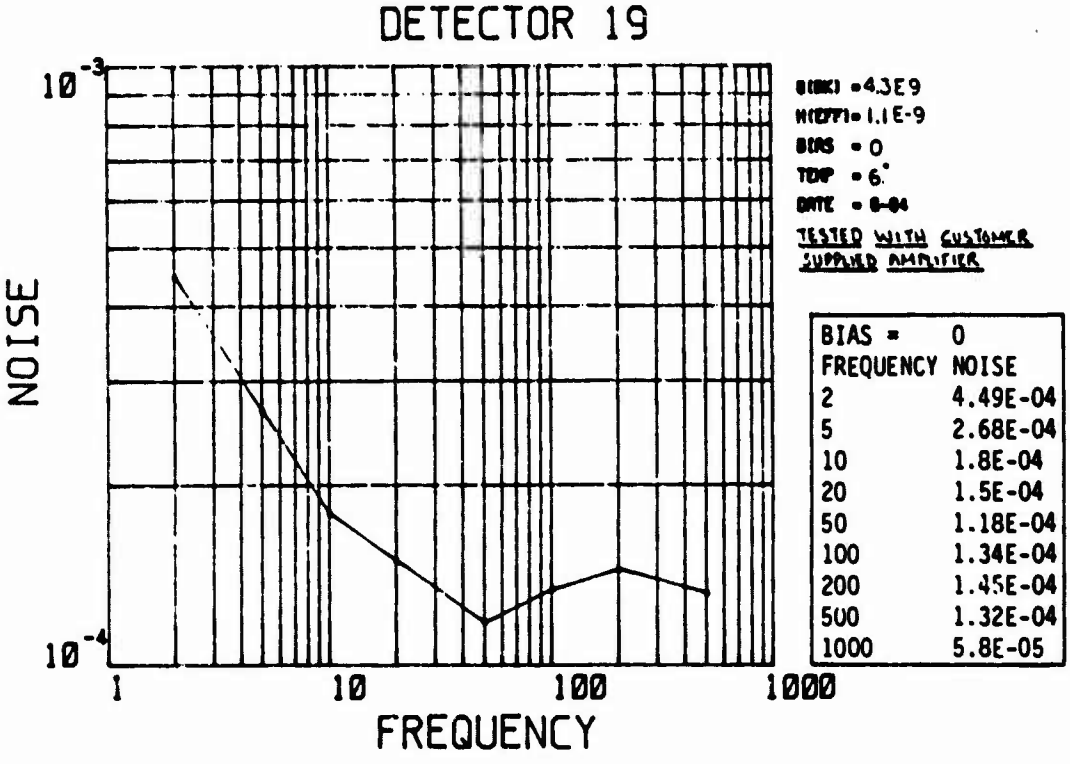

Figure 25-3. Detector Noise vs. Frequency

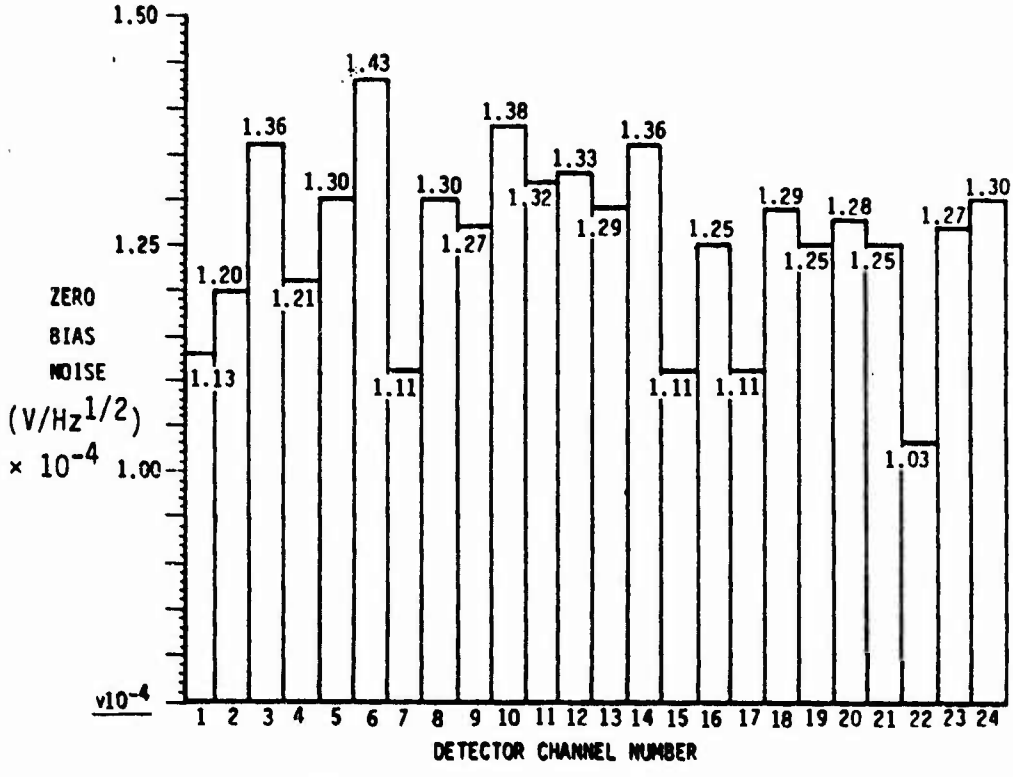

Figure 25-4. Detector Zero Bias Noise

NOTE: Zero bias noise taken at 50 Hz using customer supplied amplifier.

3.6.3 Signal and Noise vs. Bias

Figure 26-1 and 26-2 show plots of signal and noise vs. bias.

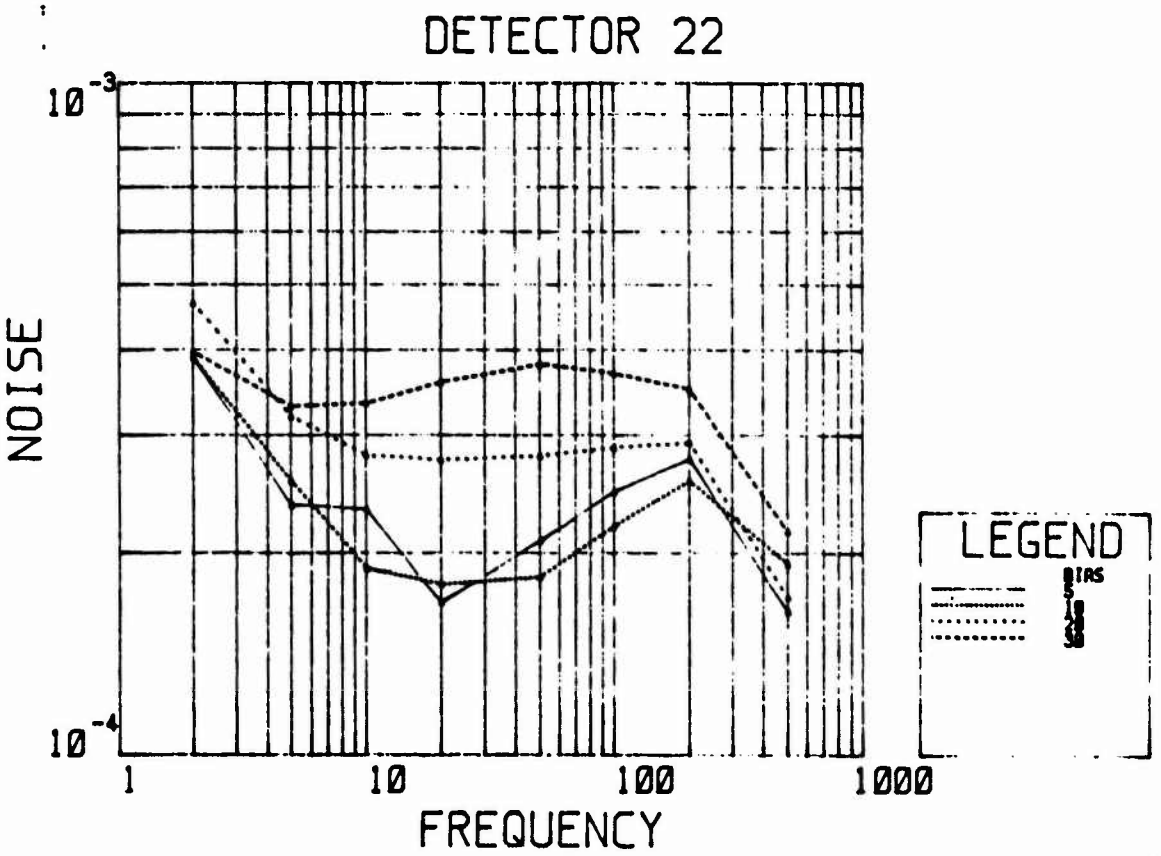

Figure 26-1. Noise vs. Bias

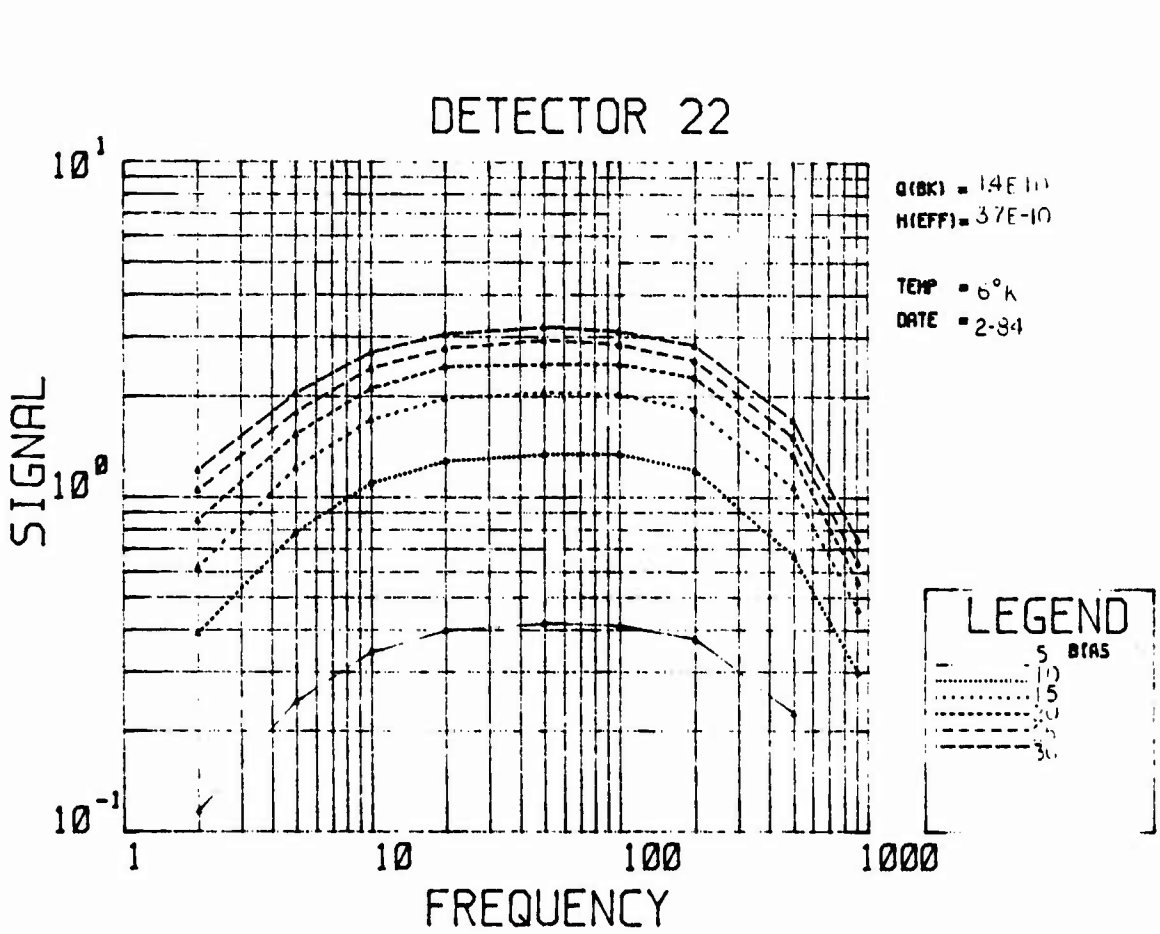

Figure 26-2. Signal vs. Bias

3.6.4 Signal and Noise vs Frequency

Refer to Figure 20 for experimental setup of dewar and refer to Table 3 for parameters used to calculate flux and background levels obtained by this setup.

Signal and noise plots for detectors 1 through 24 are presented in Figure 27-1 through 27-24. For clarity, the figure is broken down by detector, with two plots per page. The units of measure, which do not appear on these computer-generated plots are as follows:

Signal	[volts]
Noise	[$V/Hz^{1/2}$]
Frequency	[Hz]

A tabulation of data for all detectors is presented in Figure 27-25.

Table 3. Baseline Test Parameters

BB TEMP : 500 CH TEMP : 300
LAMBDA 1: 2 LAMBDA 2: 18.5
DELTA : .5
FILTERS : (1) HISTWN (2) BEAM2% (3) 3
RR/WATT : HISTGA
APERTURE: .025 DISTANCE: 12

FILTER LAMBDA	HISTWN TRANSMISSION	BEAM2%	3	HISTGA
2	.7	.02	.5	.031
2.5	.7	.02	.5	.055
3	.7	.02	.5	.061
3.5	.7	.02	.5	.11
4	.7	.02	.5	.1
4.5	.7	.02	.5	.186
5	.7	.02	.5	.224
5.5	.7	.02	.5	.249
6	.7	.02	.5	.205
6.5	.7	.02	.5	.219
7	.7	.02	.5	.241
7.5	.7	.02	.5	.402
8	.7	.02	.5	.375
8.5	.7	.02	.5	.336
9	.7	.02	.5	.383
9.5	.7	.02	.5	.418
10	.7	.02	.5	.489
10.5	.7	.02	.5	.575
11	.7	.02	.5	.678
11.5	.7	.02	.5	.758
12	.7	.02	.5	.845
12.5	.7	.02	.5	.815
13	.7	.02	.5	.864
13.5	.7	.02	.5	.839
14	.7	.02	.5	.896
14.5	.7	.02	.5	.973
15	.7	.02	.5	.969
15.5	.7	.02	.5	.934
16	.7	.02	.5	.822
16.5	.7	.02	.5	.732
17	.7	.02	.5	.794
17.5	.7	.02	.5	.624
18	.7	.02	.5	.278
18.5	.7	.02	.5	.118

BACKGROUND PHOTON FLUXES (PHOTONS SQUARE CM SECOND) :

QIBB = 1.38E+10 QIBB) = 1.02E-11

EFFECTIVE FLUX (WATTS/SQUARE CM) = 3.77E-11

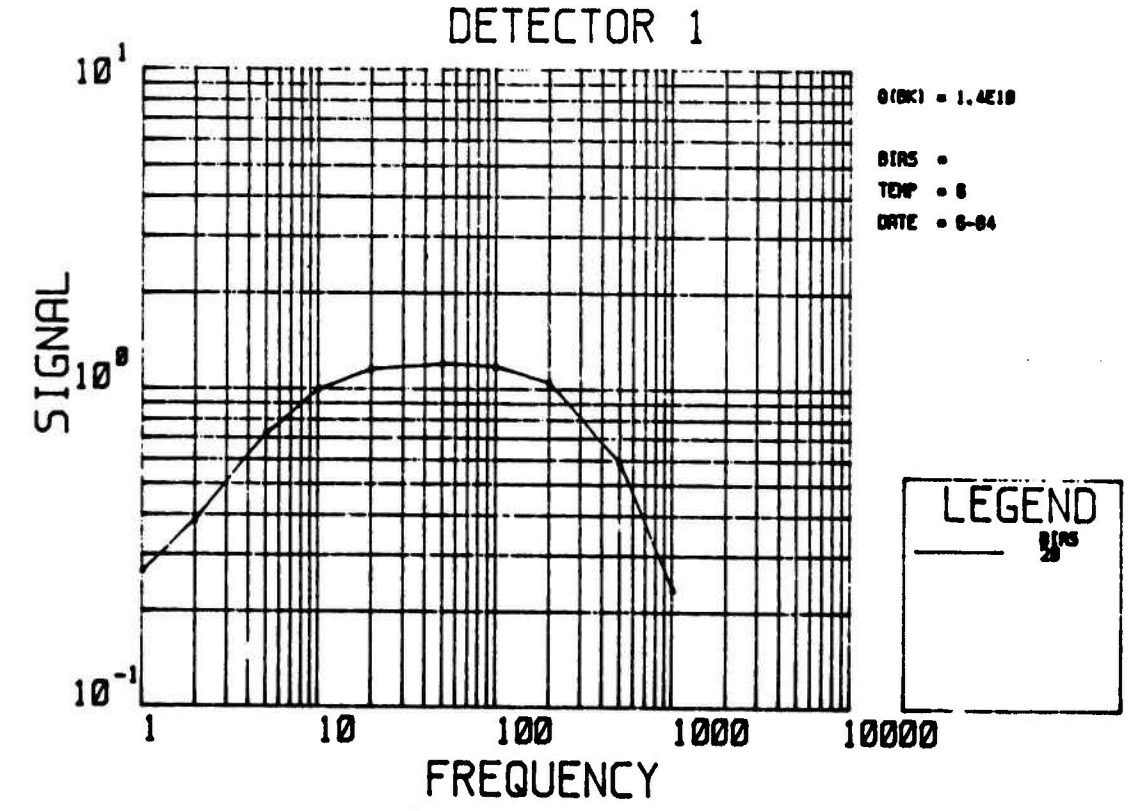

Signal vs Frequency

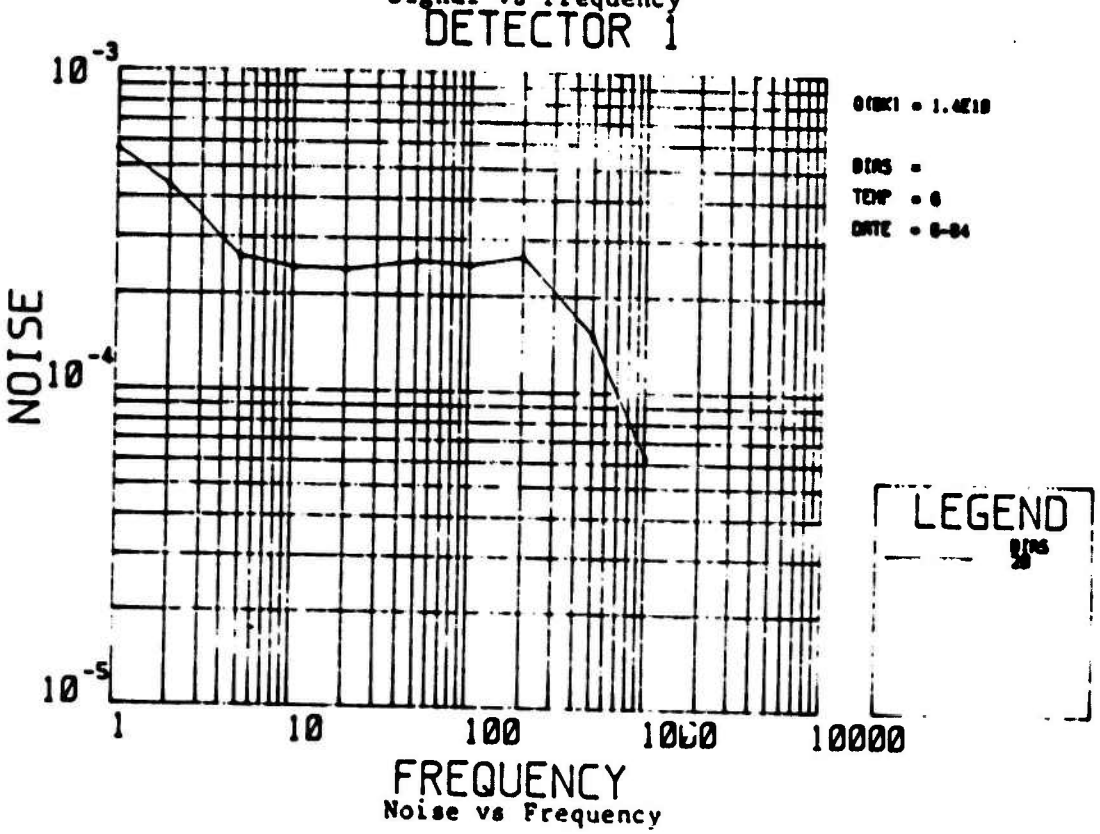

Noise vs Frequency

Figure 27-1. Detector 1

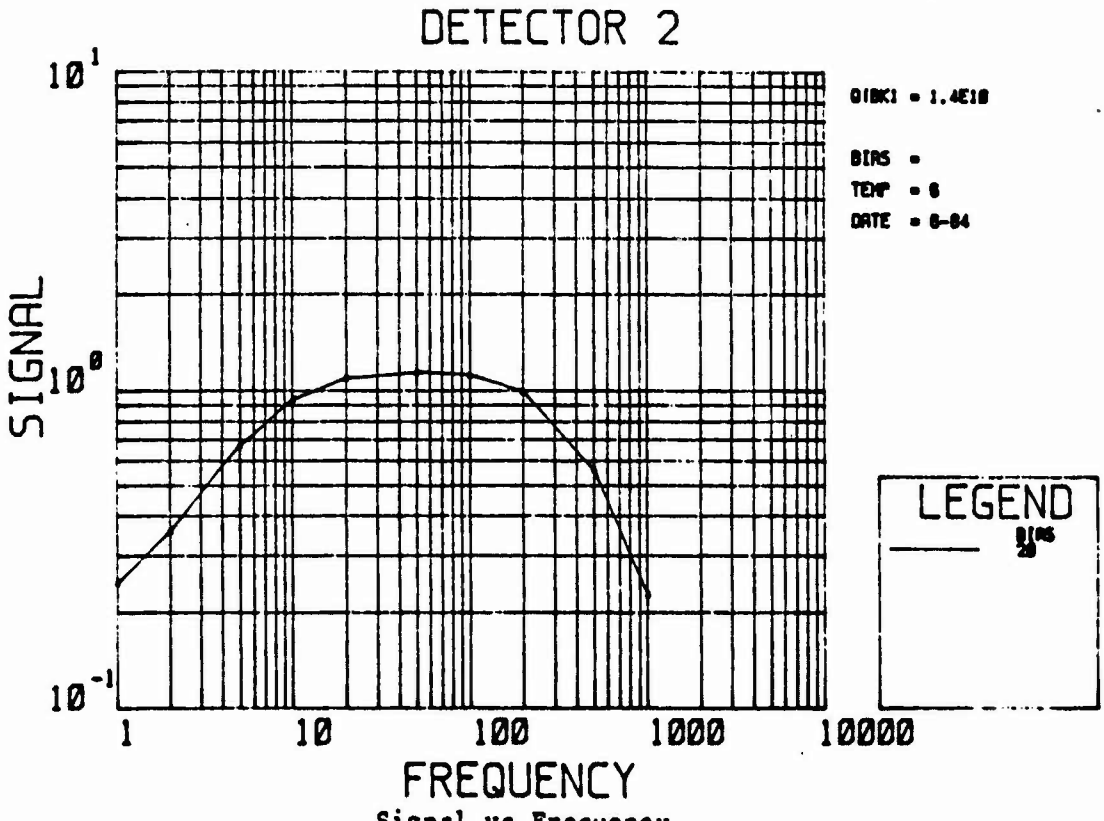

Signal vs Frequency

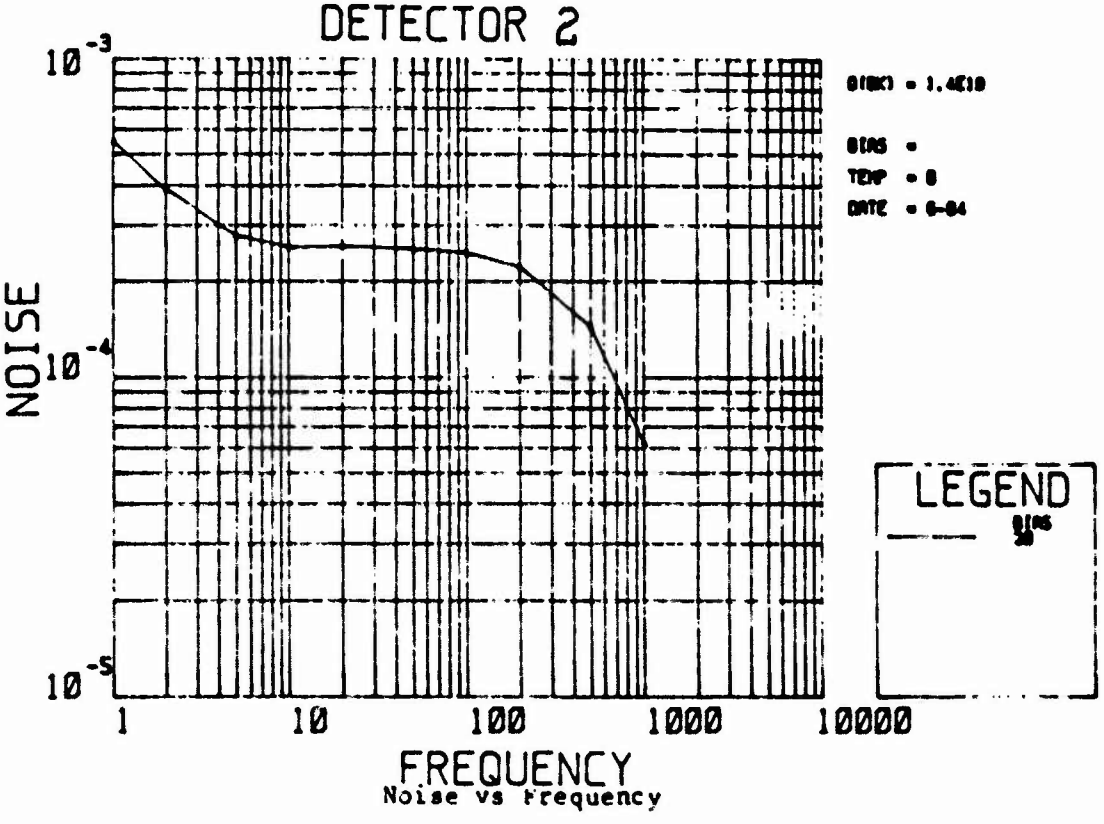

Noise vs Frequency

Figure 27-2. Detector 2

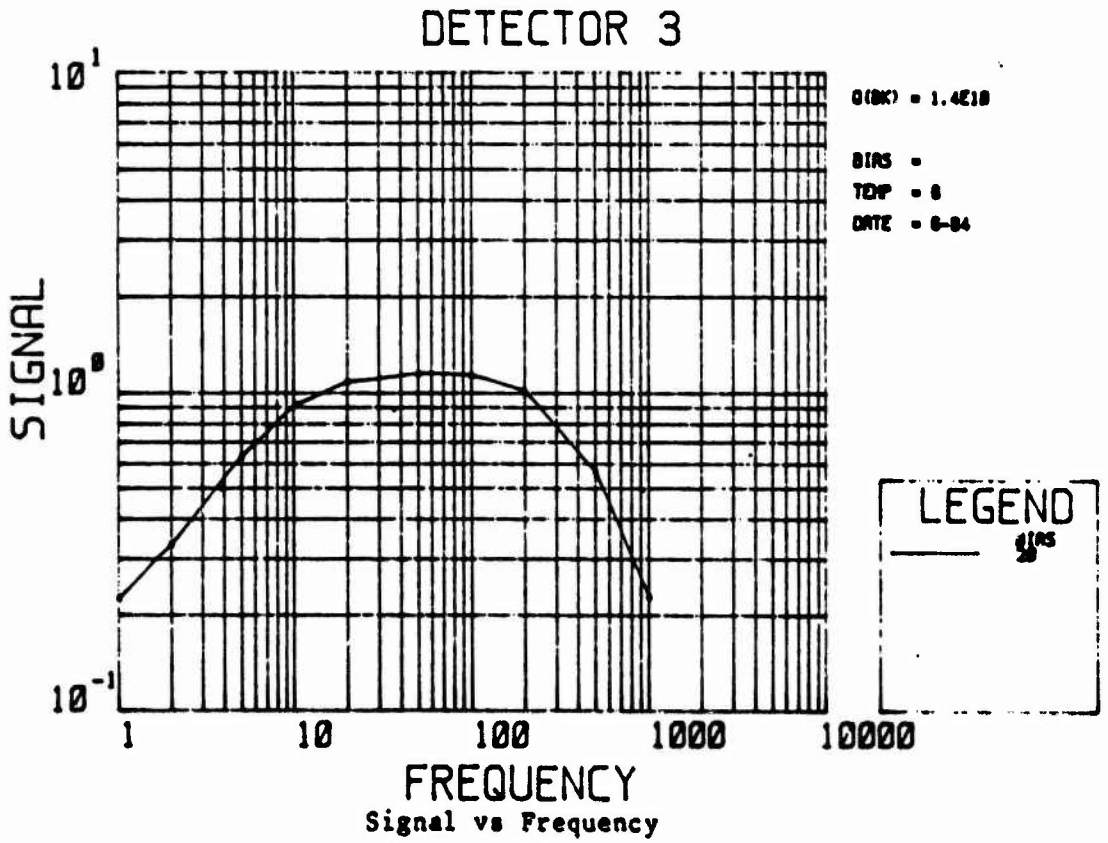

Signal vs Frequency

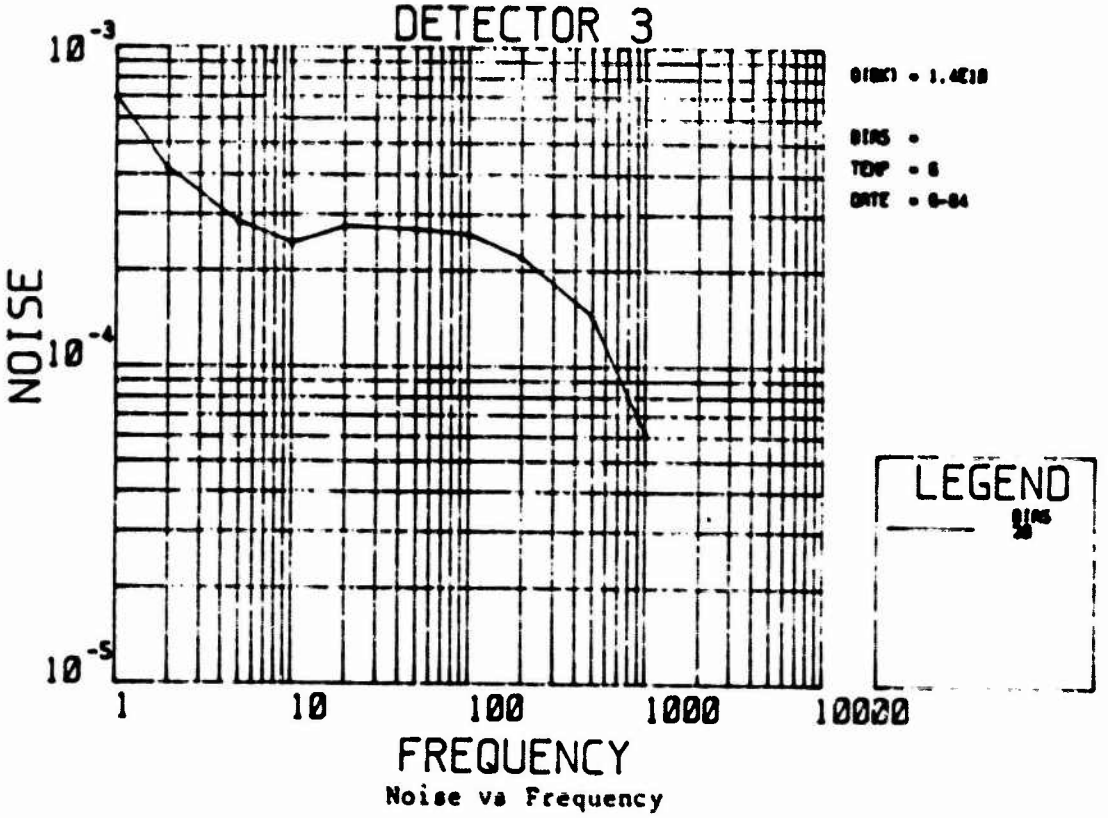

Noise vs Frequency

Figure 27-3. Detector 3

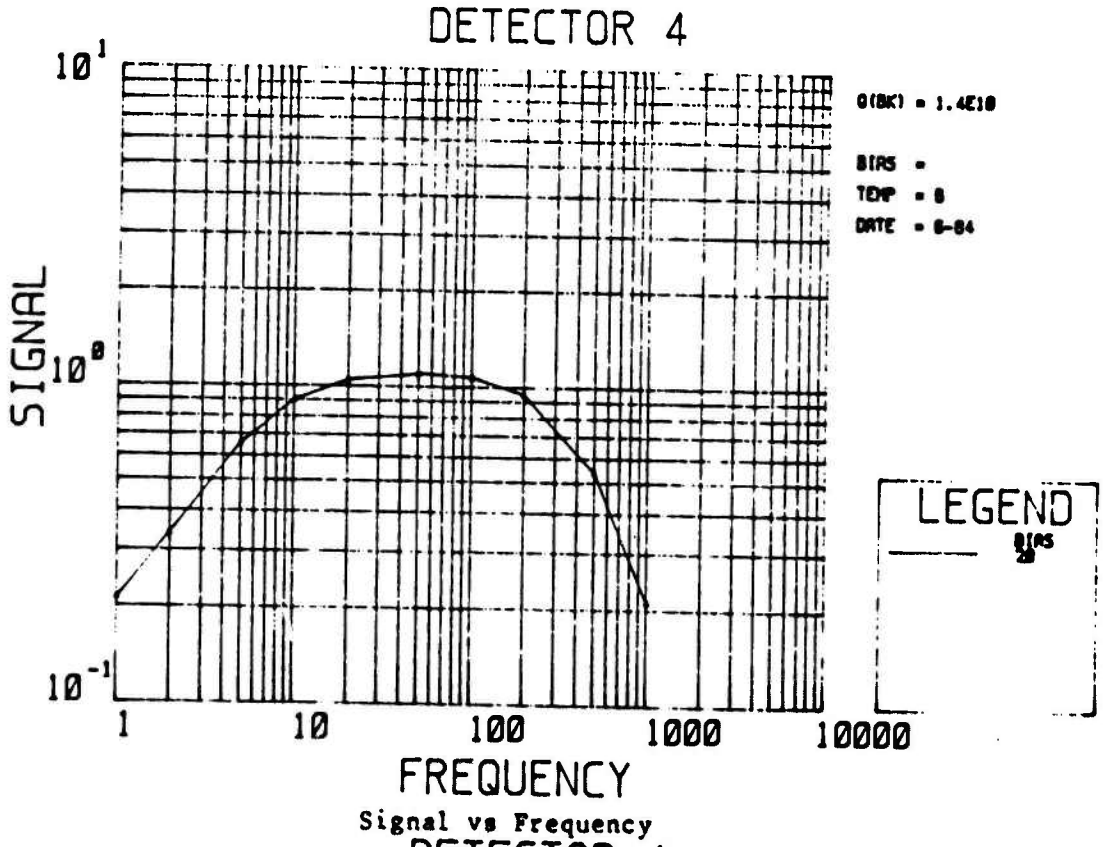

Signal vs Frequency

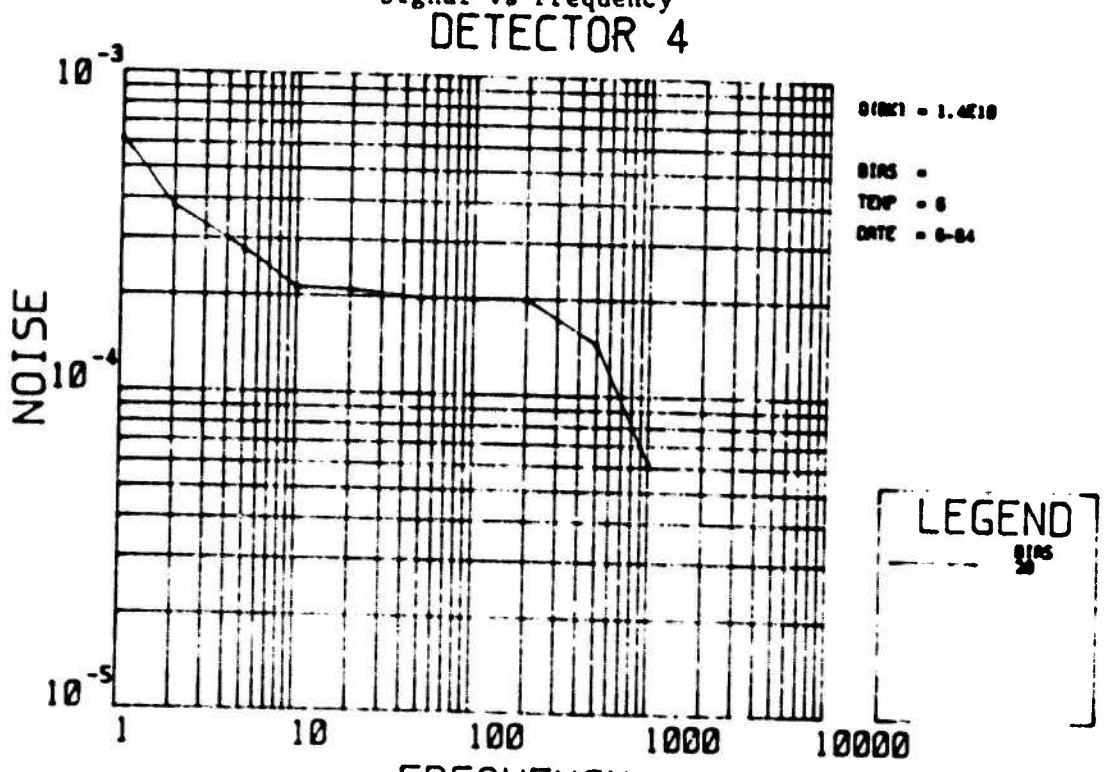

Noise vs Frequency

Figure 27-4. Detector 4

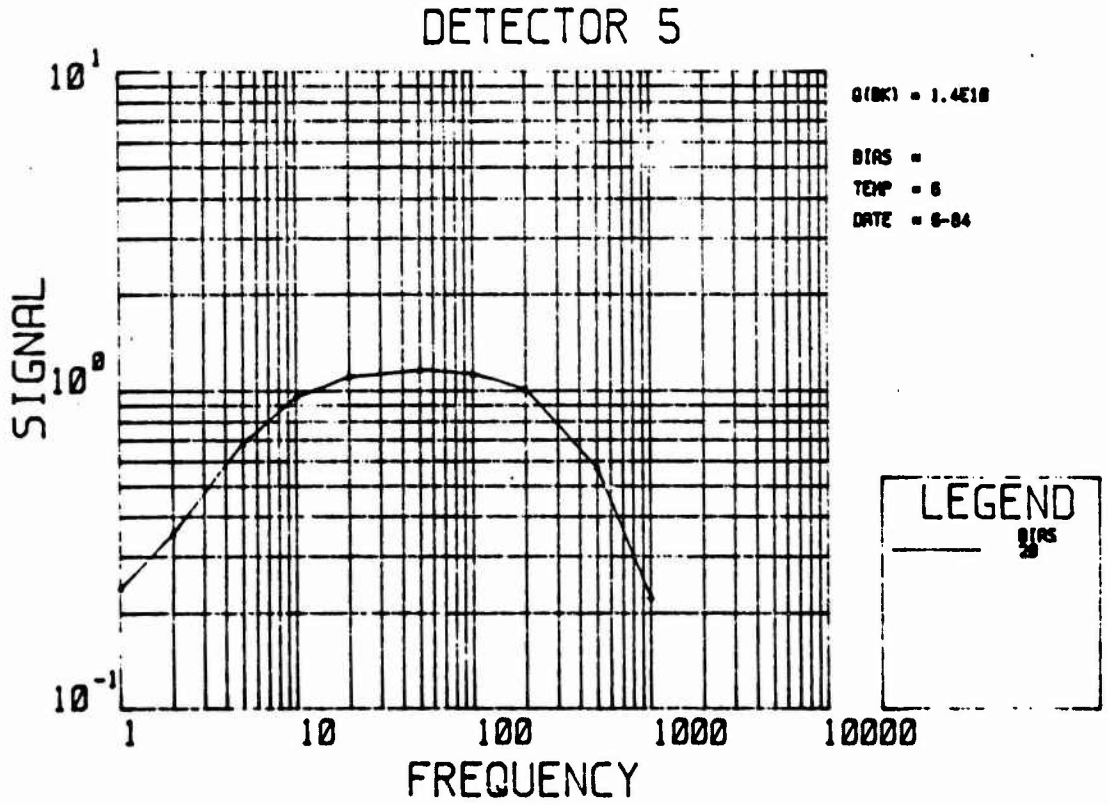

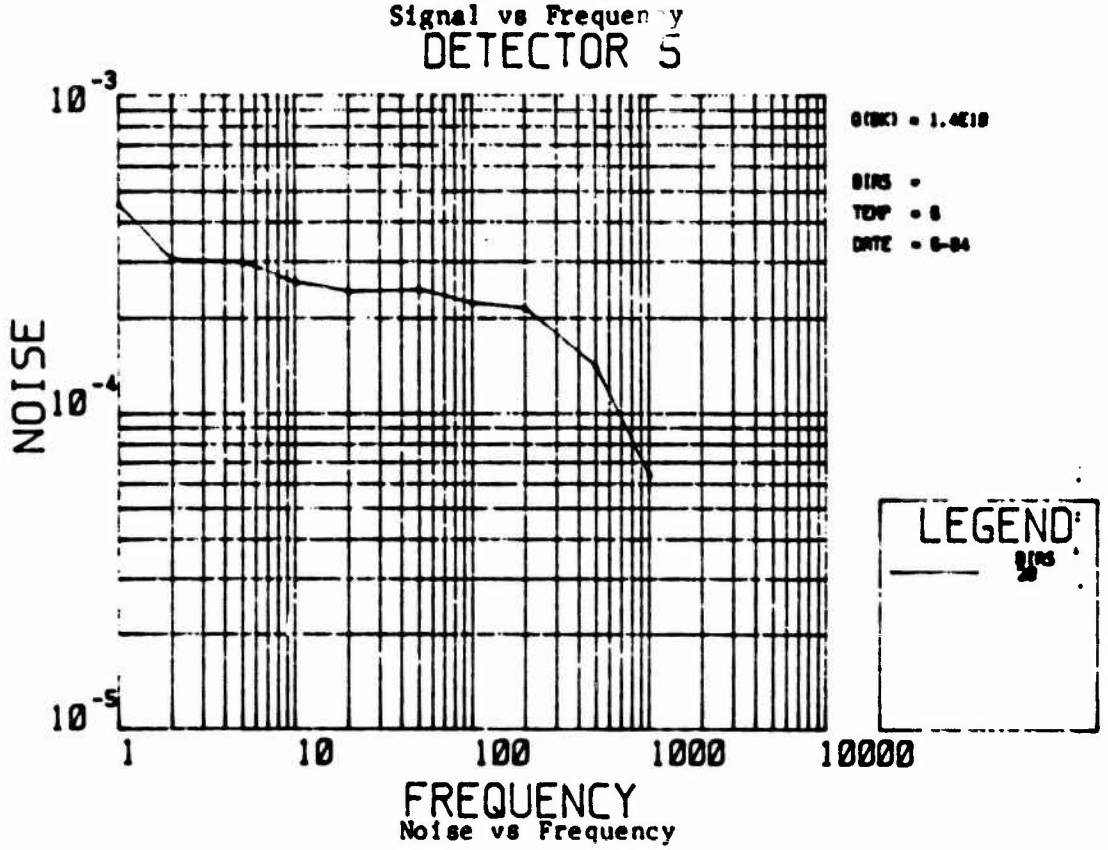

Figure 27-5. Detector 5

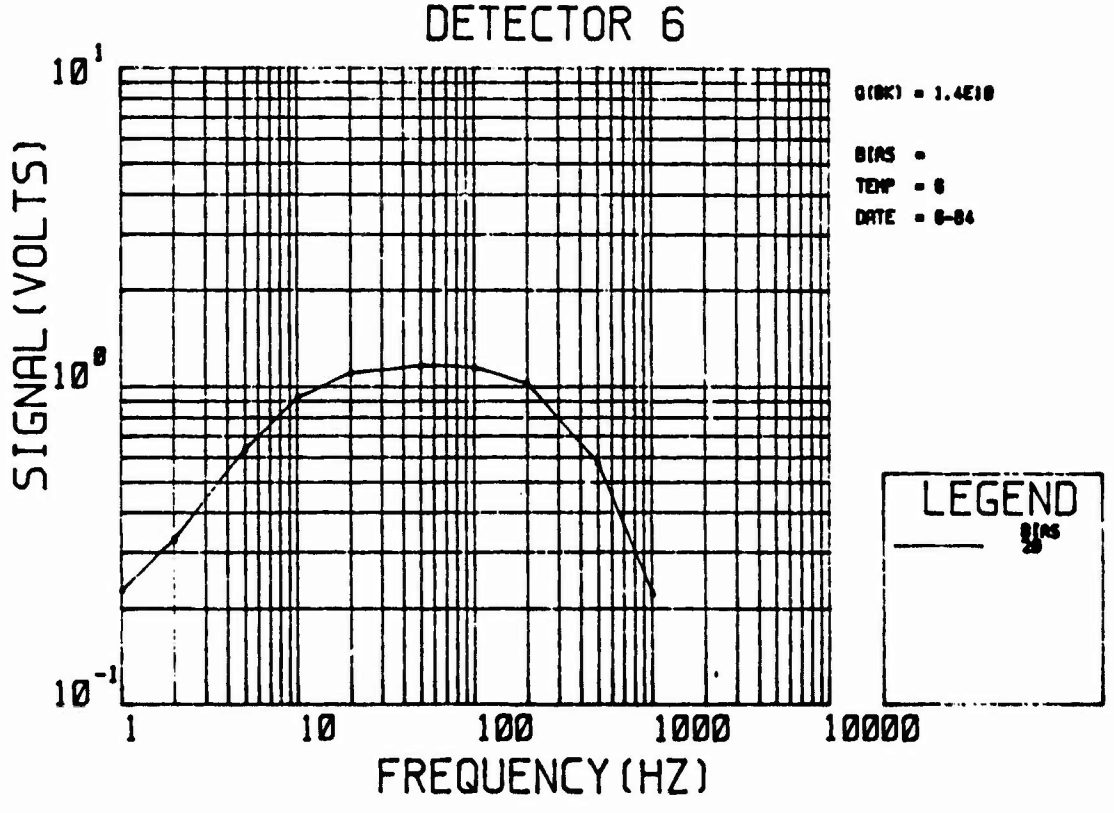

Signal vs Frequency

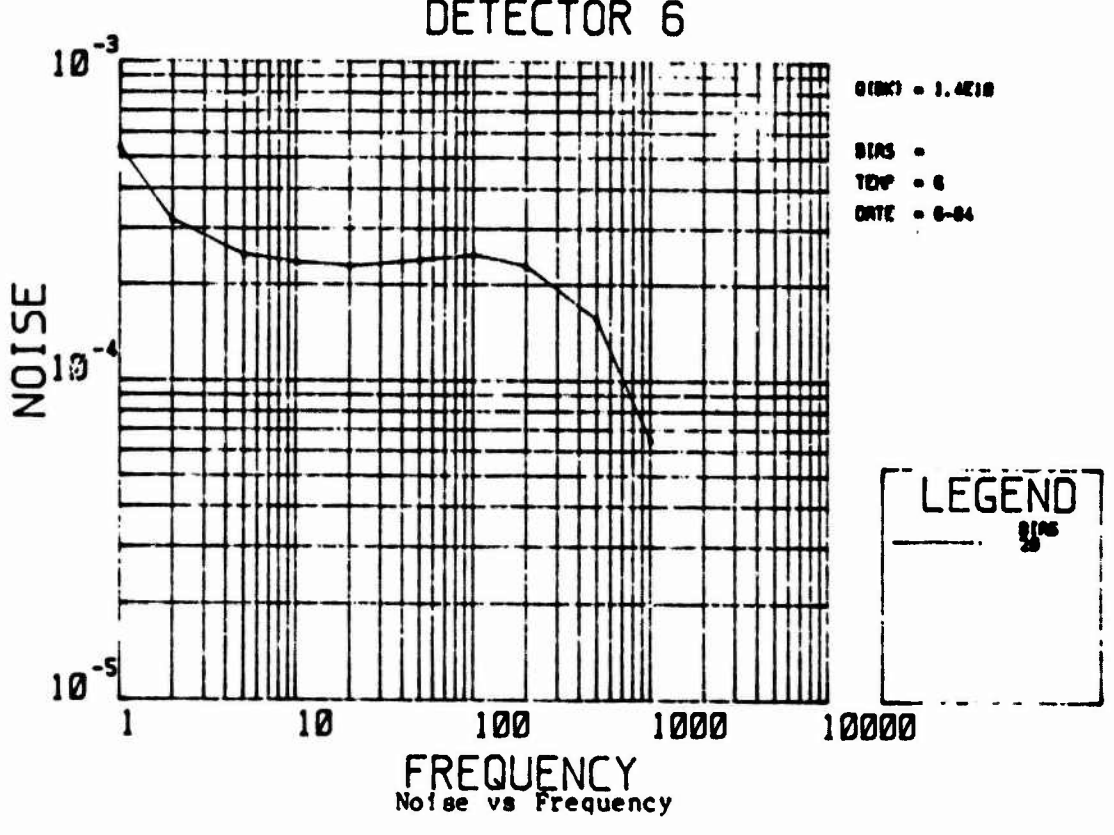

Noise vs Frequency

Figure 27-6. Detector 6

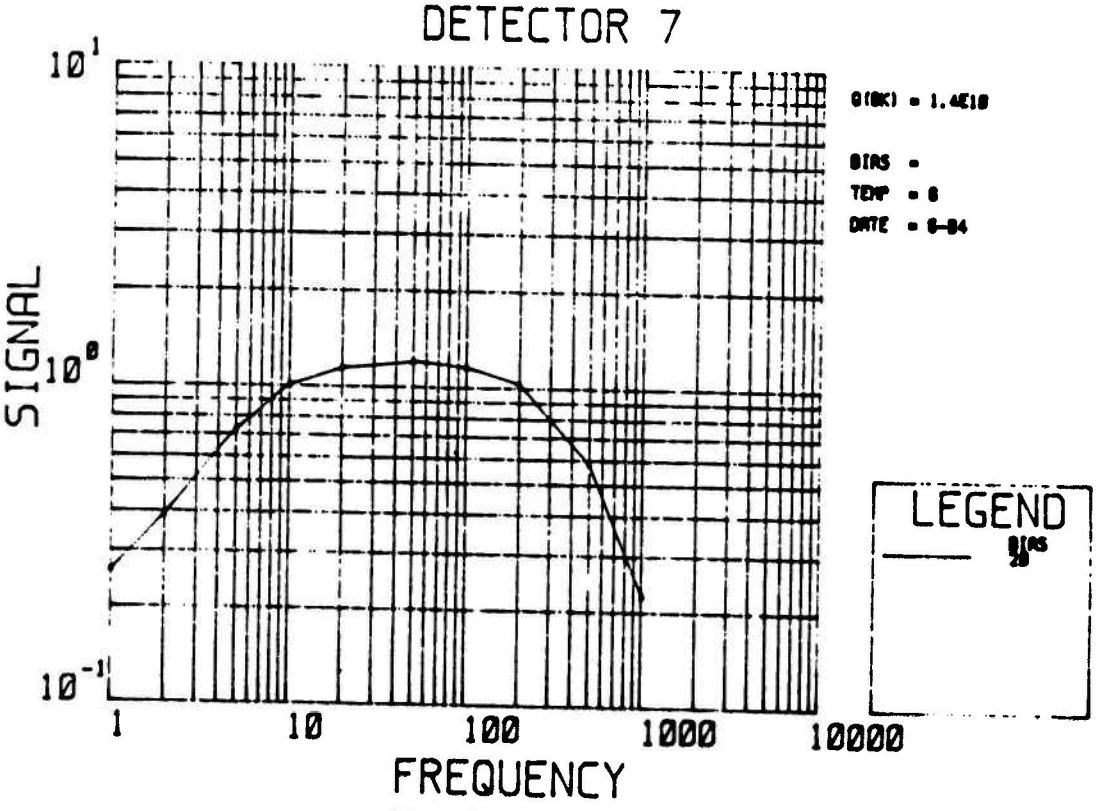

Signal vs Frequency

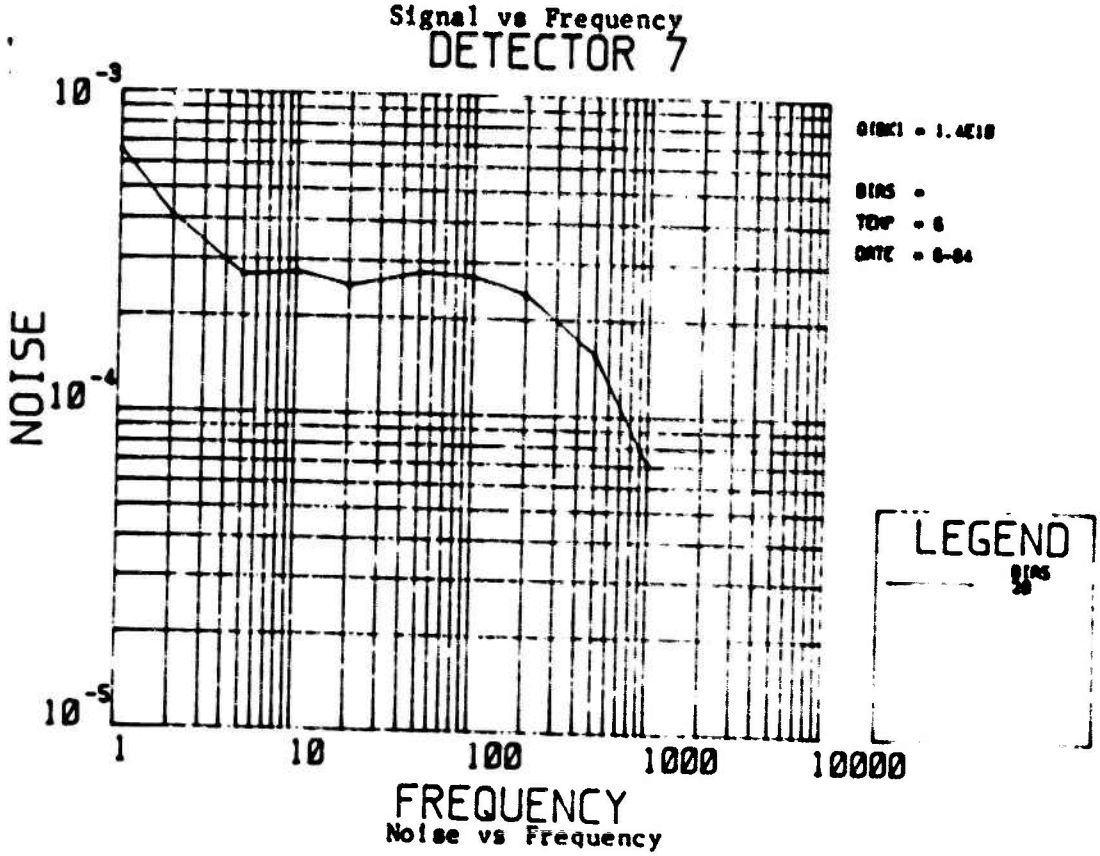

Noise vs Frequency

Figure 27-7. Detector 7

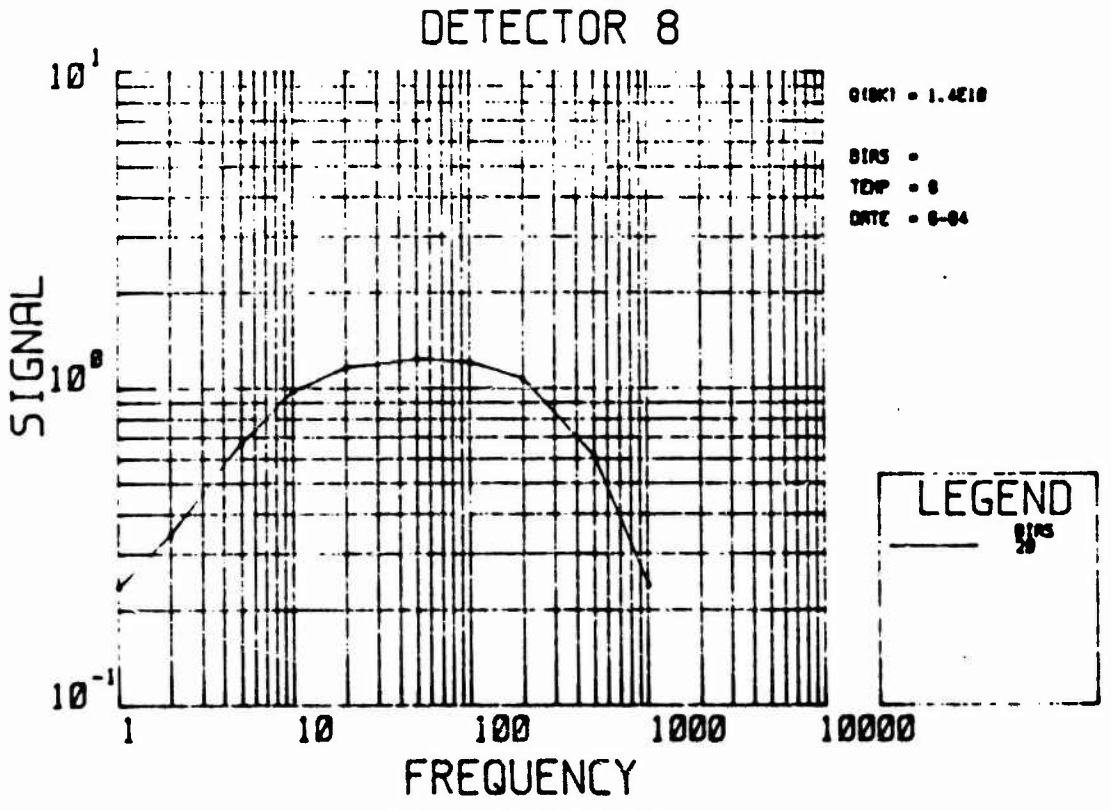

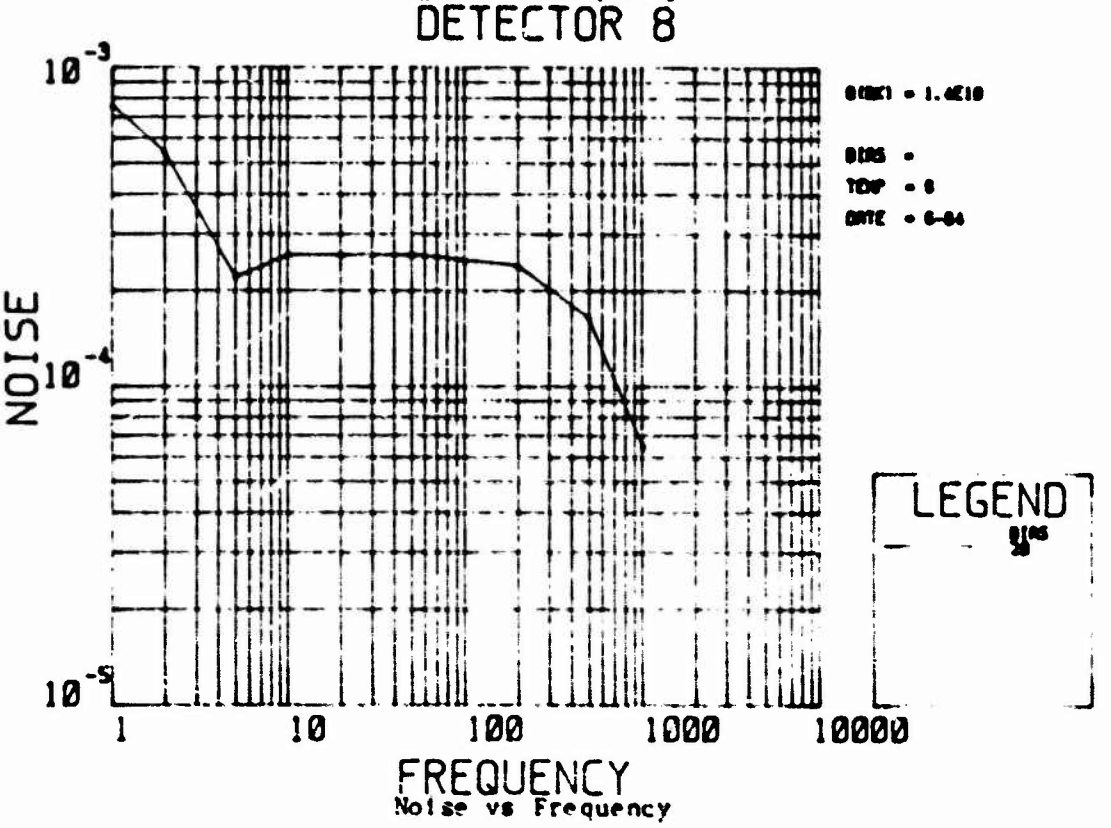

Figure 27-8. Detector 8

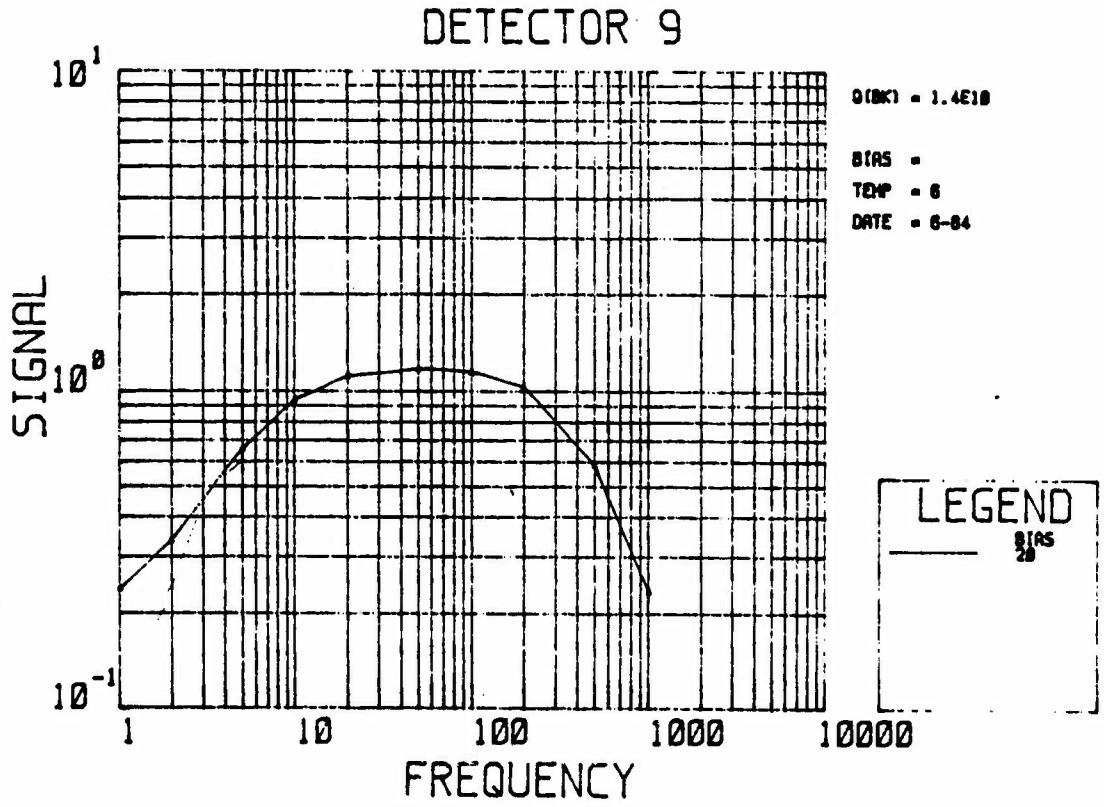

Signal vs Frequency

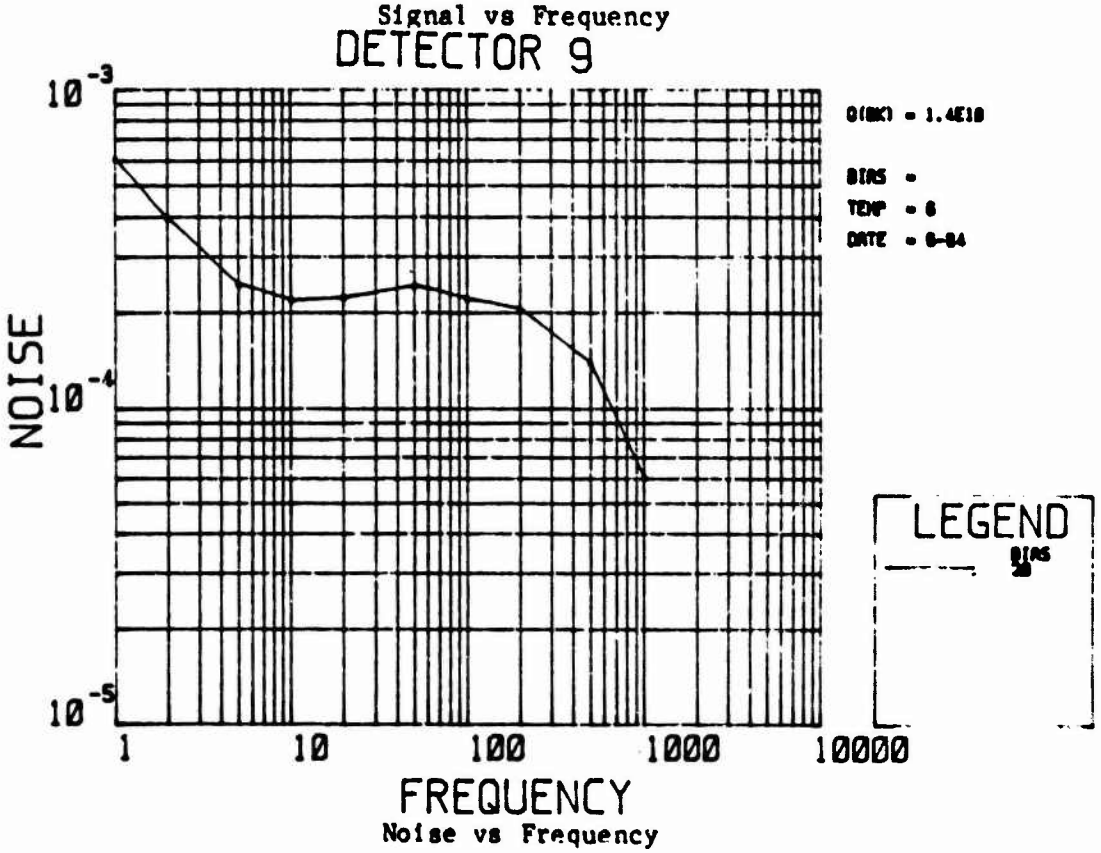

Noise vs Frequency

Figure 27-9. Detector 9

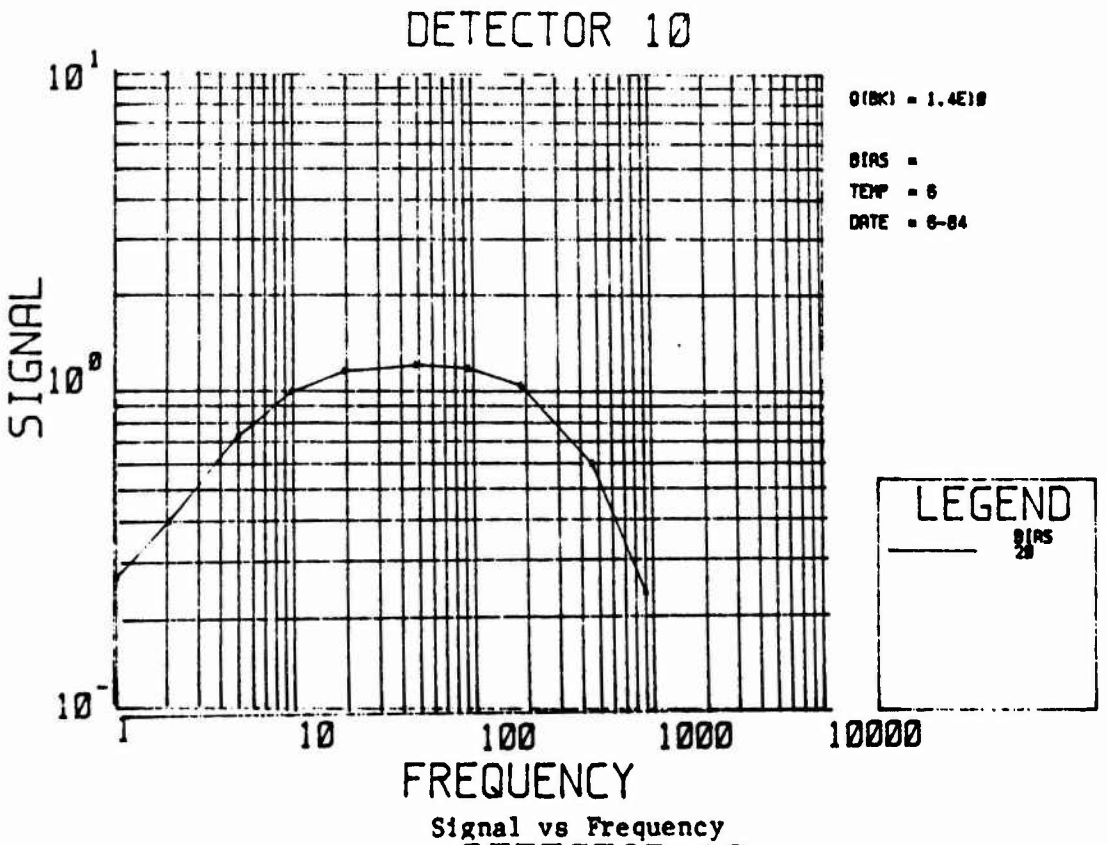

Signal vs Frequency

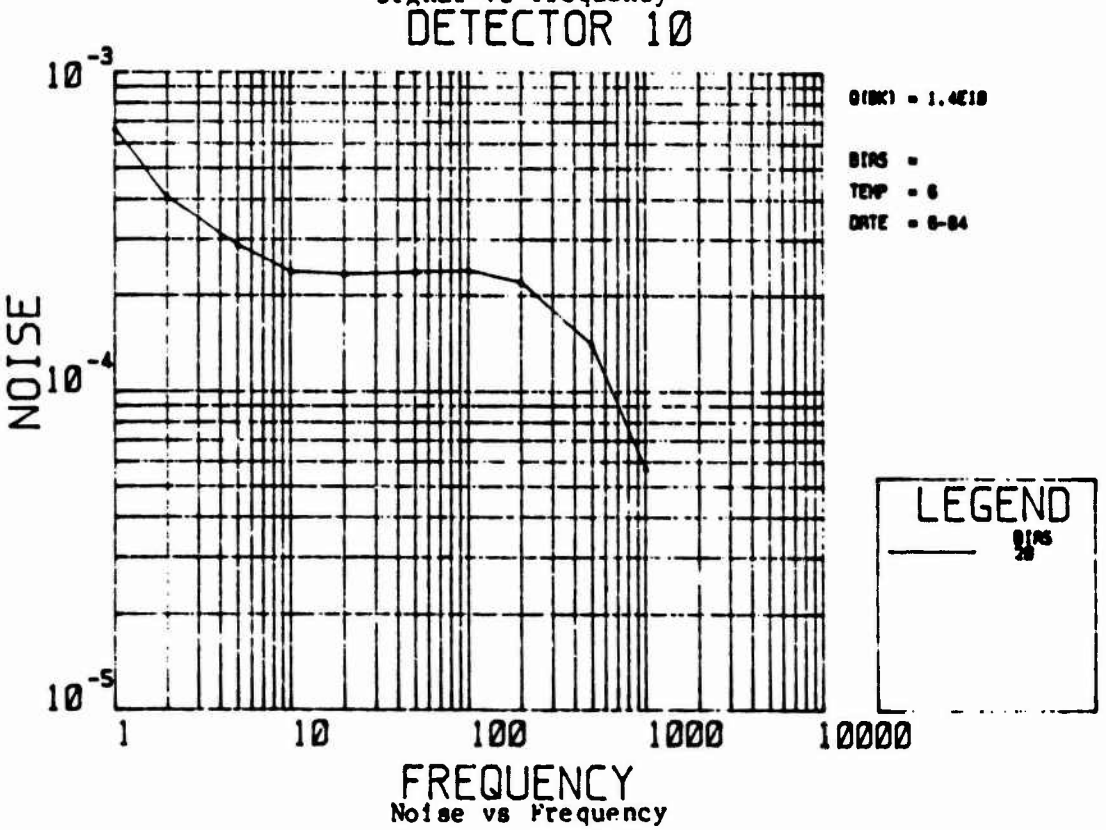

Noise vs Frequency

Figure 27-10. Detector 10

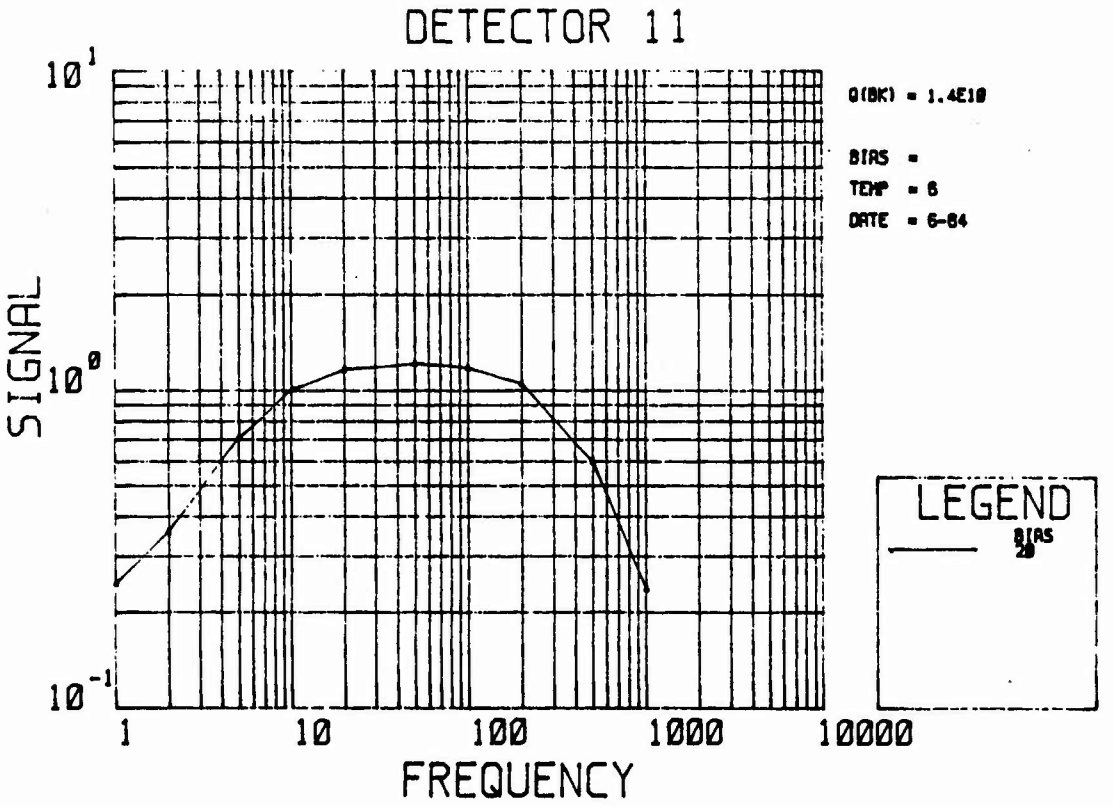

Signal vs Frequency

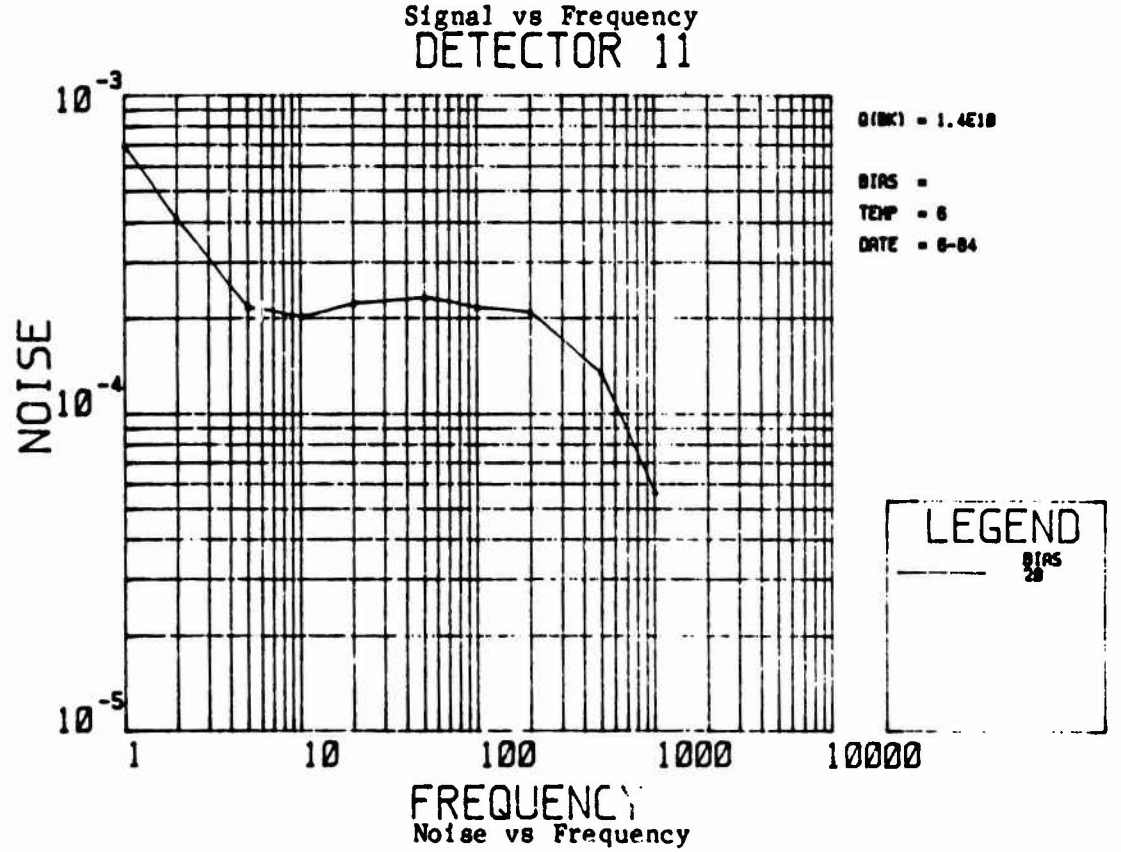

Noise vs Frequency

Figure 27-11. Detector 11

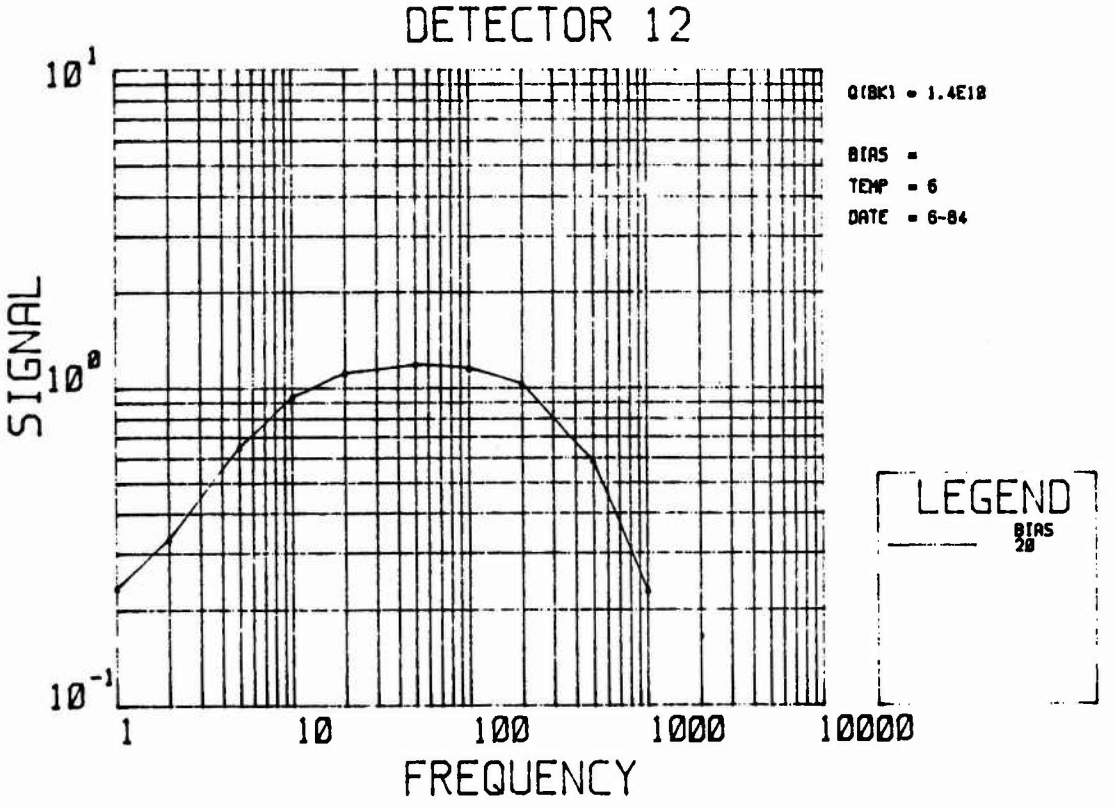

Signal vs Frequency

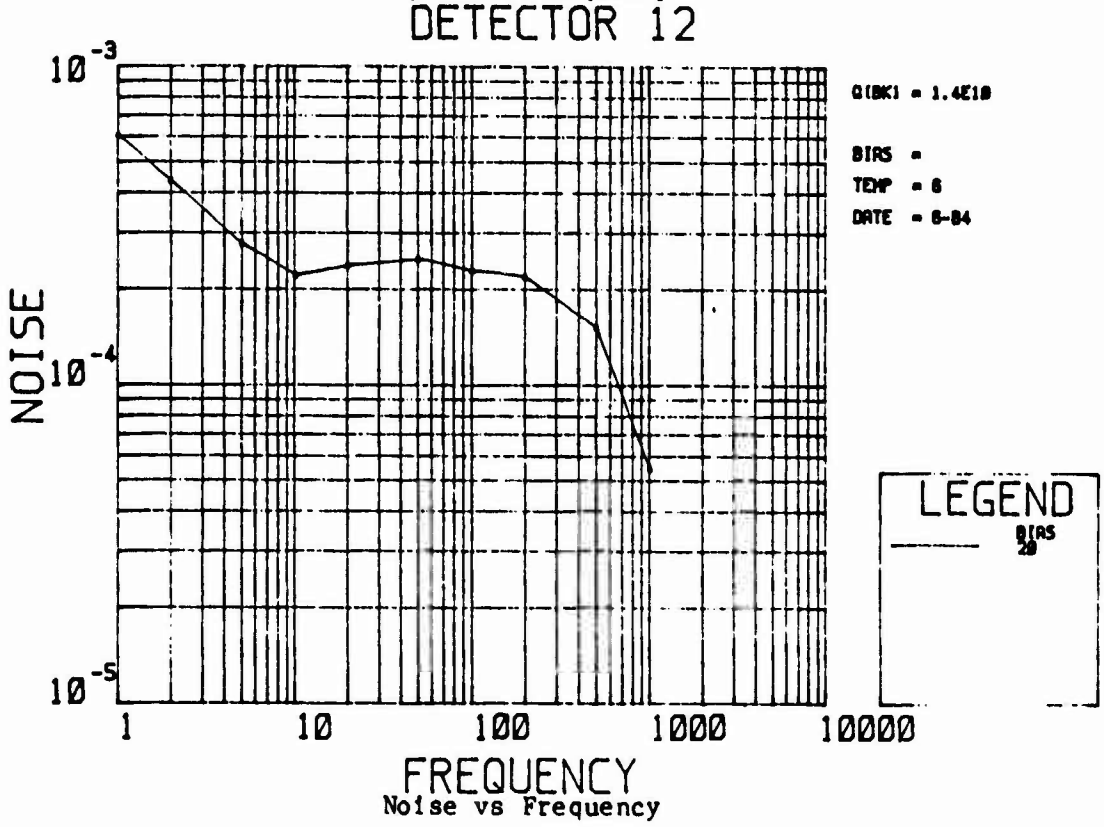

Noise vs Frequency

Figure 27-12. Detector 12

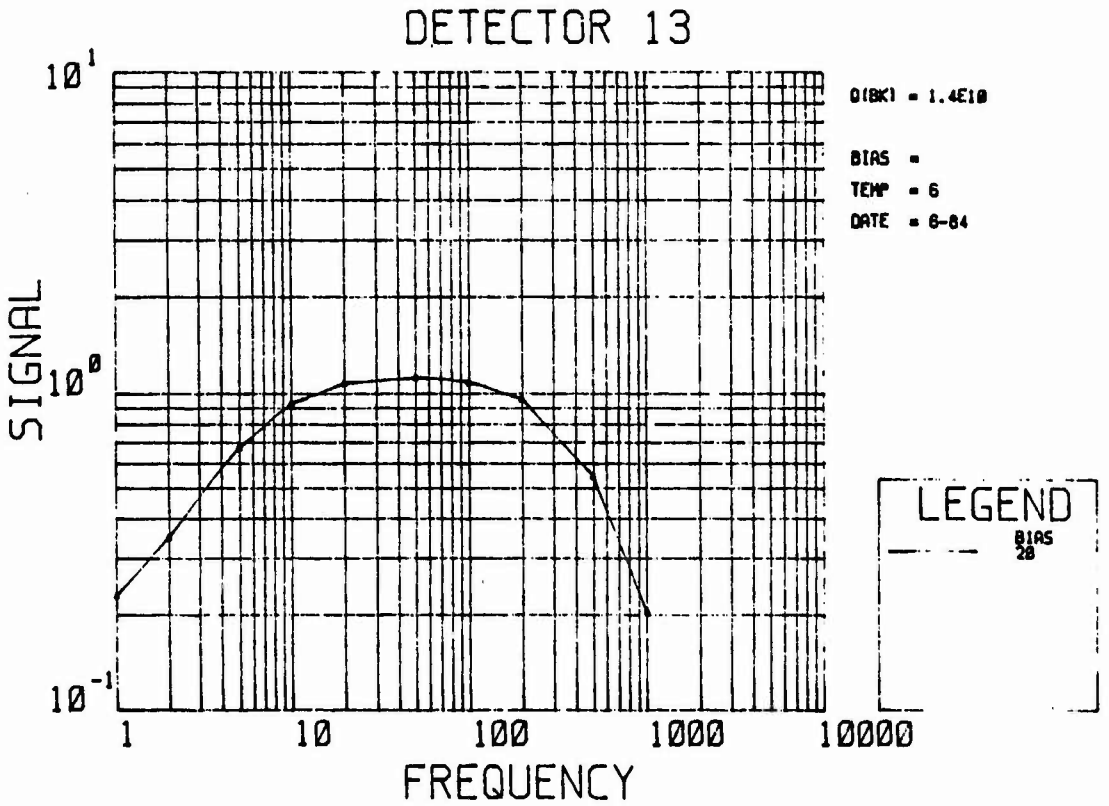

Signal vs Frequency

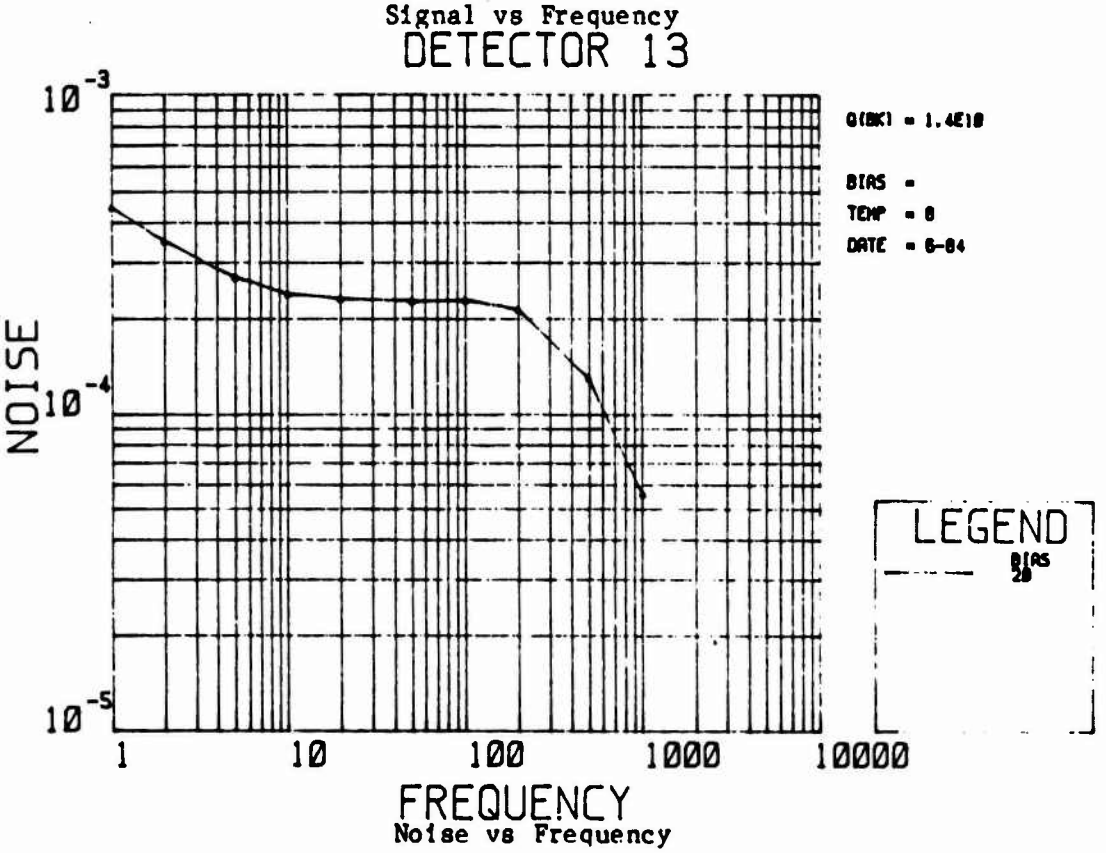

Noise vs Frequency

Figure 27-13. Detector 13

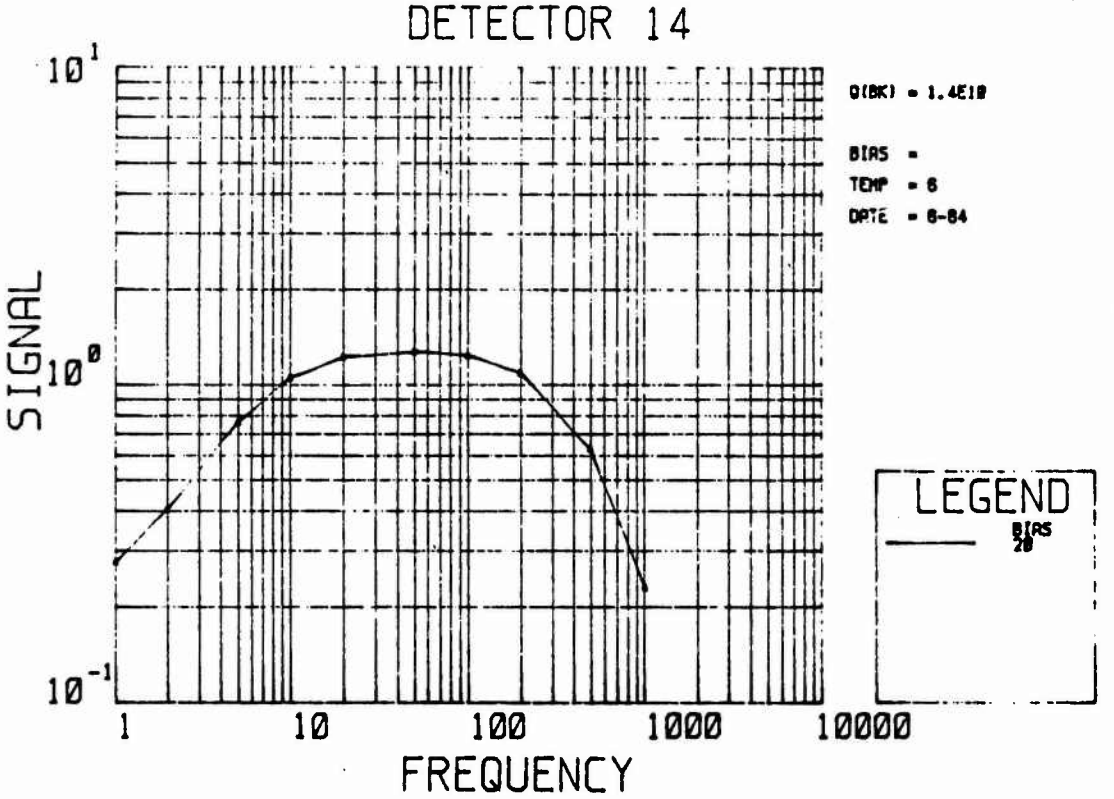

Signal vs Frequency

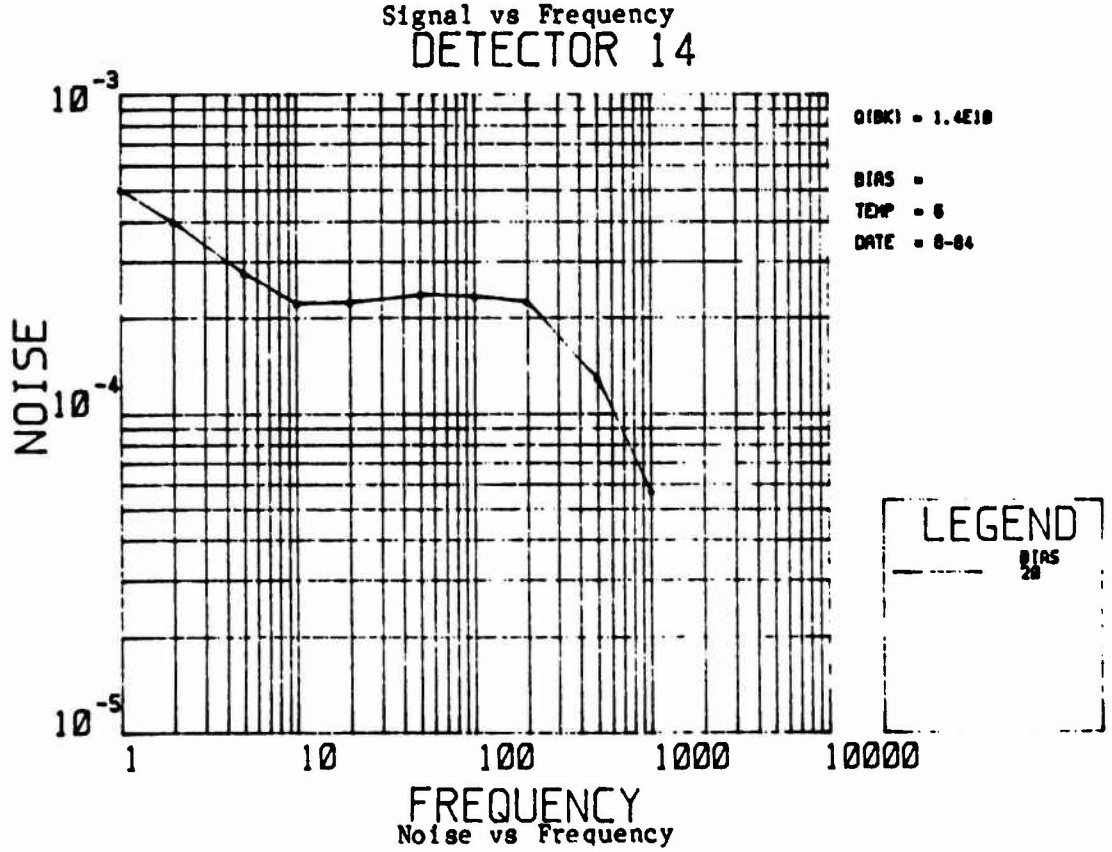

Noise vs Frequency

Figure 27-14. Detector 14

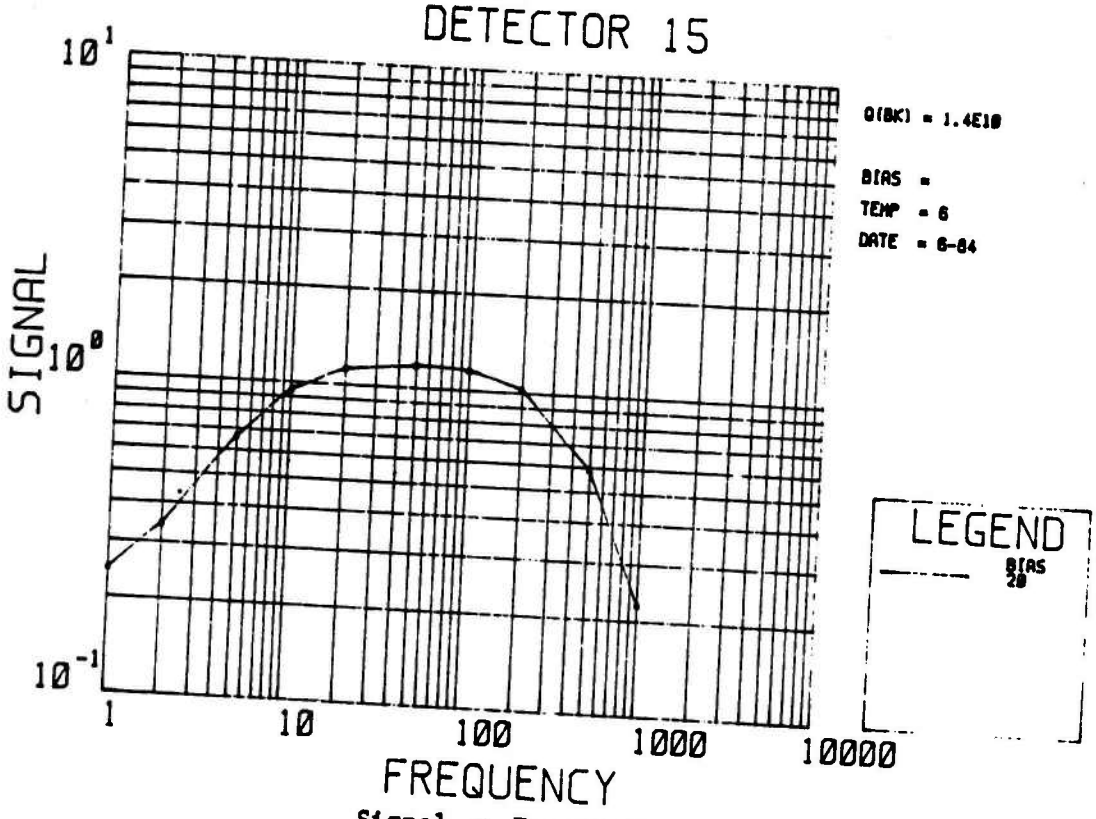

Signal vs Frequency

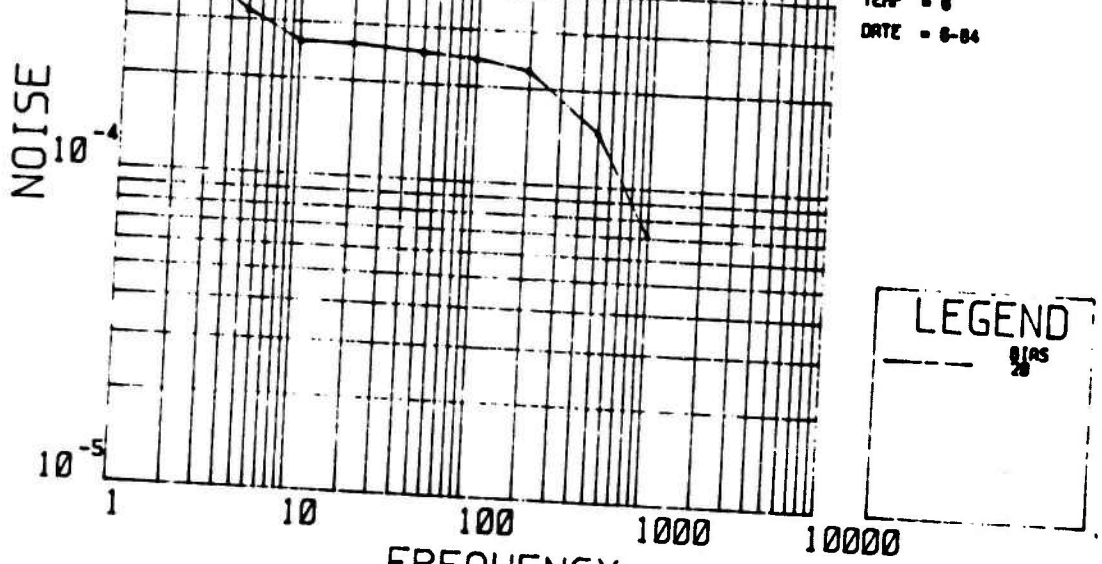

Noise vs Frequency

Figure 27-15. Detector 15

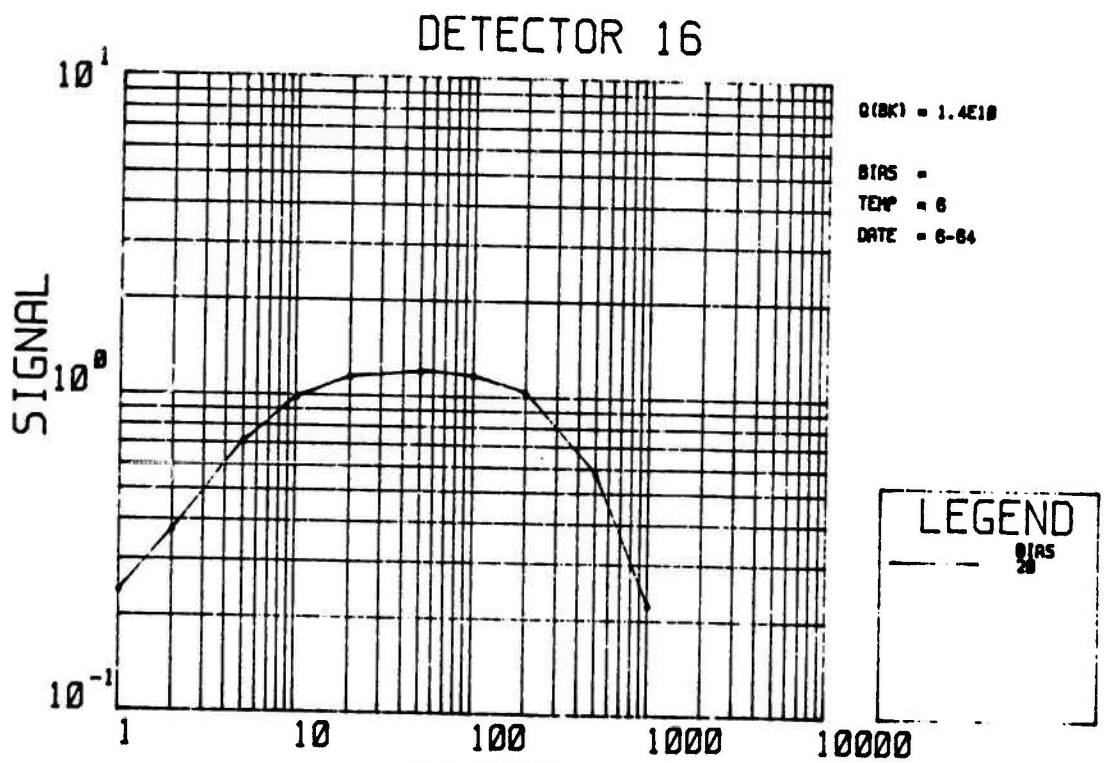

Signal vs Frequency

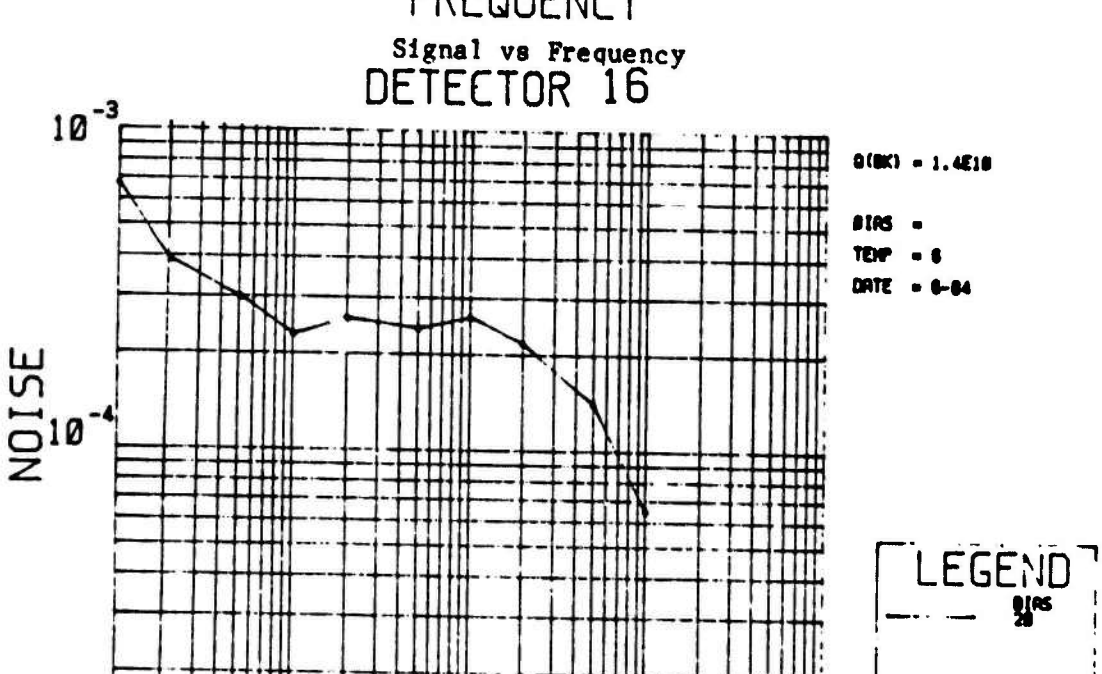

Noise vs Frequency

Figure 27-16. Detector 16

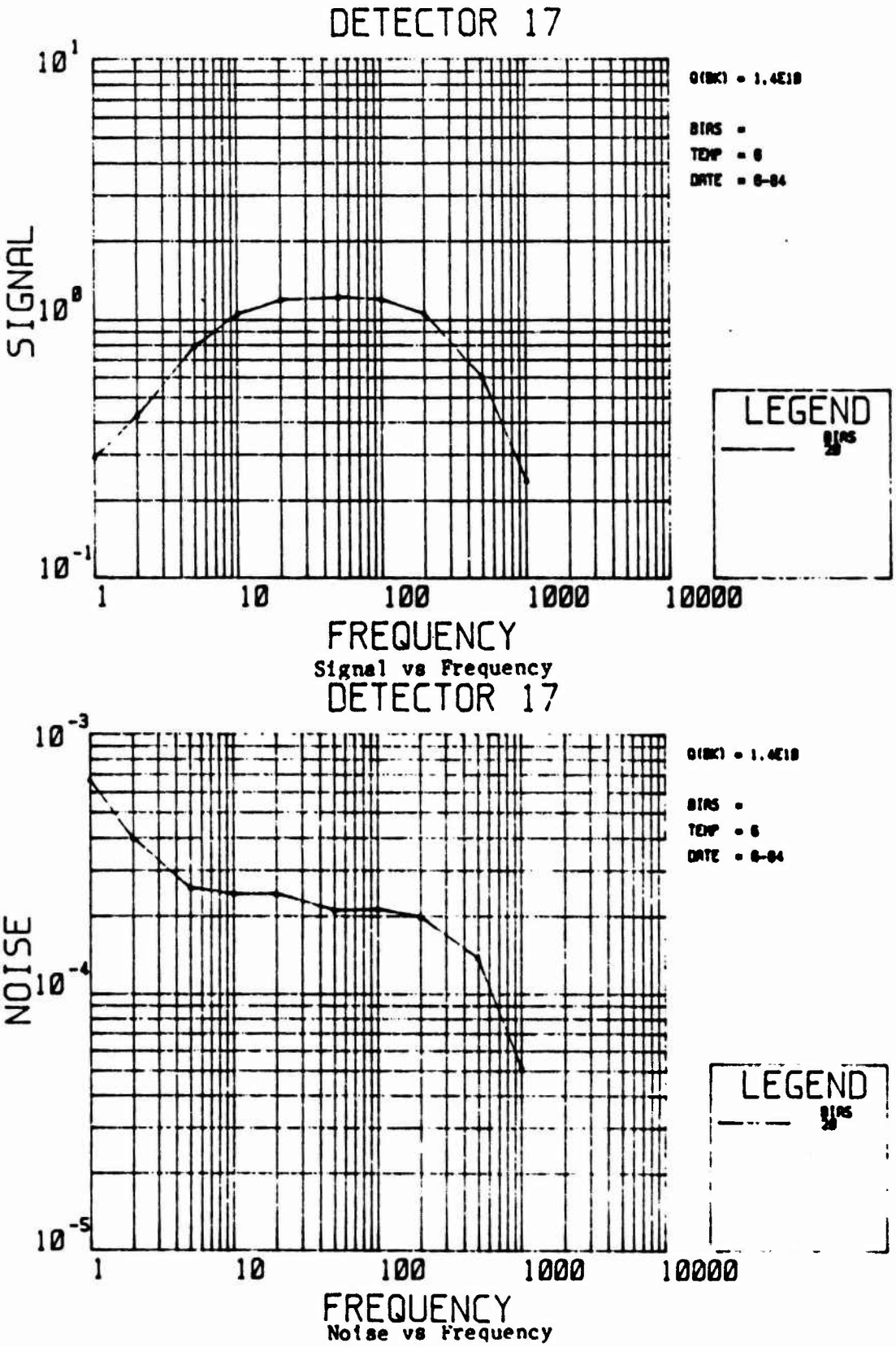

Figure 27-17. Detector 17

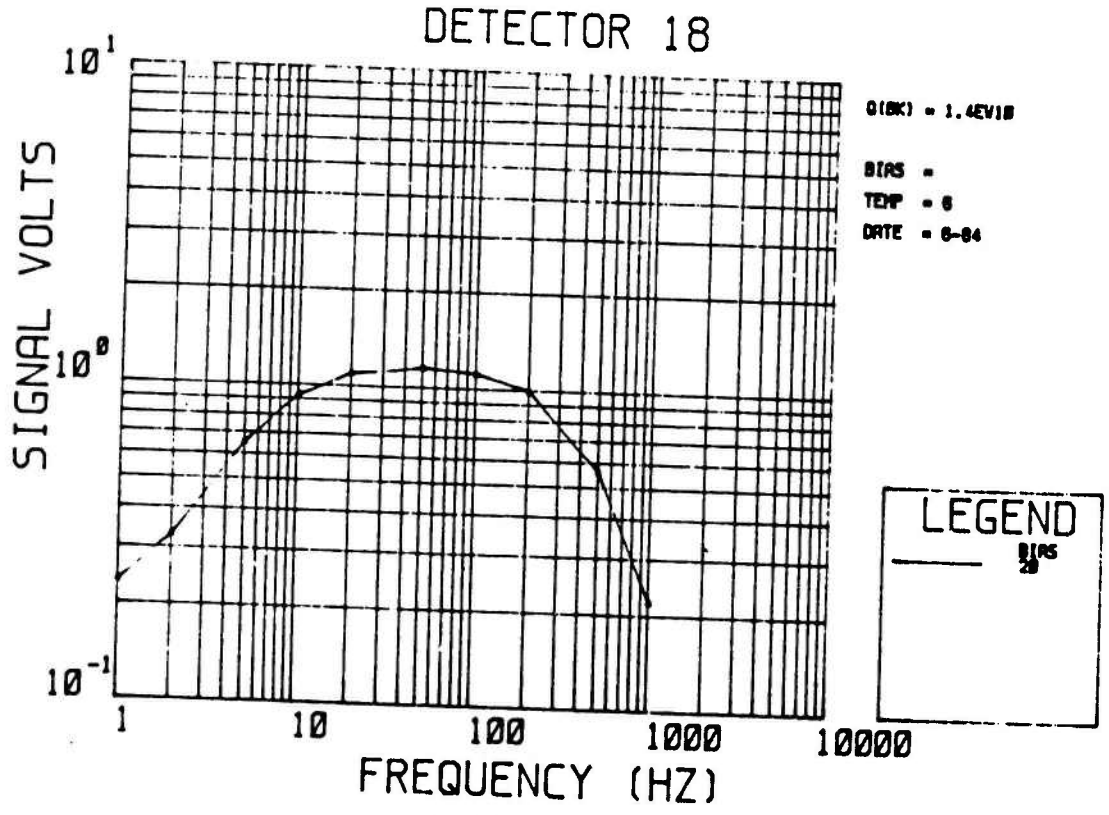

Signal vs Frequency

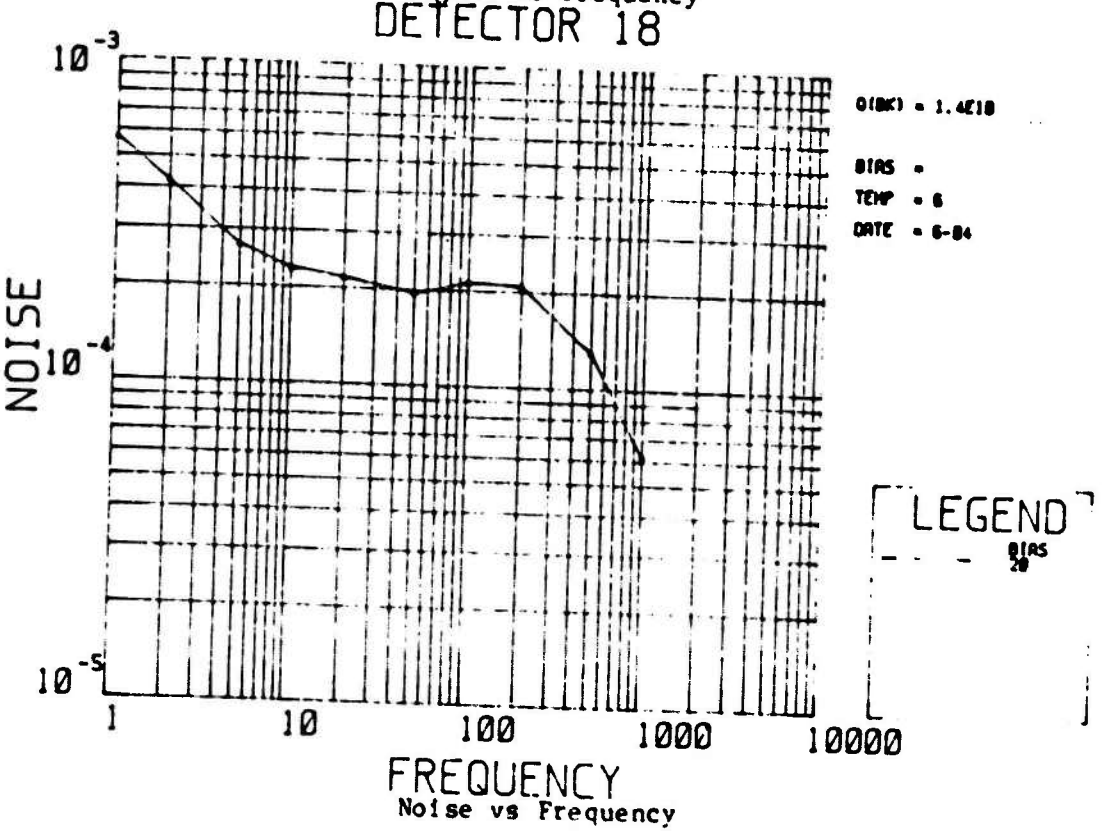

Noise vs Frequency

Figure 27-18. Detector 18

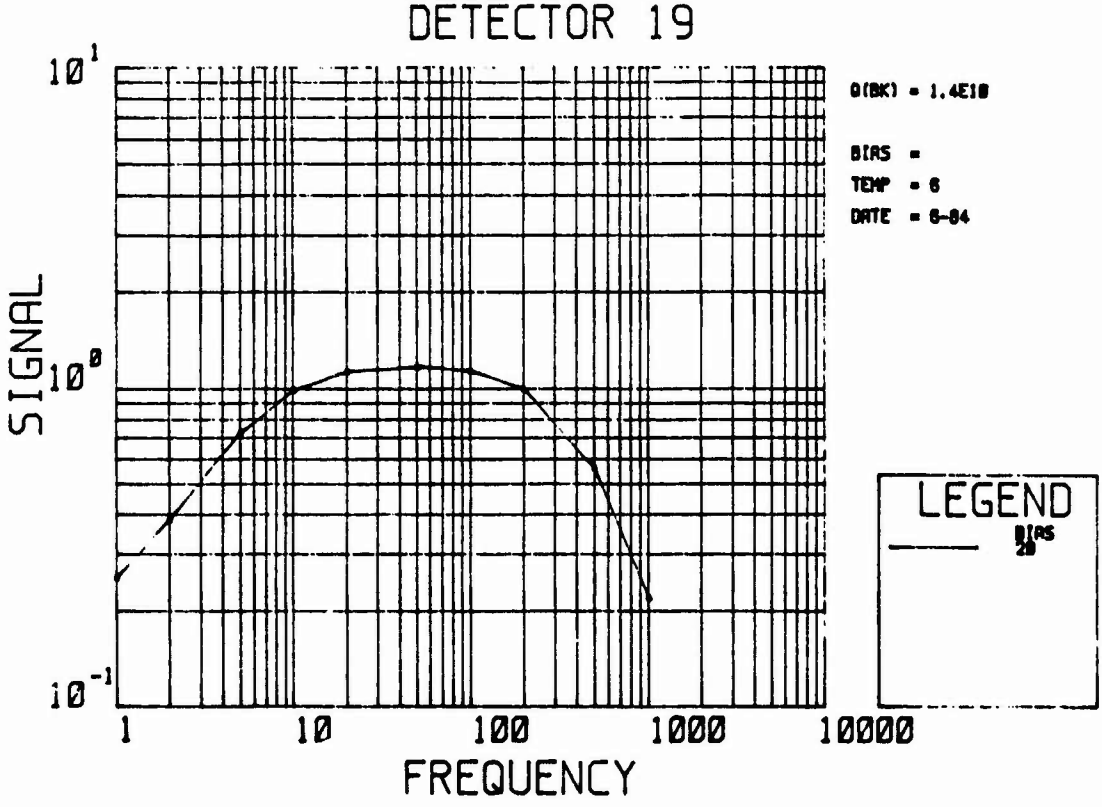

Signal vs Frequency

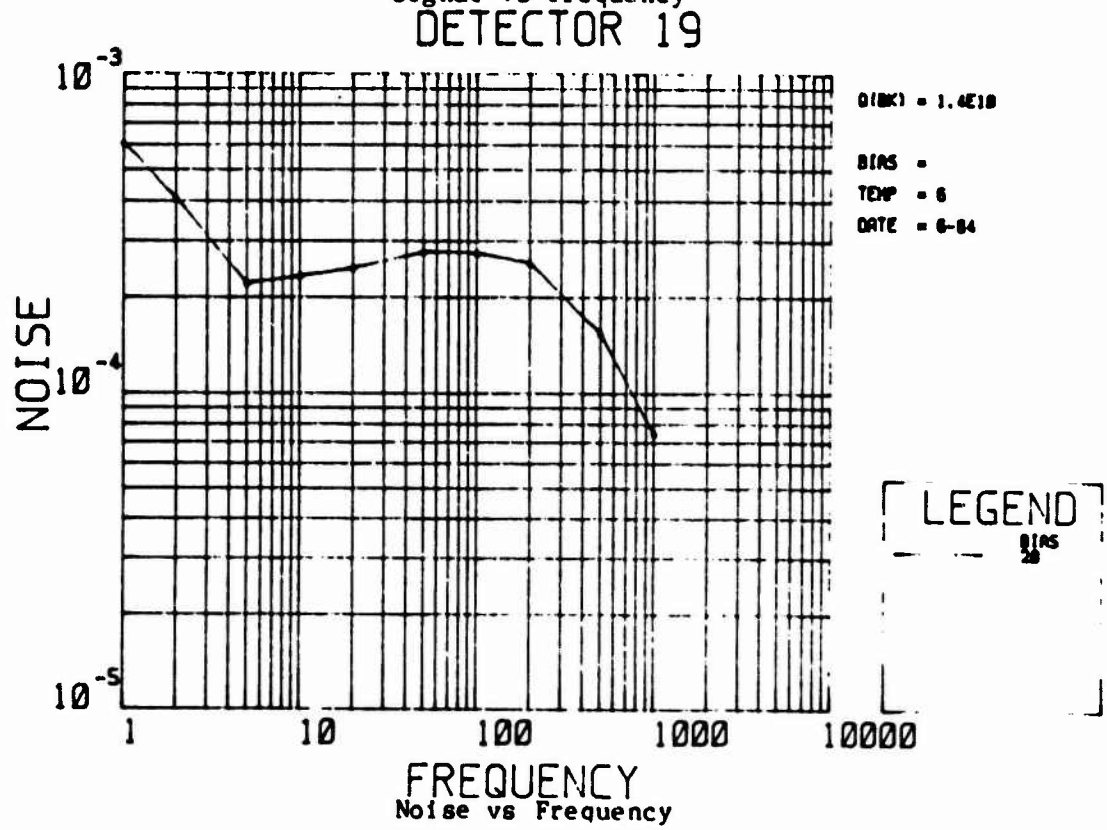

Noise vs Frequency

Figure 27-19. Detector 19

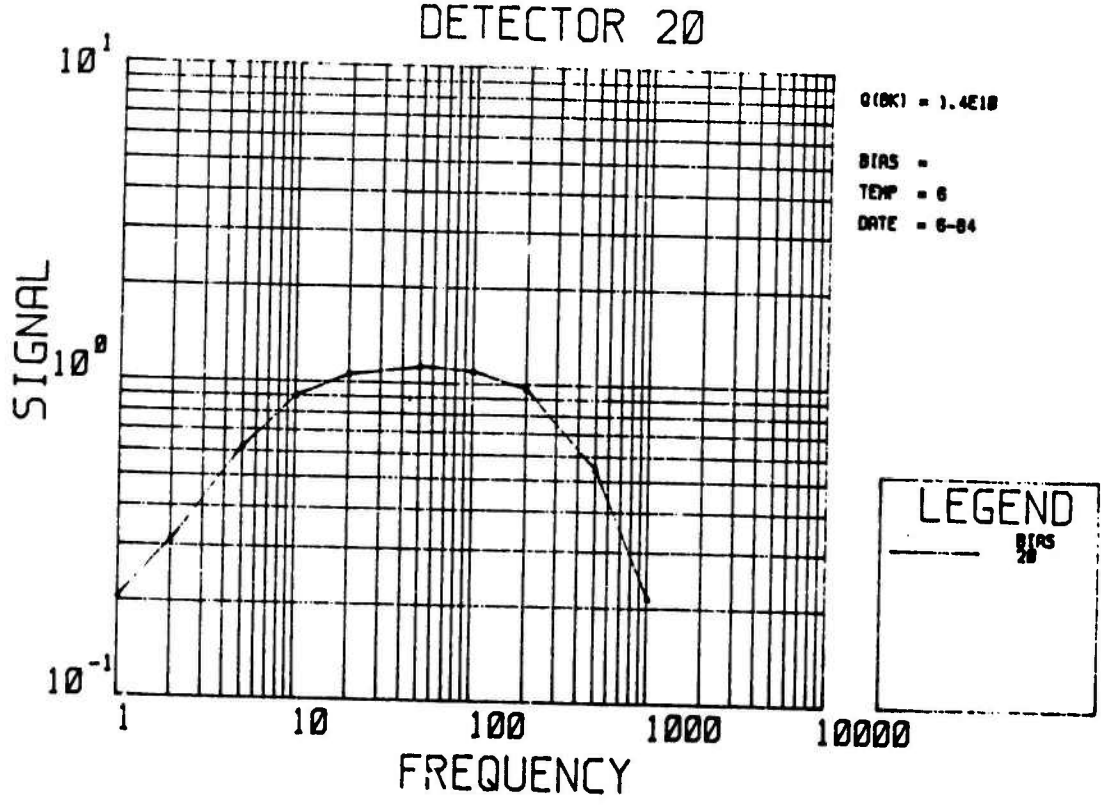

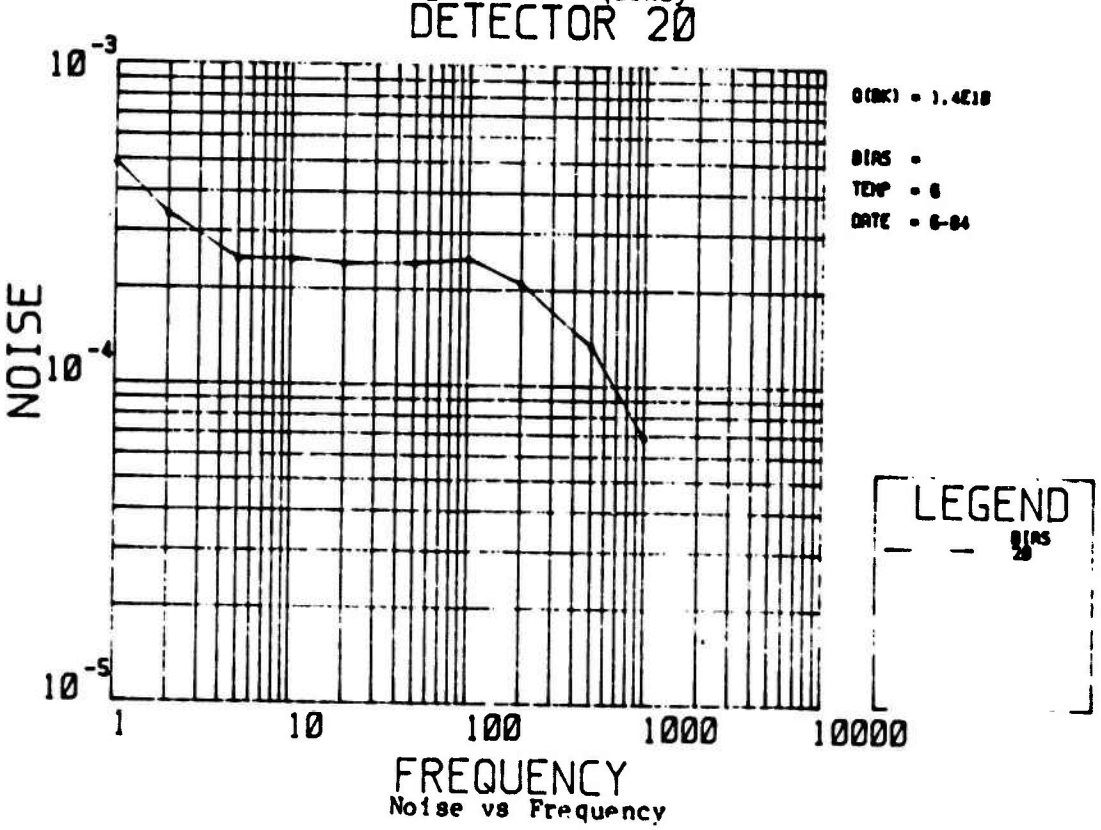

Figure 27-20. Detector 20

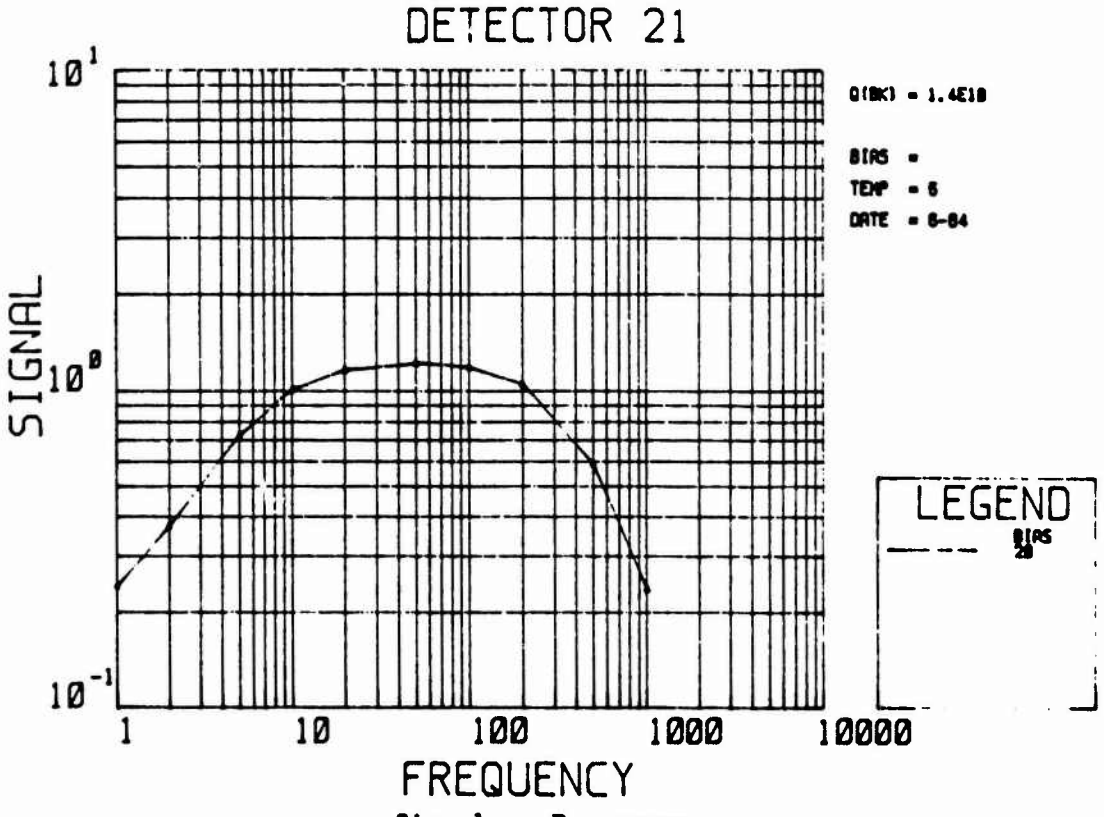

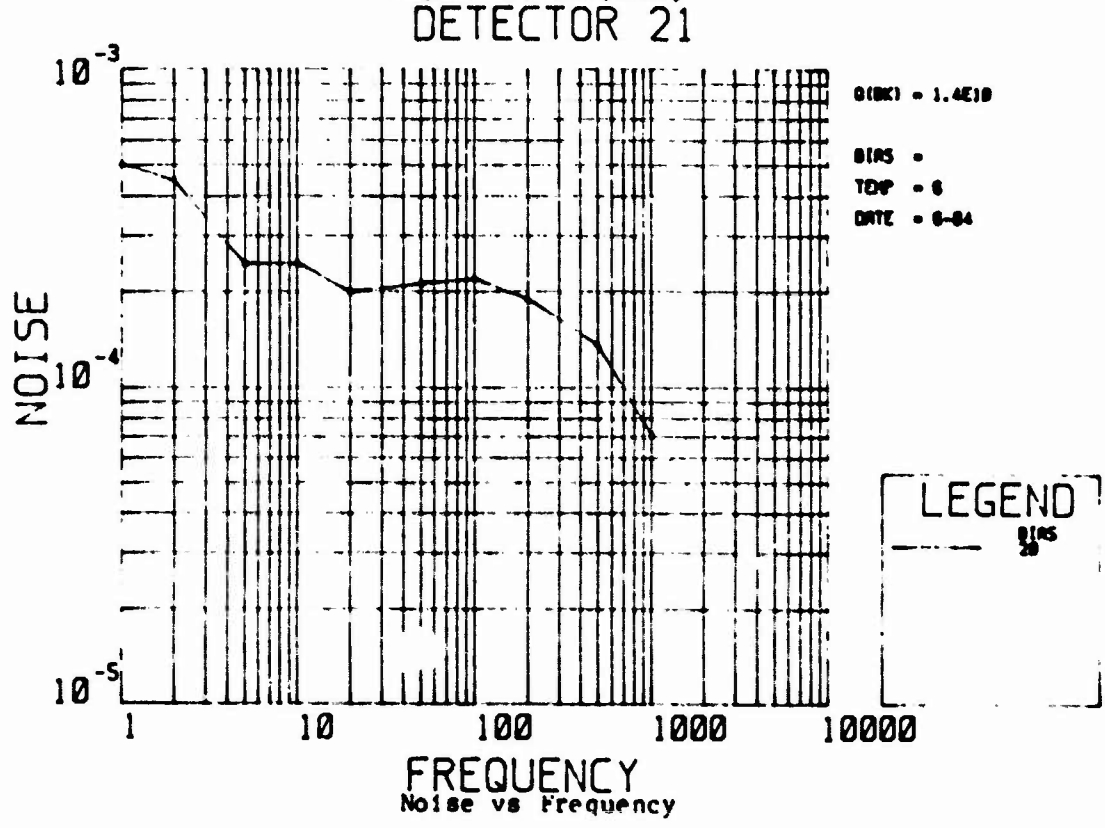

Figure 27-21. Detector 21

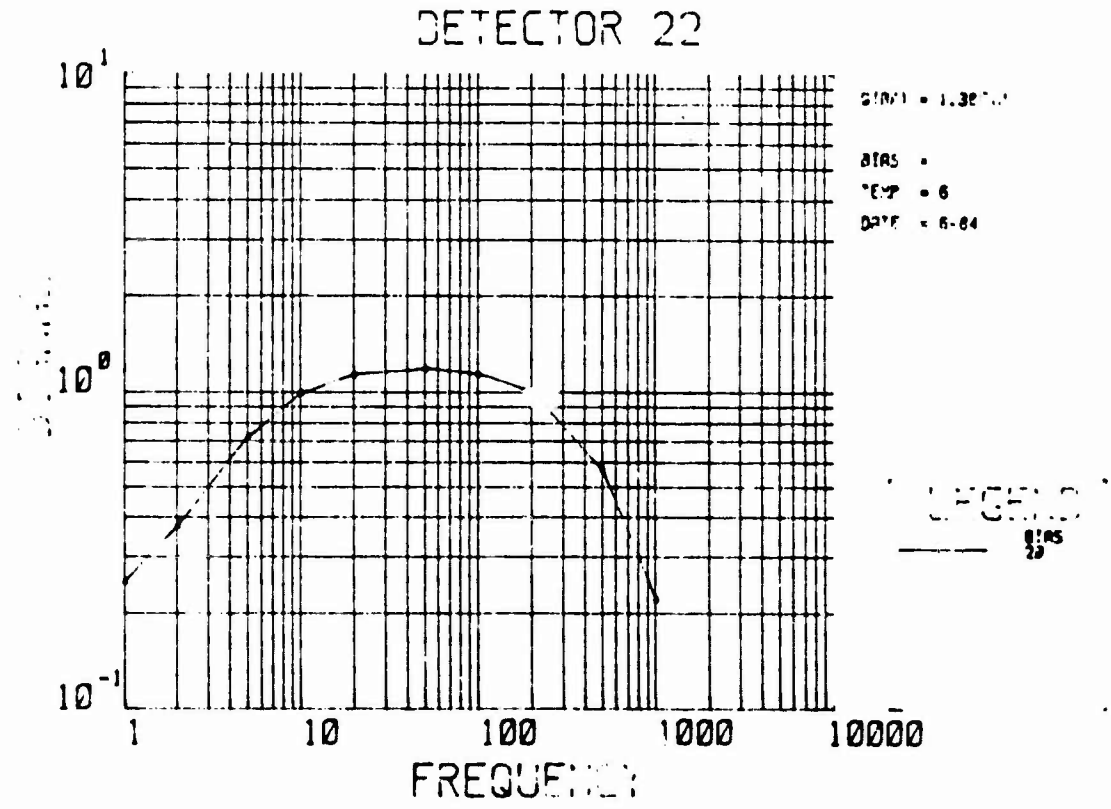

Signal vs Frequency

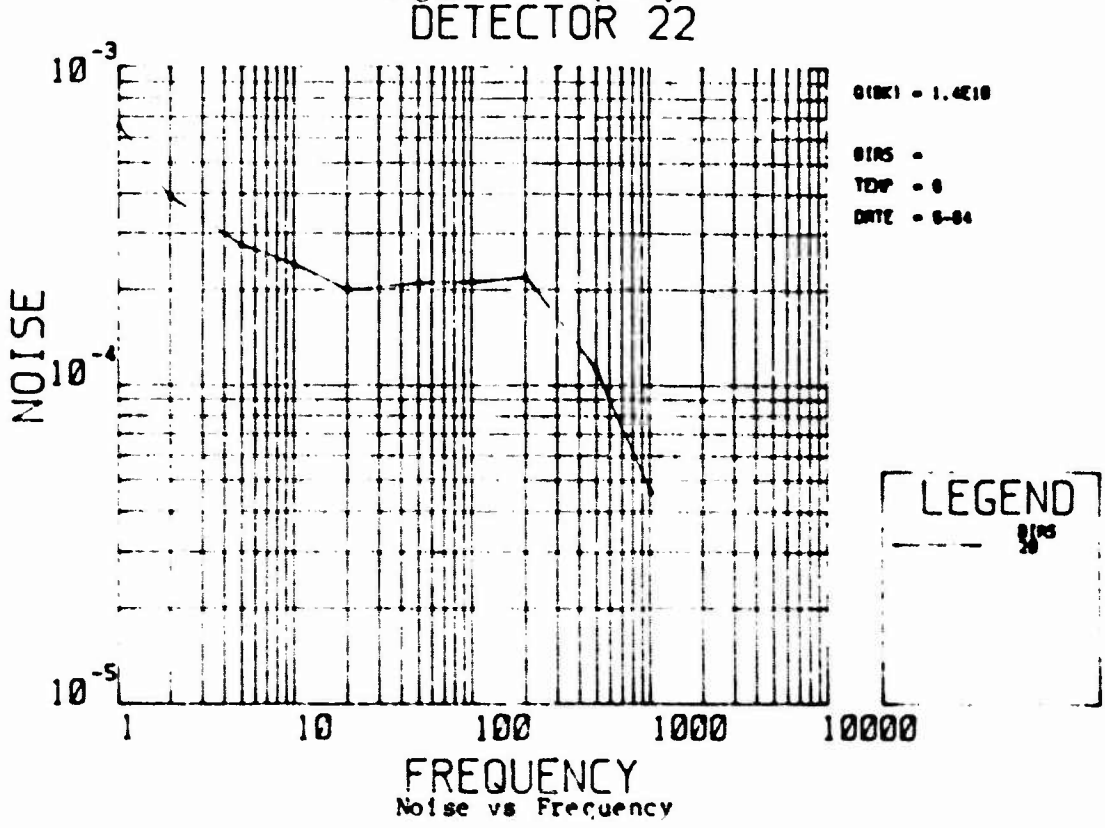

Noise vs Frequency

Figure 27-22. Detector 22

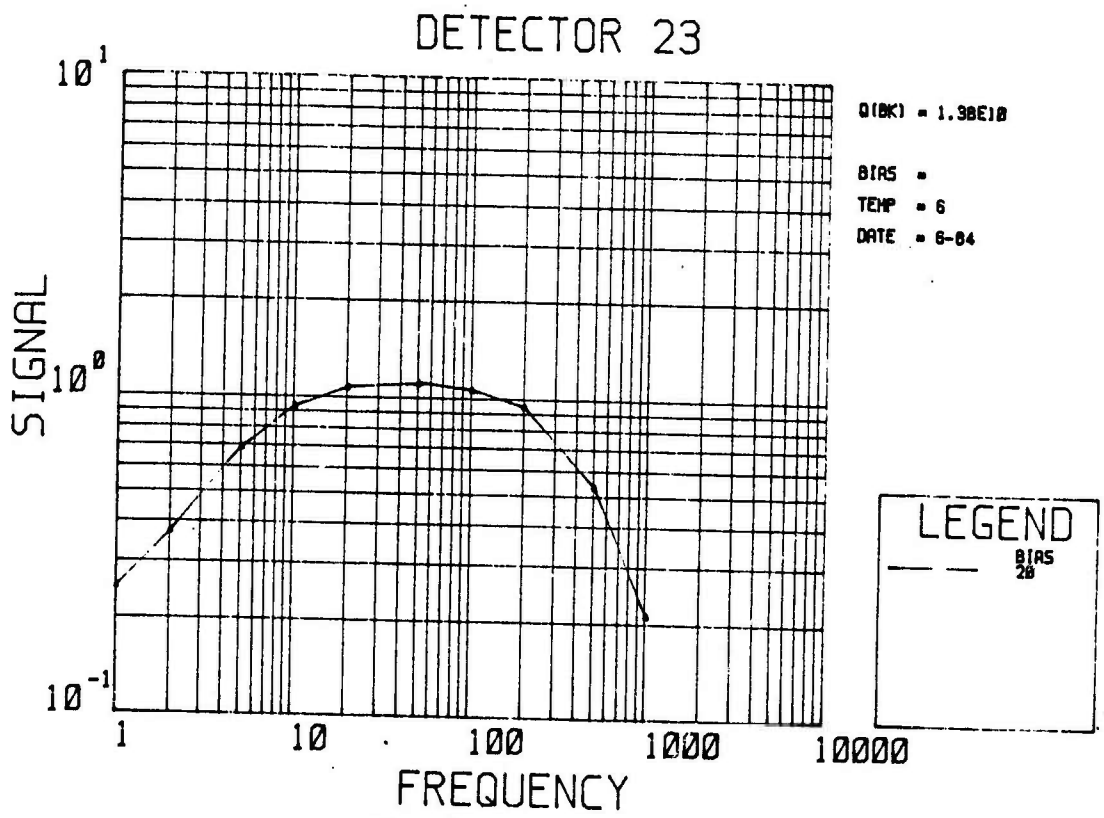

Signal vs Frequency

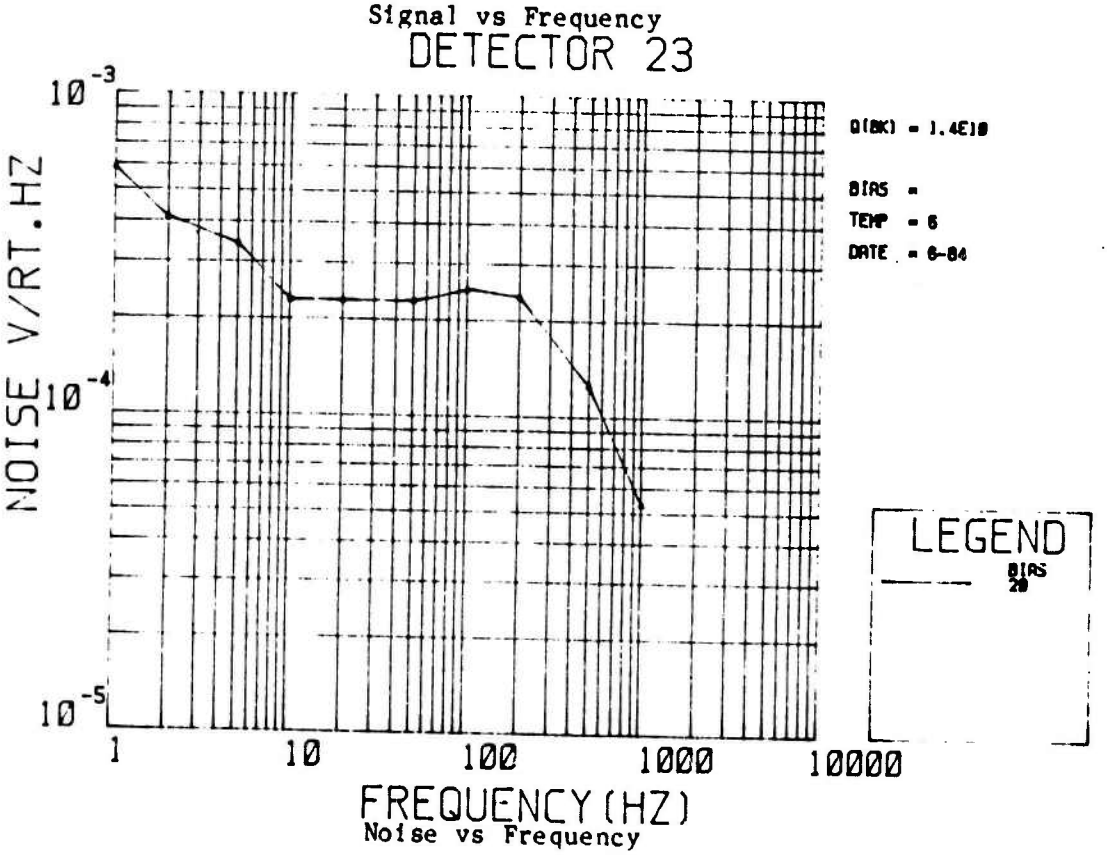

Noise vs Frequency

Figure 27-23. Detector 23

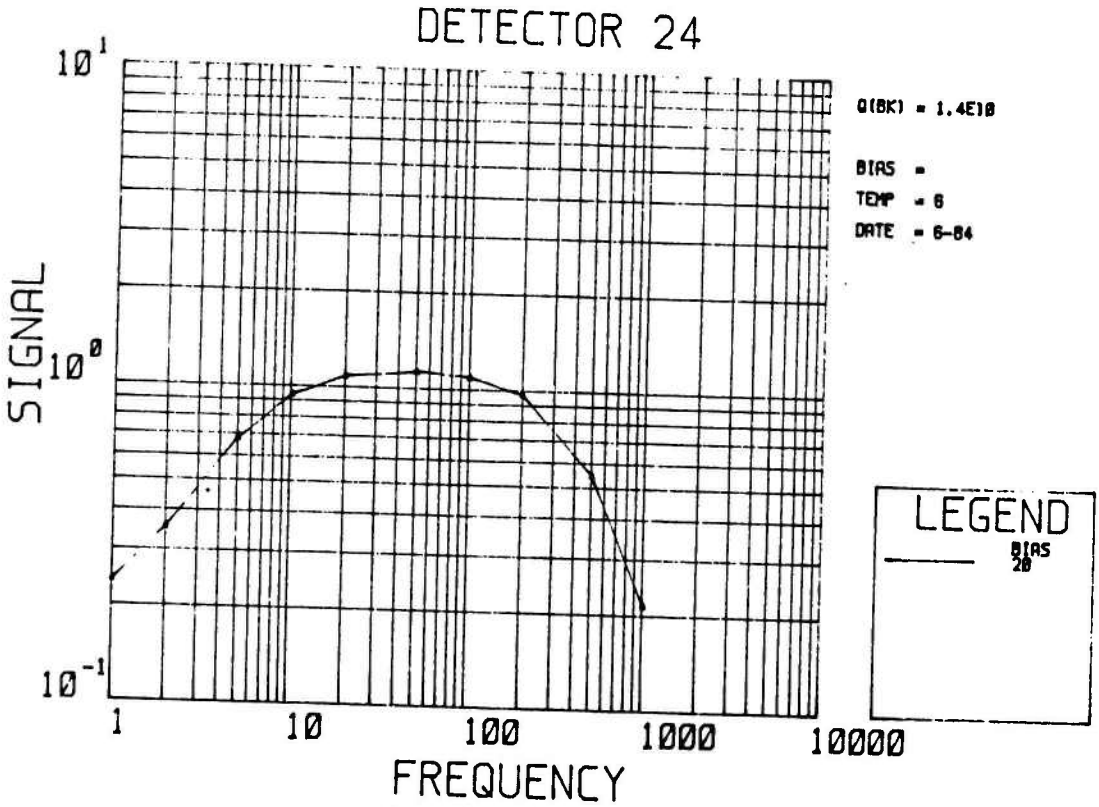

Signal vs Frequency

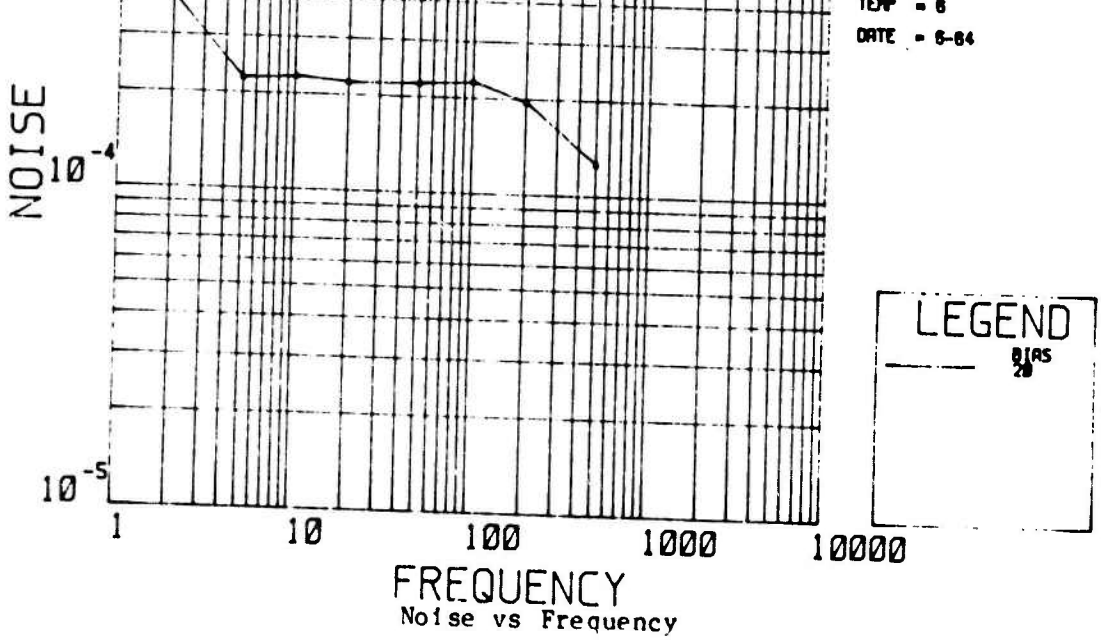

Noise vs Frequency

Figure 27-24. Detector 24

			Q_{BK} = 1.38 × 10^{10} ph/cm^2/sec H_{EFF} = 3.77 × 10^{10} w/cm^2 T = 6K BIAS = 20V F = 50 Hz AREA = 8.06 E-3 cm^2		
DET NO.	SIGNAL × 10^{-3} (VOLTS)	NOISE × 10^{-6} ($V/\sqrt{Hz}$)	SNR	RESP. (A/W)	NEP ($W/\sqrt{Hz}$) × 10^{-16}
1	1210	257	4710	2.30	6.45
2	1145	254	4510	2.15	6.74
3	1160	250	4640	2.18	6.55
4	1100	200	5500	2.07	5.52
5	1165	247	4720	2.19	6.44
6	1170	240	4880	2.20	6.23
7	1200	278	4320	2.26	7.04
8	1240	260	4770	2.33	6.37
9	1180	247	4780	2.22	6.36
10	1210	238	5080	2.28	5.98
11	1220	234	5210	2.29	5.83
12	1190	250	4760	2.24	6.38
13	1120	227	4930	2.11	6.16
14	1265	236	5360	2.38	5.67
15	1175	250	4700	2.21	6.47
16	1200	241	4980	2.26	6.10
17	1220	211	5780	2.29	5.26
18	1150	194	5930	2.16	5.13
19	1170	210	5570	2.20	5.45
20	1125	241	4669	2.12	6.51
21	1220	213	5730	2.29	5.31
22	1180	210	5619	2.22	5.41
23	1110	229	4847	2.09	6.27
24	1130	220	5136	2.13	5.92

Figure 27-25. Tabulation of Baseline Measurements

3.6.5 Signal and Noise vs Temp

Plots of signal and noise vs temperature are shown in Figure 28.

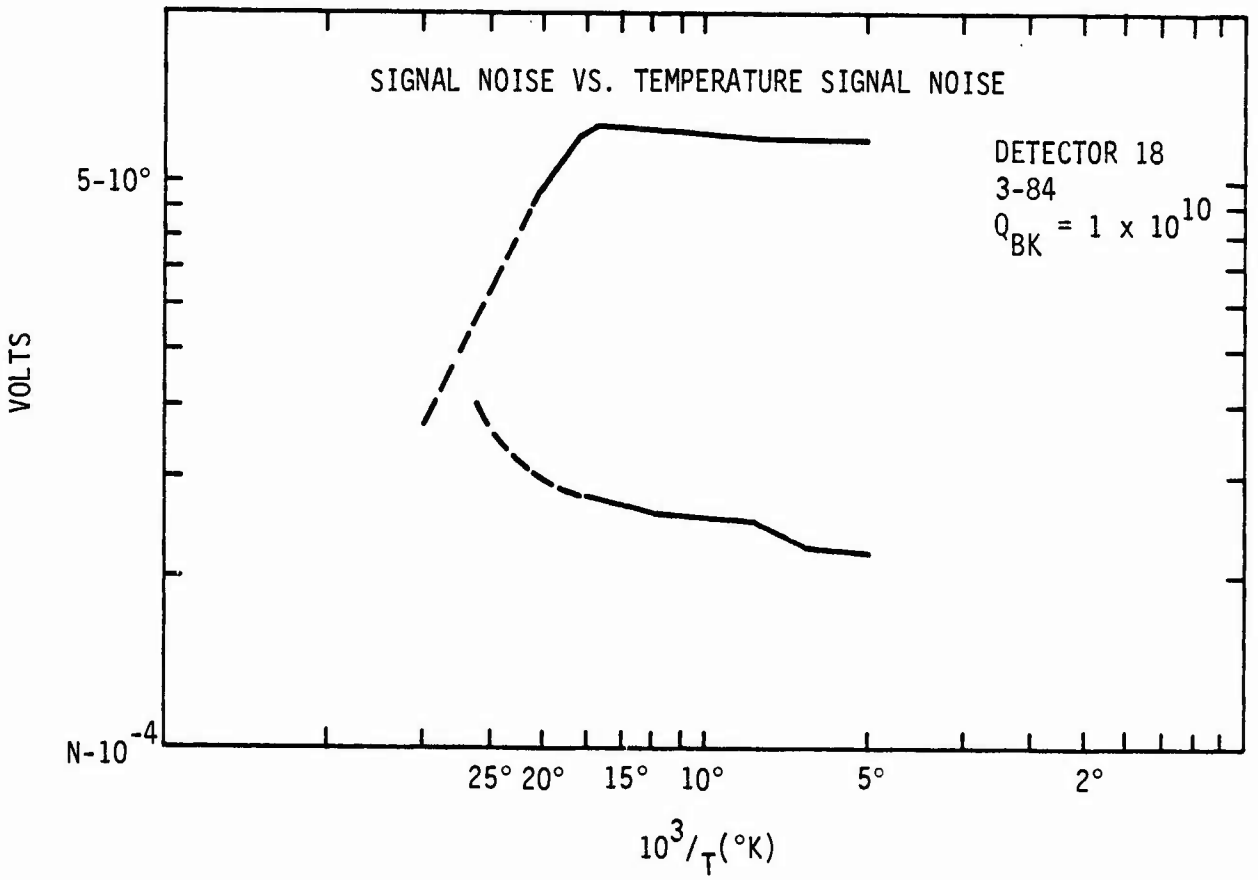

Figure 28-1. Signal and Noise vs Temperature Detector 18

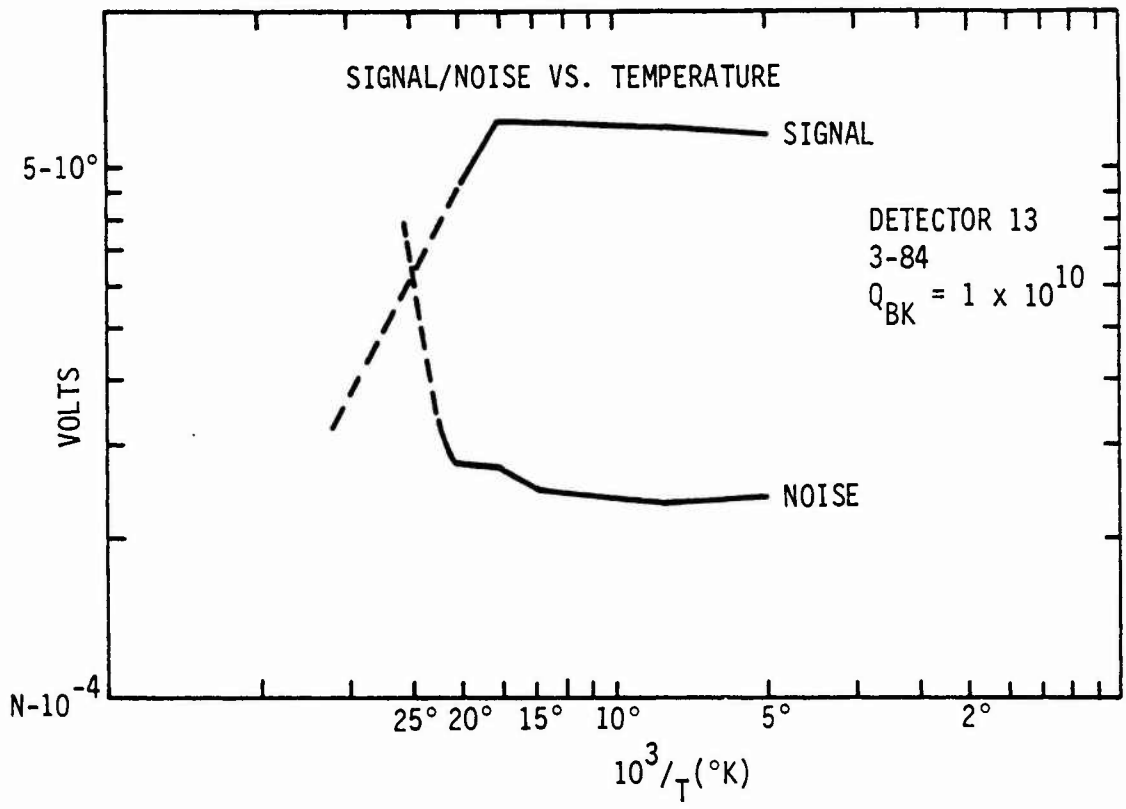

Figure 28-2. Signal and Noise vs. Temperature Detector 13

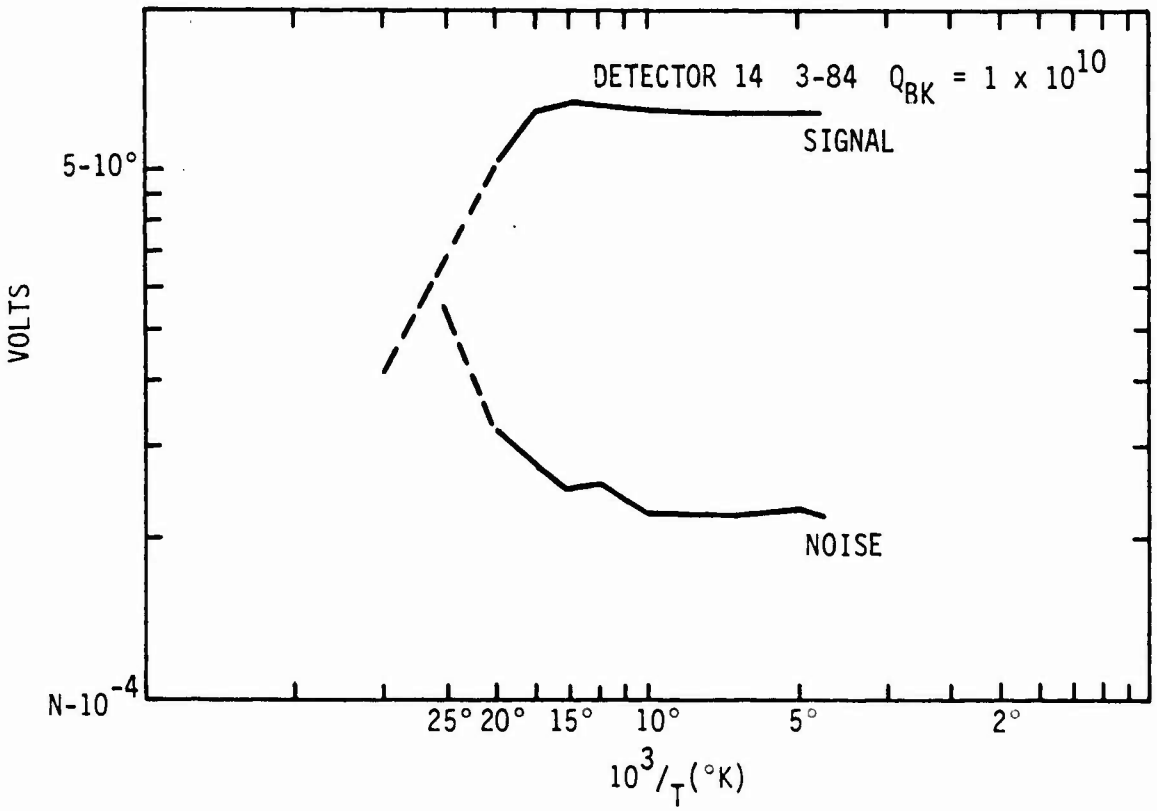

Figure 28-3. Signal and Noise vs Temperature Detector 14

3.6.6 Dynamic Range Measurements on Selected Detectors

Measurements were performed on selected BEAM detectors for the purpose of determining their dynamic range capabilities. The experimental apparatus which was used in this study is shown in Figure 26-1. The optical filtering consists of: (1) a Corning blue glass filter on the liquid helium (LHe) cap which provides a 30% transmittance passband at 4.2K from 1.6 to 2.7 μm, and a background attenuation of 10^{-6}; (2) a germanium filter comounted on the LHe cap which has a 50% transmittance; (3) a 0.60 inch aperture on the LN_2 shield with another 50% Ge N.D. filter; and (4) a KRS-5 window on the ambient dewar cap which has a transmission value of about 72% in the 2.7-μm region. The detector signal V_{sig} was monitored as a function of signal flux density Q_s. The signal flux density was varied over nearly five orders of magnitude by using several blackbody apertures (0.125 to 0.60 inch) with one blackbody temperature setting (500K). A chopping frequency of 2 Hz was used during the tests.

Dynamic range is calculated from the expression:

$$DR = \frac{V_{s,max}}{V_N} \tag{3}$$

where

$V_{s,max}$ is the maximum signal voltage observed from a detector

V_N is the noise voltage from a detector

The noise voltage V_N is that which was measured at the background level used for the dynamic range test. The lowest flux levels used during the dynamic range measurements were limited by the smallest available aperture size.

Representative samples of dynamic range (linearity) data taken on the BEAM FPA are shown in Figures 26-2 through 26-4. It will be concluded from the data that the signal output as a function of incident energy is linear over the range measured, or from the noise level to amplifier saturation, and that (with the assumption that the signal is linear from the background noise level to the signal obtained with the smallest aperture). The dynamic range exceeds the 10^4 requirement.

The upper signal was limited to the aperture on the blackbody which matched the smallest aperture internal to the dewar.

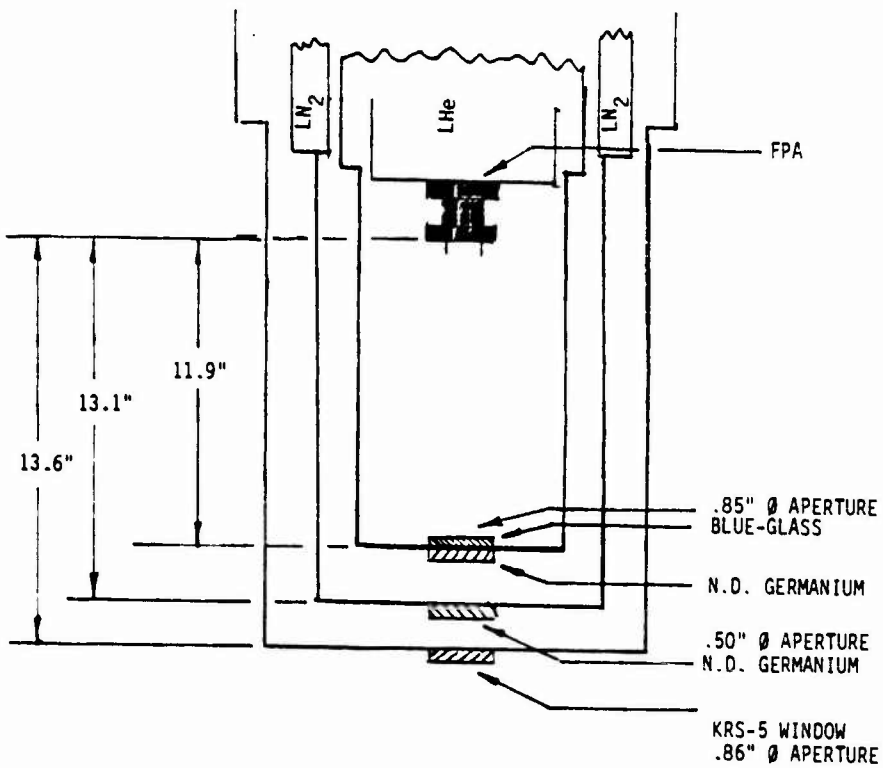

Figure 29-1. Test Setup

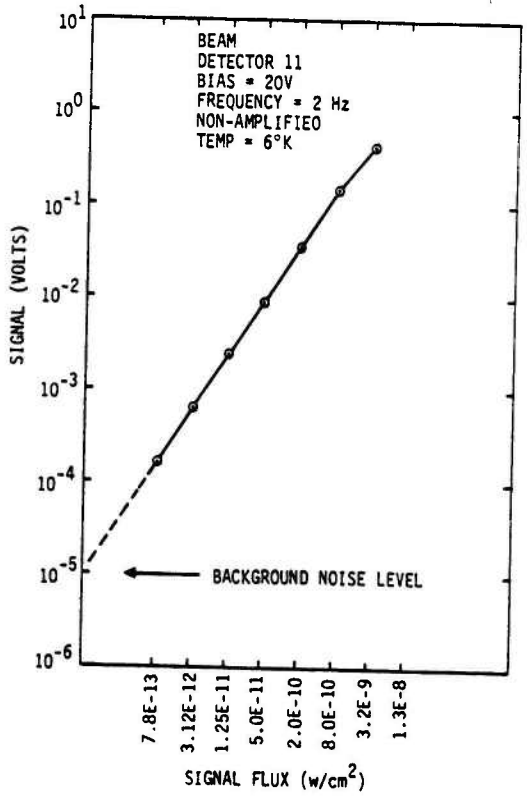

Figure 29-2. Signal vs Flux - Detector 11

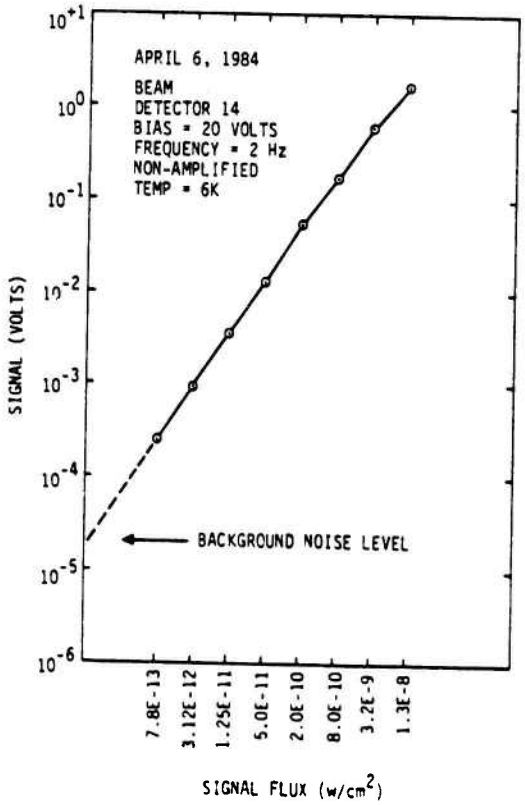

Figure 29-3. Signal vs Flux - Detector 14

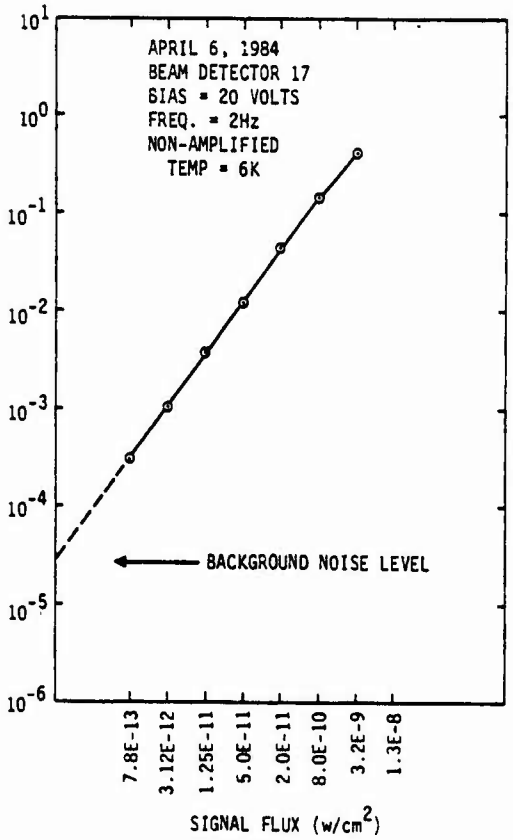

Figure 29-4. Signal vs Flux - Detector 17

3.6.7 Typical Signal vs. Frequency (Source Follower)

A typical response curve is shown in Figure 30-1. Typical curves for a preamplifier and a postamplifier are shown in Figure 30-2.

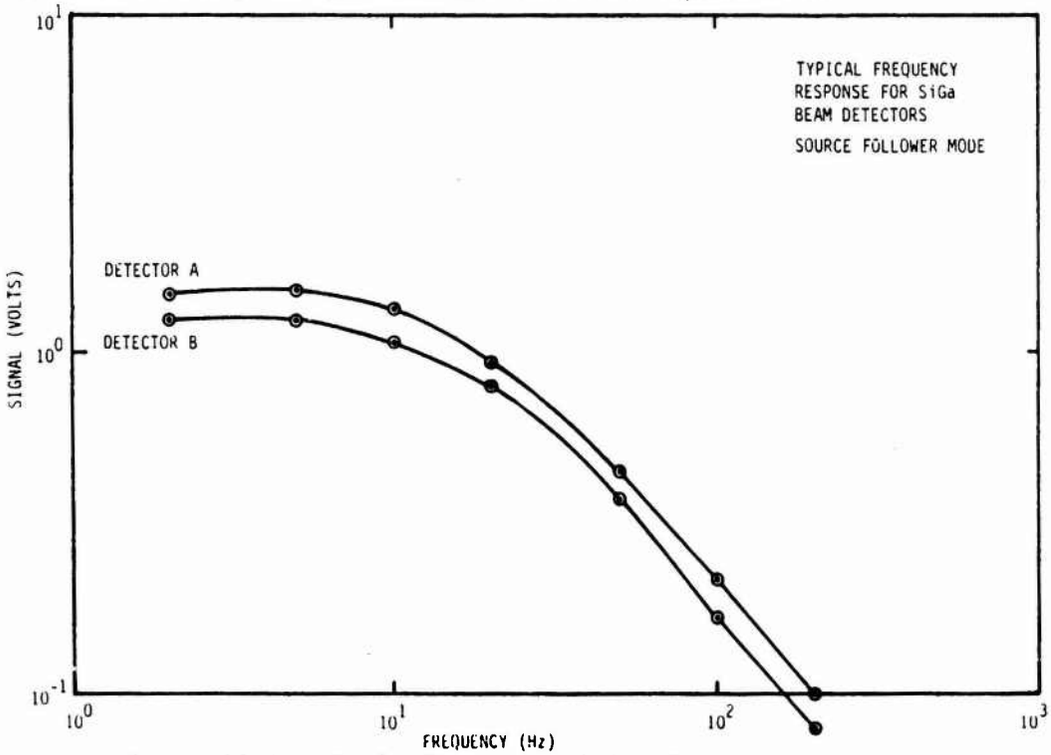

Figure 30-1. Typical Non-amplified Frequency Response for SiGa BEAM Detectors (Source Follower Mode)

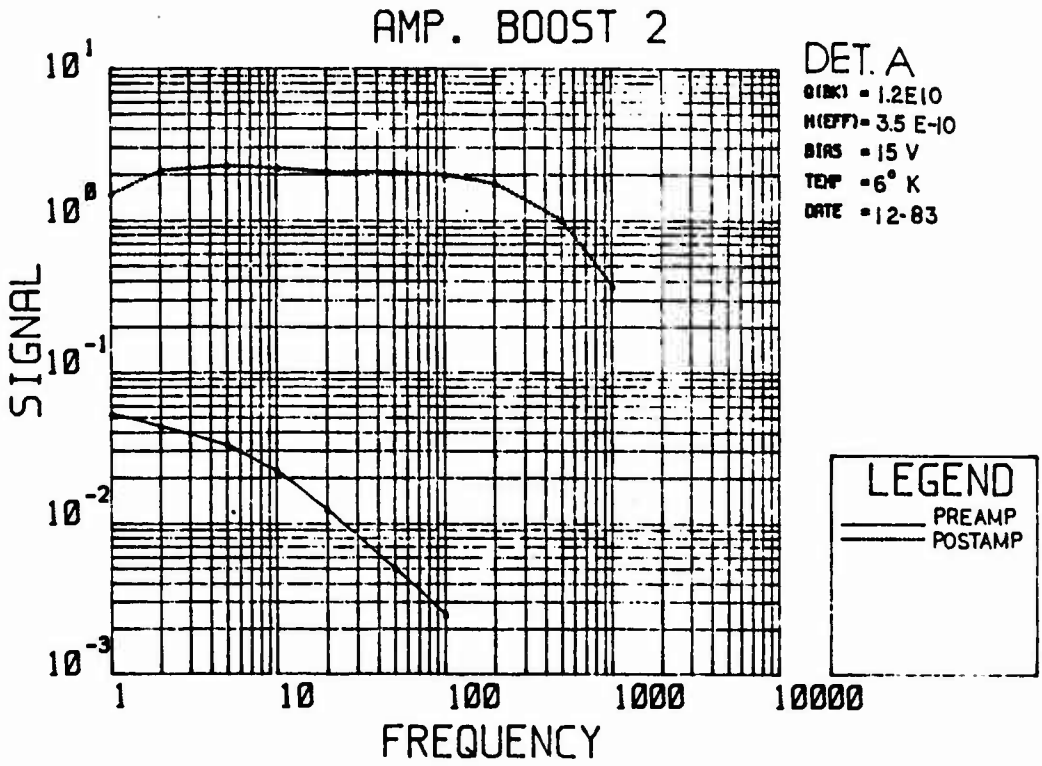

Figure 30-2. Typical Signal vs Frequency

3.7 FINAL MEASUREMENTS

Following the baseline set of measurements. the FPA's spectral filters were installed atop the unit. The FPA was then cooled down to 6K and a new set of data was taken at optimum bias and at a single frequency. This exercise was done at two background levels as shown in the following tables. The calculated NEP and responsivity along with the associated background and signal flux levels are also included in these tables.

Environmental tests were conducted on the FPA and the above tests were run again at both background levels with no apparent change in signal or noise. This insured performance repeatability of all 24 channels of the beam FPA.

TEST WITH BANDPASS FILTERS

SET UP: 2.0% TRANS. N.D. FILTER @4.2°K

50% TRANS. N.D. FILTER @77.°K

70% TRANS. KRS-5 WINDOW @295°K

XX% TRANS. BANDPASS FILTERS @4.2°K

0.025" DIA. APERTURE

11.95" DETECTOR-APERTURE DISTANCE

Table 4. Filter Transmission Data-Band 1.

RR TEMP : 500 CH TEMP : 300
LAMBDA 1: 2 LAMBDA 2: 19.5
DELTA : .5
FILTERS : (1) BEAMZ% (2) HISTWN (3) 3 (4) BIHIST (5) MGF2
RR/WATT : HISTGA
APERTURE: .825 DISTANCE: 12

FILTER LAMBDA	BEAMZ% TRANSMISSION	HISTWN	3	BIHIST	MGF2
2	.02	.7	.5	0	.94
2.5	.02	.7	.5	0	.95
3	.02	.7	.5	0	.95
3.5	.02	.7	.5	.76	.95
4	.02	.7	.5	.82	.96
4.5	.02	.7	.5	.83	.96
5	.02	.7	.5	.5	.95
5.5	.02	.7	.5	0	.95
6	.02	.7	.5	0	.93
6.5	.02	.7	.5	0	.92
7	.02	.7	.5	0	.83
7.5	.02	.7	.5	0	.8
8	.02	.7	.5	0	.58
8.5	.02	.7	.5	0	.42
9	.02	.7	.5	0	.23
9.5	.02	.7	.5	0	.14
10	.02	.7	.5	0	.08
10.5	.02	.7	.5	0	0
11	.02	.7	.5	0	0
11.5	.02	.7	.5	0	0
12	.02	.7	.5	0	0
12.5	.02	.7	.5	0	0
13	.02	.7	.5	0	0
13.5	.02	.7	.5	0	0
14	.02	.7	.5	.015	0
14.5	.02	.7	.5	.03	0
15	.02	.7	.5	.02	0
15.5	.02	.7	.5	.01	0
16	.02	.7	.5	.025	0
16.5	.02	.7	.5	.035	0
17	.02	.7	.5	.03	0
17.5	.02	.7	.5	.02	0
18	.02	.7	.5	.01	0
18.5	.02	.7	.5	.02	0

BACKGROUND PHOTON FLUXES (PHOTONS/CM SQUARE/SECOND) :

Table 5. Band 1 Final Performance Data at Background $\approx 9 \times 10^7$.

BAND 1 (3-5 μm)	BIAS = $^+25$V TEMP. = 6°K FREQ. = 50 Hz	$Q_{BK} = 8.7 \times 10^7$ ph/cm^2/sec $H_{EFF} = 2.14$ E-11 w/cm^2 $AREA_D = 8.06$ E-3 cm^2 GAIN = 35			
DETECTOR	SIGNAL ($\times 10^{-3}$V)	NOISE ($\times 10^{-6}$ V/√Hz)	S/N	RESPON. (A/W)	NEP $\times 10^{-16}$ (W/√Hz)
1	67	112	598	2.23	2.88
4	67	112	598	2.23	2.88
7	66	112	589	2.18	2.93
10	71.5	125	572	2.38	3.02
13	63.7	97	657	2.11	2.63
16	63.7	97	657	2.11	2.63
19	68.5	97	706	2.28	2.44
22	76	112	679	2.52	2.54
WORST				2.11	3.02
AVG				2.26	2.78

Table 6. Band 1 Final Performance Data at Background $\approx 5 \times 10^9$.

BAND 1 (3-5 μm)	BIAS = +20V TEMP. = 6°K FREQ. = 50 Hz		$Q_{BK} = 4.35 \times 10^9$ ph/cm^2/sec $H_{EFF} = 9.5 \times 10^{-11}$ w/cm^2 $AREA_D$ = 8.06 E-3 cm^2 GAIN = 35		
DETECTOR	SIGNAL ($\times 10^{-3}$V)	NOISE ($\times 10^{-6}$ V/$\sqrt{Hz}$)	S/N ($\times 10^3$)	RESPON. (A/W)	NEP $\times 10^{-16}$ (W/$\sqrt{Hz}$)
1	234	125	1.87	1.71	4.20
4	234	125	1.87	1.71	4.20
7	225	125	1.80	1.64	4.36
10	240	112	2.14	1.75	3.66
13	210	125	1.68	1.53	4.67
16	221	125	1.77	1.61	4.44
19	222	125	1.78	1.62	4.4
22	234	118	1.98	1.70	3.9
WORST				1.53	4.67
AVG				1.66	4.23

NOTE: 500K blackbody source with 8.9% ND filter.

Table 7. Band 2 Filter Transmission Data

BB TEMP : 500 CH TEMP : 300
LAMBDA 1: 2 LAMBDA 2: 18.5
DELTA : .5
FILTERS : (1) BEAMZ% (2) HISTWN (3) NDGE50 (4) HISBP2 (5) HISBL2
RR/WATT : HISTGA
APERTURE: .025 DISTANCE: 12

FILTER LAMBDA	BEAMZ% TRANSMISSION	HISTWN	NDGE50	HISBP2	HISBL2
2	.02	.7	.5	0	0
2.5	.02	.7	.5	0	0
3	.02	.7	.5	0	0
3.5	.02	.7	.5	0	0
4	.02	.7	.5	0	.1
4.5	.02	.7	.5	0	.24
5	.02	.7	.5	0	.85
5.5	.02	.7	.5	.74	.94
6	.02	.7	.5	.83	.94
6.5	.02	.7	.5	.84	.94
7	.02	.7	.5	.15	.88
7.5	.02	.7	.5	0	.77
8	.02	.7	.5	0	.52
8.5	.02	.7	.5	0	.245
9	.02	.7	.5	0	.18
9.5	.02	.7	.5	0	.14
10	.02	.7	.5	0	.08
10.5	.02	.7	.5	0	0
11	.02	.7	.5	0	0
11.5	.02	.7	.5	0	0
12	.02	.7	.5	0	0
12.5	.02	.7	.5	0	0
13	.02	.7	.5	0	0
13.5	.02	.7	.5	0	0
14	.02	.7	.5	0	0
14.5	.02	.7	.5	0	0
15	.02	.7	.5	0	0
15.5	.02	.7	.5	0	0
16	.02	.7	.5	0	0
16.5	.02	.7	.5	0	0
17	.02	.7	.5	0	0
17.5	.02	.7	.5	0	
18	.02	.7	.5	0	
18.5	.02	.7	.5	0	

BACKGROUND PHOTON FLUXES (PHOTONS/SQUARE CM/SECOND) :

Table 8. Band 2 Final Performance Data at ≈ 5×10^8 Background

BAND 2 (5-7 μm)	BIAS = $^{+}25$V TEMP = 6°K FREQ = 50 Hz		$Q_{BK} = 4.74 \times 10^8$ ph/cm^2/sec $H_{EFF} = 3.48 \times 10^{-11}$ w/cm^2 $AREA_D = 8.06 \times 10^{-3}$ cm^2 GAIN = 35		
DETECTOR	SIGNAL ($\times 10^{-3}$ VOLTS)	NOISE ($\times 10^{-6}$ V/√Hz)	S/N $\times 10^3$	RESPONSIVITY A/W	NEP $\times 10^{-16}$ W/√Hz
2	205	97	2.11	4.2	1.33
5	225	112	2.01	4.6	1.40
8	220	125	1.76	4.5	1.59
11	220	112	1.96	4.5	1.43
14	215	87	2.47	4.4	1.14
17	215	112	1.92	4.4	1.46
20	192	112	1.71	3.9	1.64
23	190	112	1.70	3.9	1.65
WORST				3.9	1.65
AVG				4.3	1.46

Table 9. Band 2 Final Performance Data at ≈ 3×10^{10} Background

BAND 1 (3-5 μm)	BIAS = +20V TEMP. = 6°K FREQ. = 50 Hz		$Q_{BK} = 2.37 \times 10^{10}$ ph/cm^2/sec $H_{EFF} = 1.44 \times 10^{-10}$ w/cm^2 $AREA_D = 8.06$ E-3 cm^2 GAIN = 35		
DETECTOR	SIGNAL ($\times 10^{-3}$V)	NOISE ($\times 10^{-6}$ V/√Hz)	S/N ($\times 10^3$)	RESPON. (A/W)	NEP $\times 10^{-16}$ (W/√Hz)
2	670	274	2.45	3.28	4.78
5	670	274	2.45	3.28	4.78
8	750	274	2.74	3.67	4.27
11	735	262	2.81	3.59	4.20
14	675	262	2.58	3.30	5.54
17	675	224	3.01	3.3	3.88
20	580	237	2.45	2.84	4.8
23	665	280	2.38	3.25	4.92
WORST				2.84	5.54
AVG				3.31	4.65

NOTE: 500K blackbody signal source with 8.5% ND filter.

Table 10. Filter Transmission Data - Band 3

BB TEMP : 500 CH TEMP : 300
LAMBDA 1: 2 LAMBDA 2: 18.5
DELTA : .5
FILTERS : (1) BEAM2% (2) HISTWN (3) NDGE50 (4) HISTB3 (5) 1
RR/WATT : HISTGA
APERTURE: .025 DISTANCE: 12

FILTER LAMBDA	BEAM2% TRANSMISSION	HISTWN	NDGE50	HISTB3	1
2	.02	.7	.5	0	1
2.5	.02	.7	.5	0	1
3	.02	.7	.5	0	1
3.5	.02	.7	.5	0	1
4	.02	.7	.5	0	1
4.5	.02	.7	.5	0	1
5	.02	.7	.5	0	1
5.5	.02	.7	.5	0	1
6	.02	.7	.5	0	1
6.5	.02	.7	.5	0	1
7	.02	.7	.5	0	1
7.5	.02	.7	.5	0	1
8	.02	.7	.5	.02	1
8.5	.02	.7	.5	.63	1
9	.02	.7	.5	.72	1
9.5	.02	.7	.5	.74	1
10	.02	.7	.5	.76	1
10.5	.02	.7	.5	.77	1
11	.02	.7	.5	.77	1
11.5	.02	.7	.5	.77	1
12	.02	.7	.5	.76	1
12.5	.02	.7	.5	.75	1
13	.02	.7	.5	.74	1
13.5	.02	.7	.5	.7	1
14	.02	.7	.5	.66	1
14.5	.02	.7	.5	.6	1
15	.02	.7	.5	0	1
15.5	.02	.7	.5	0	1
16	.02	.7	.5	0	1
16.5	.02	.7	.5	0	1
17	.02	.7	.5	0	1
17.5	.02	.7	.5	0	1
18	.02	.7	.5	0	1
18.5	.02	.7	.5	0	1

BACKGROUND PHOTON FLUXES (PHOTONS/SQUARE CM/SECOND) :

Table 11. Band 3 Final Performance Data at 6×10^9 Background

BAND 3 (8-14 μm)	BIAS = + 25V TEMP = 6°K FREQ = 50 Hz		$Q_{BK} = 5.7 \times 10^9$ ph/cm^2/sec $H_{EFF} = 1.4 \times 10^{-10}$ w/cm^2 DET. AREA = 8.06×10^{-3} cm^2 GAIN = 35		
DETECTOR	SIGNAL ($\times 10^{-3}$V)	NOISE ($\times 10^{-6}$ V/Hz$^{1/2}$)	S/N $\times 10^3$	RESPONSIVITY (A/W)	NEP $\times 10^{-16}$ W/√Hz
3	890	189	4.71	4.5	2.40
6	875	189	4.63	4.4	2.44
9	865	187	4.63	4.4	2.44
12	851	187	4.55	4.3	2.48
15	823	187	4.40	4.2	2.56
18	814	189	4.31	4.1	2.62
21	880	187	4.71	4.46	2.40
24	815	187	4.36	4.1	2.59
WORST				4.1	2.62
AVG				4.31	2.49

Table 12. Band 3 Final Performance Data at 3×10^{11} Background

BAND 1 (3-5 μm)	BIAS = +20V TEMP. = 6 K FREQ. = 50 Hz			$Q_{BK} = 2.85 \times 10^{11}$ ph/cm^2/sec $H_{EFF} = 6.05 \times 10^{-10}$ w/cm^2 $AREA_D = 8.06$ E-3 cm^2 GAIN = 35	
DETECTOR	SIGNAL ($\times 10^{-3}$V)	NOISE ($\times 10^{-6}$ V/$\sqrt{Hz}$)	S/N $\times 10^3$	RESPON. (A/W)	NEP $\times 10^{-15}$ (W/$\sqrt{Hz}$)
3	2700	901	3.0	3.16	1.63
6	2660	984	2.7	3.12	1.80
9	2870	959	2.99	3.36	1.63
12	2800	997	2.81	3.78	1.74
15	2600	922	2.82	3.05	1.73
18	2560	872	2.94	3.0	1.66
21	2660	950	2.80	3.12	1.74
24	2400	810	2.96	2.80	1.65
WORST				2.80	1.80
AVG				3.17	1.70

NOTE: 500K blackbody source with 8.5% ND filter.

Section 4
ENVIRONMENTAL TEST RESULTS

The HIGH STAR SOUTH FPA was subjected to environmental tests including vibration in three perpendicular axes for a period of three minutes and in accordance with the frequency range, amplitude rate, and power spectral density values indicated in Table 13.

The ICS units were absent from the otherwise complete BEAM FPA during environmental testing. The fact that the vibration and shock tests were performed at atmospheric pressure would have rendered the thin sapphire diaphragm of the ICS unit susceptible to damage that could be incurred by pressure differentials created across the diaphragm during shake and shock. The durability of the ICS units has been demonstrated on the Celestial Mapping Project, ELC, HIGH STAR II, SCOOP, ZIP, FIRSSE and SOFT programs in which their operational lifetime was spent in reduced-pressure environments. The power spectral density/frequency profile to which the BEAM FPA unit was subjected is recorded in the graphs of Figures 31-1, 31-2, and 31-3 for the X, Y, and Z axes, respectively, and as defined in Figure 32.

The BEAM FPA was also subjected to a series of 100g peak amplitude half-sine pulses of 11-ms duration in each of the three axes. One shock pulse was inflicted on the FPA in one direction of each axis and with one shock pulse in the opposite direction of each axis. The experimental setup used in the shock tests is shown in Figure 33 where the BEAM FPA is mounted base-up for shock tests in the Z-axis. A calibration shock-pulse profile reveals a 100g peak amplitude, 11-ms half-sine shock pulse that is typical of the shock-pulse to which the ELC FPA was subjected. Figures 34 and 35 represent the profile of shock pulse applied to the focal plane. Figure 36 shows a calibrator profile.

Table 13. Vibration Testing Parameter Values for BEAM FPA Environmental Testing

FREQUENCY RANGE (Hz)	AMPLITUDE RATE	POWER SPECTRAL DENSITY
20-100	+6 dB/OCT	0.0 to 0.1 g^2/Hz
100-2000	0 dB/OCT	0.1 g^2/Hz

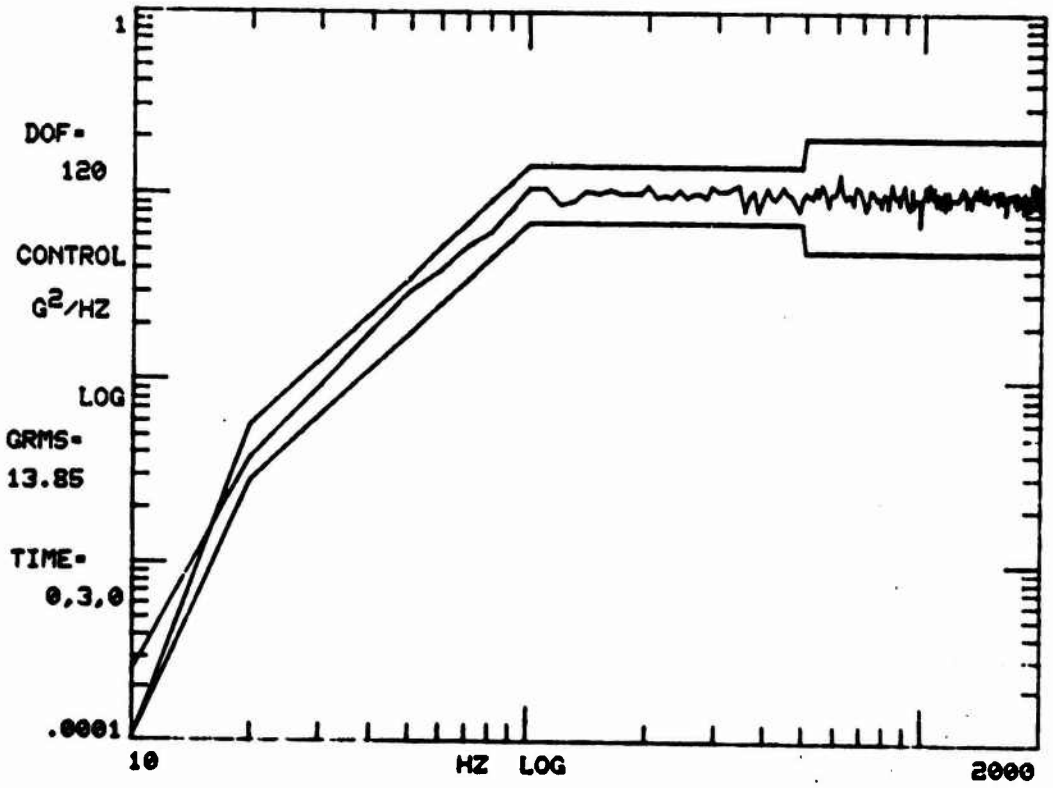

Figure 31-1. HIGH STAR SOUTH Qualification Vibration (X Axis)

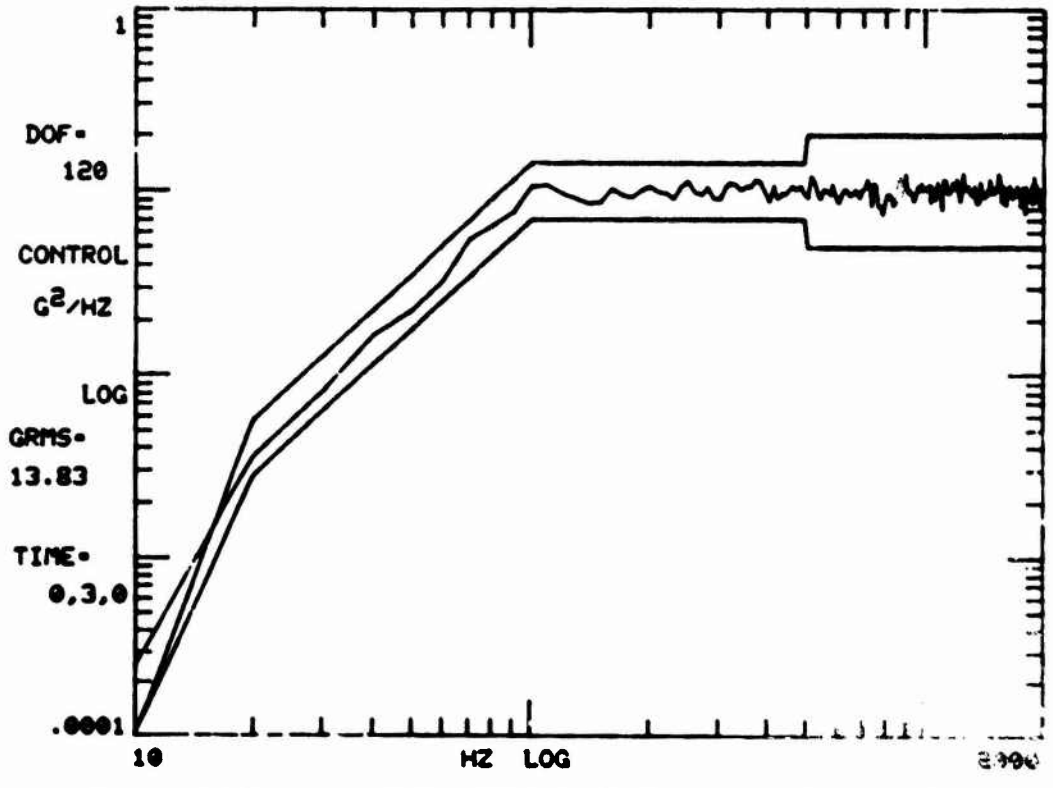

Figure 31-2. HIGH STAR SOUTH Qualification Vibration (Y Axis)

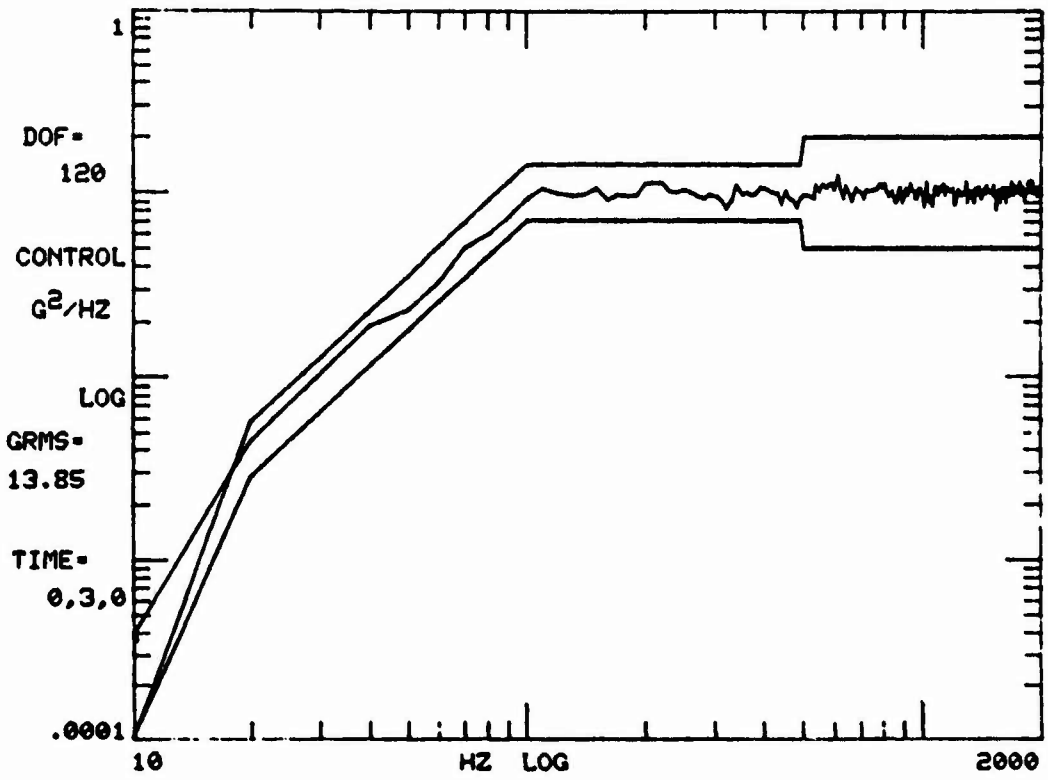

Figure 31-3. HIGH STAR SOUTH Qualification Vibration (Z Axis)

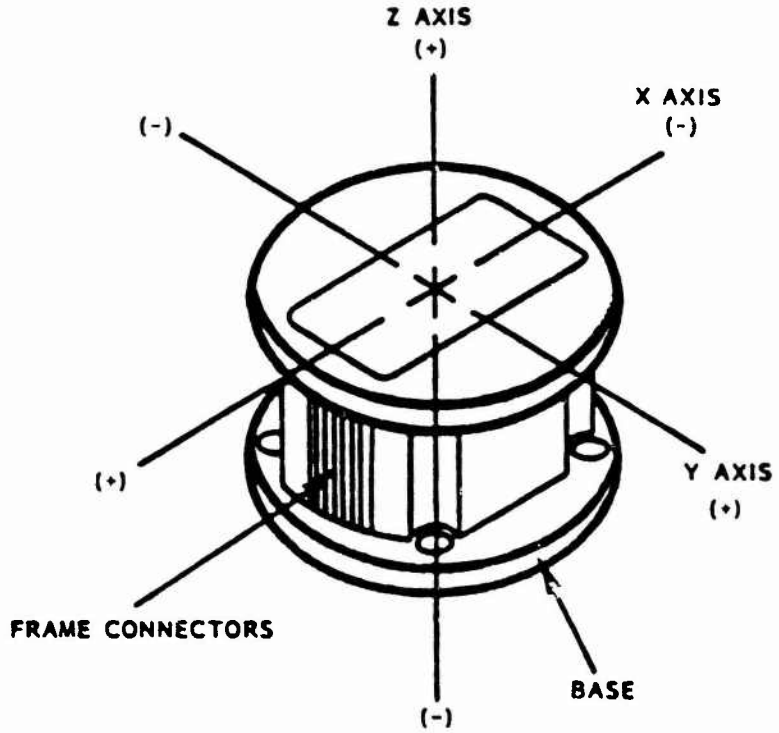

Figure 32. Definition of X, Y, and Z Axes of BEAM FPA

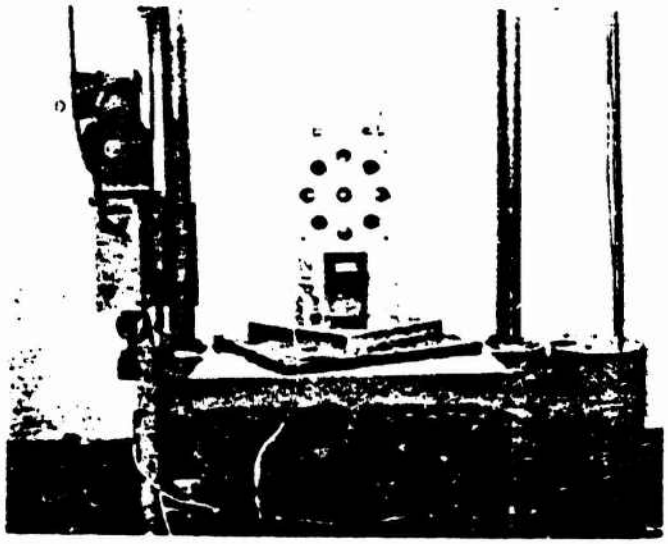

Figure 33. BEAM FPA on Shock Tower

(a) +X Axis
20g/div
5 ms/div
6-12-84

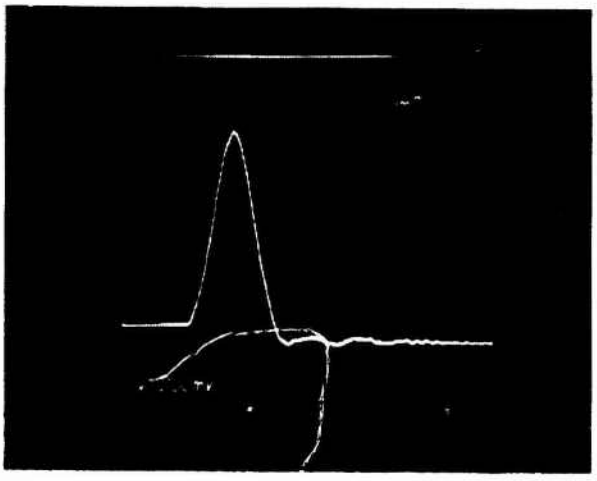

(b) +Y Axis
20g/div
5 ms/div
6-12-84

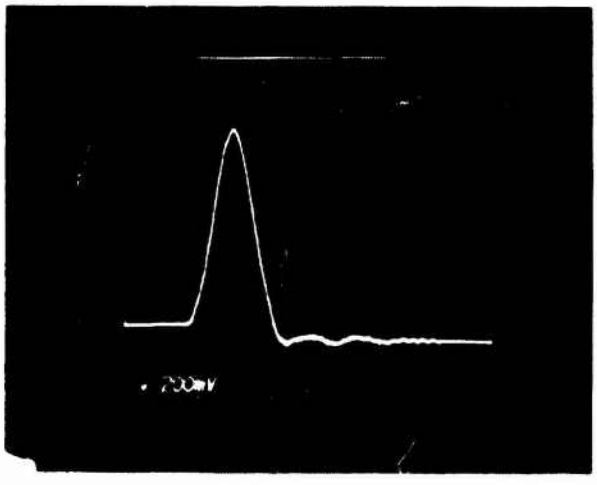

(c) +2 Axis
20g/div
5 ms/div
6-12-84

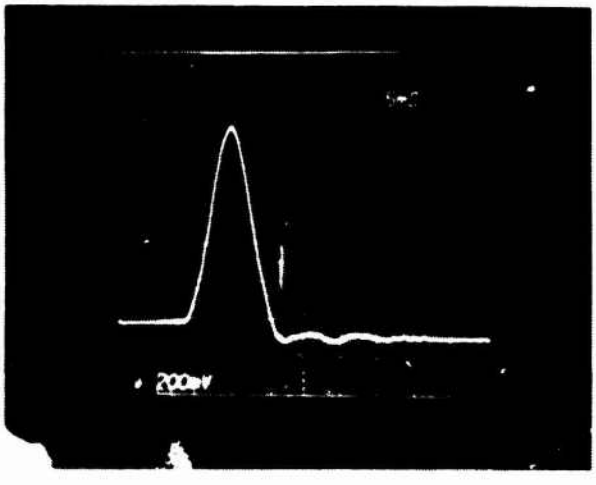

Figure 34. FPA Shock Pulse Profile (+X,+Y,+Z axes)

(a) -X Axis
20g/dw
5 ms/div
6-12-84

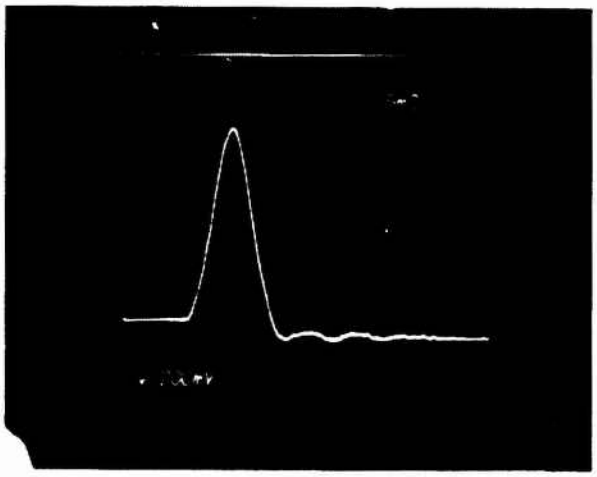

(b) -Y Axis
20g/div
5 ms/div
6-12-84

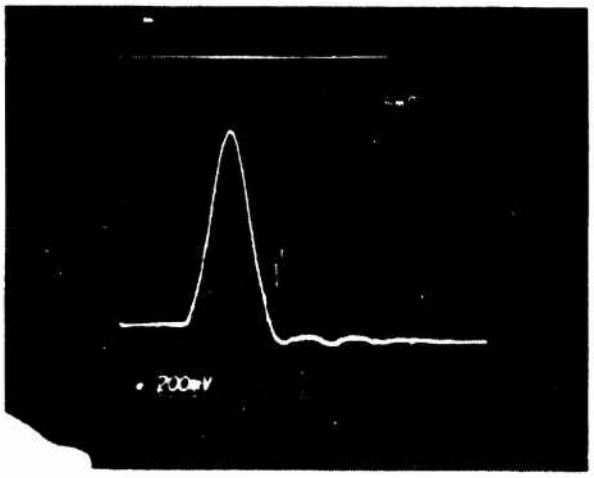

(c) -2 Axis
20g/div
5 ms/div
6-12-84

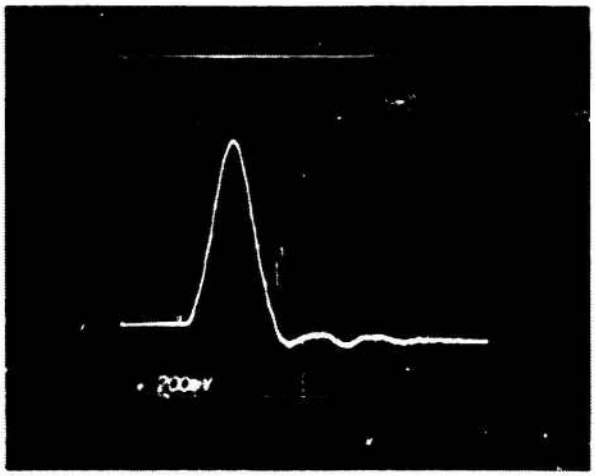

Figure 35. FPA Shock Pulse Profile (-X,-Y,-Z axes)

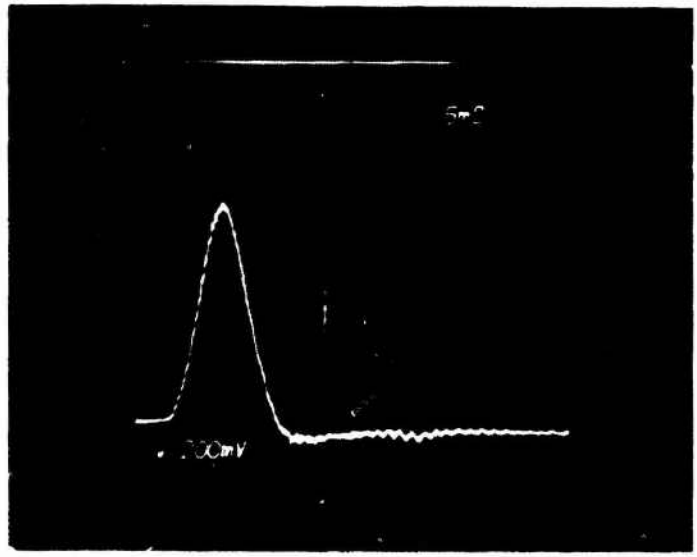

Figure 36. Calibration Profile for BEAM FPA Shock Test

4.1 THERMAL CYCLING

The FPA was subject to multiple cooldowns from 295K to 4.2K during baseline and final testing. Each time the unit was warmed up, it was exposed to atmospheric pressure then repumped to $\approx 10^{-7}$ Torr and recooled to 4.2K. This occured approximately 12 times with no apparent deviation in detector performance. Visual checks were performed when appropriate to check for thermal fractures in the epoxies or in the circuit/detector board assemblies. The components appeared normal at all times.

Section 5
MISCELLANEOUS DATA

5.1 ICS PULSE DATA

Photos of detector responses to ICS pulses are shown in Figure 37. The 24 detectors of the BEAM FPA will show response to the activation of the internal calibration sources (ICS) which are located above the detector plane and wired in parellel with each other. The response of each detector was photographed as the ICS units were pulsed. The experimental set up used in this measurement employed a Systron-Donner Model 101C pulse generator to activate the IC sources. A Textronix 7000 Series oscilloscope and Textronix C-50 Series camera recorded the output signals. All 24 are shown here with corresponding inputs.

Note: A few detectors appear somewhat lower in signal response due to their location and their relative filter positions with respect to the location of the ICS, which illuminate somewhat lateral to the direction of normal incident light. These measurements are for general comparision only, not a true calibration method.

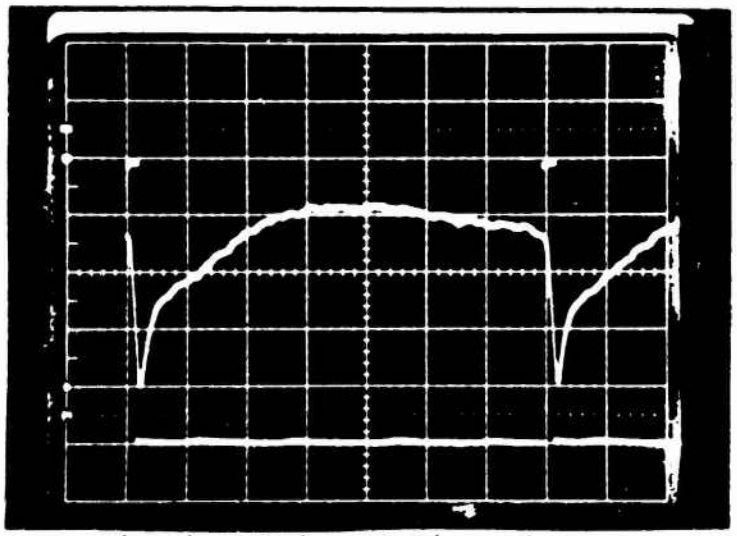

Detector 1. 1 ms Pulse, 1 V/cm Cal Source, 0.2 V/cm Signal, Band 1

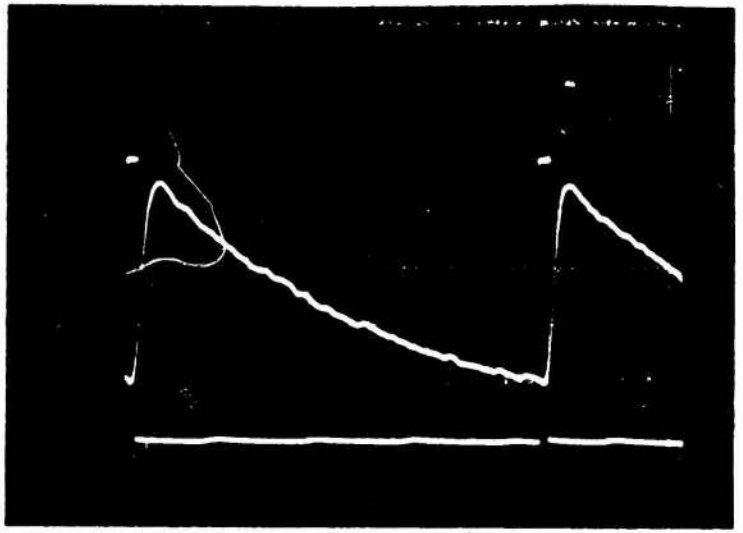

Detector 2. 1 ms Pulse, 1 V/cm Cal Source, 0.5 V/cm Signal, Band 2

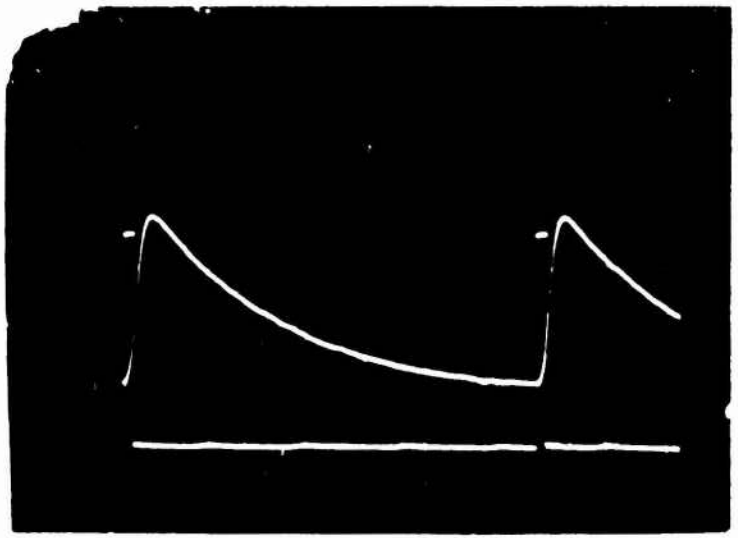

Detector 3. 1 ms Pulse, 3.6 V/cm Cal Source, 2 V/cm Signal, Band 3

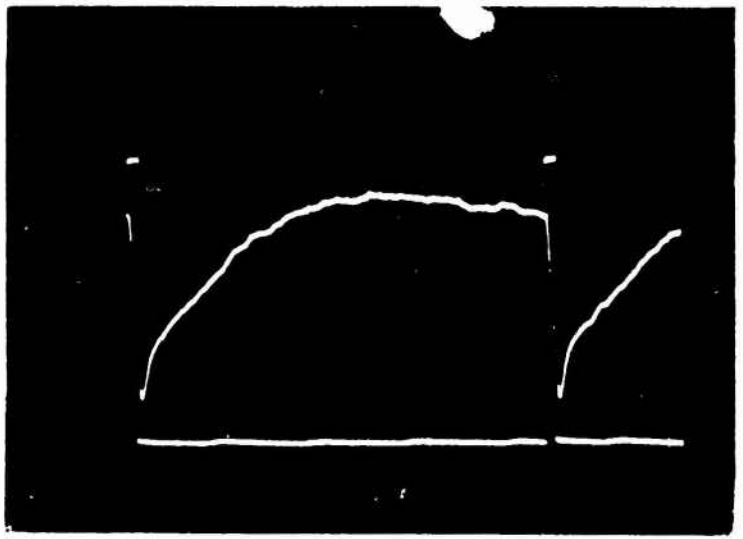

Detector 4. 1 ms Pulse, 1 V/cm Cal Source, 0.2 V/cm Signal, Band 1

Figure 37. Detector Response to ICS Pulse.

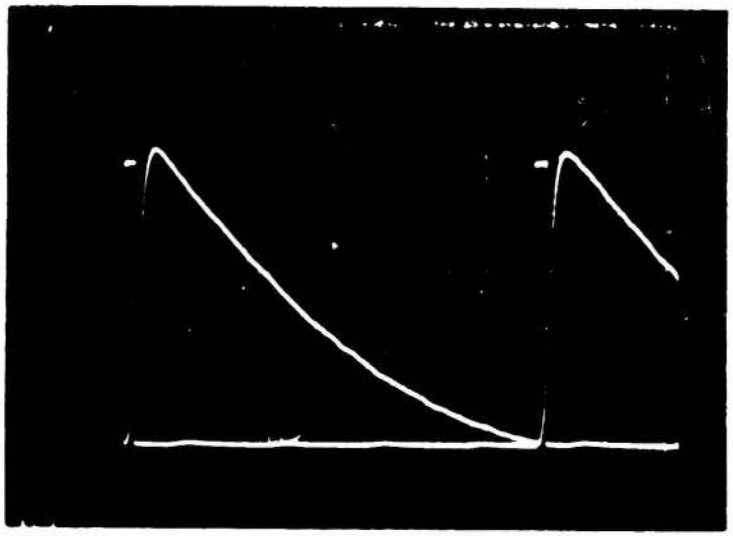

Detector 5. 1 ms Pulse, 1 V/cm Cal Source, 2/5 V/cm Signal, Band 2

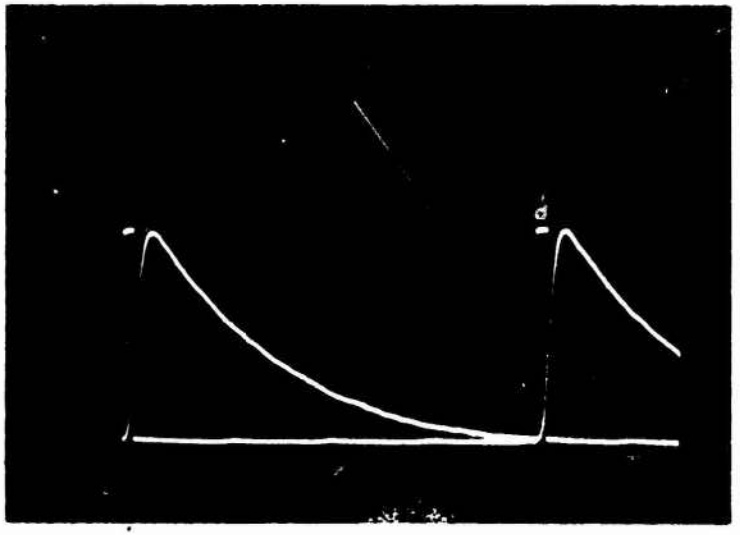

Detector 6. 1 ms Pulse, 3.6 V/cm Cal Source, 2 V/cm Signal, Band 3

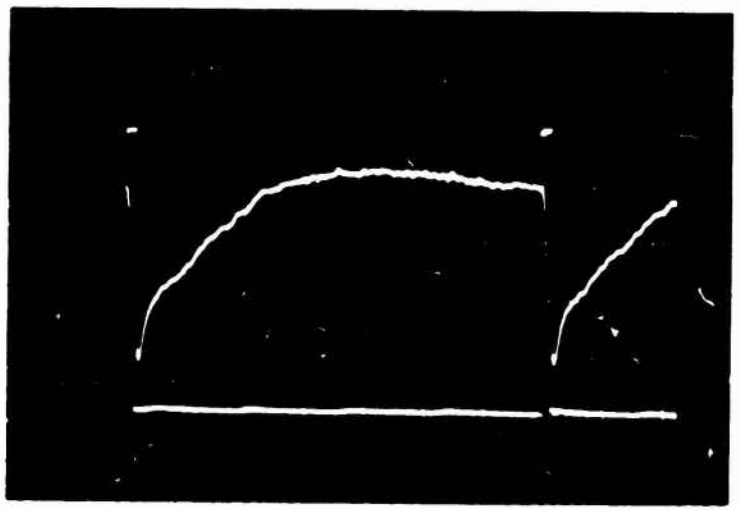

Detector 7. 1 ms Pulse, 1 V/cm Cal Source, 0.1 V/cm Signal, Band 1

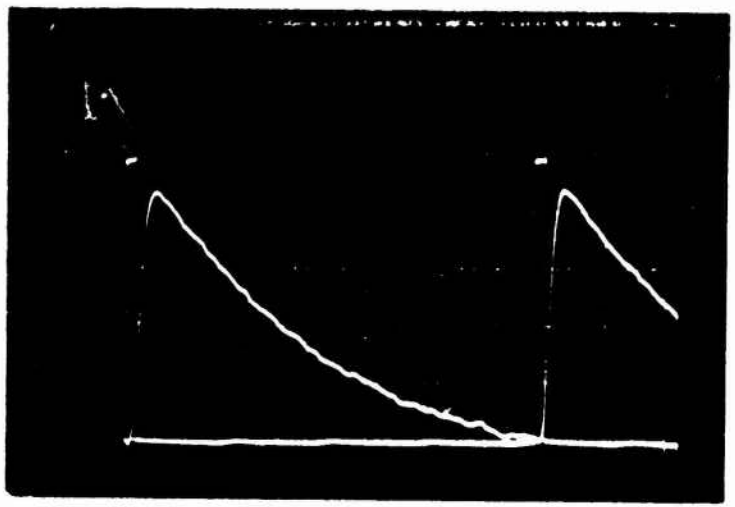

Detector 8. 1 ms Pulse, 1 V/cm Cal Source, 0.5 V/cm Signal, Band 2

Figure 37. (Continued)

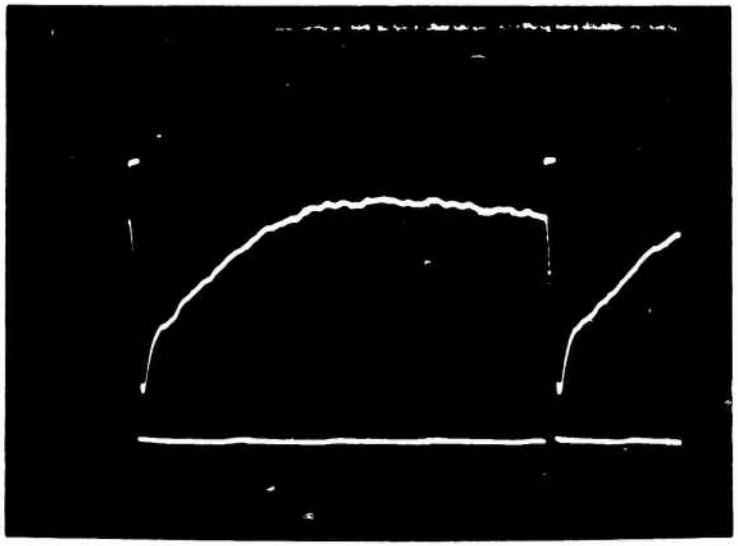

Detector 9. 1 ms Pulse, 1 V/cm Cal Source

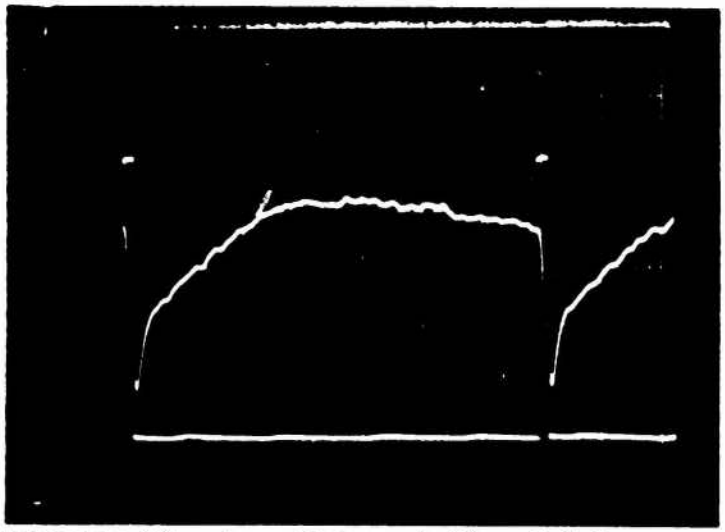

Detector 10. 1 ms Pulse, 1 V/cm Cal Source, 0.2 V/cm Signal, Band 1

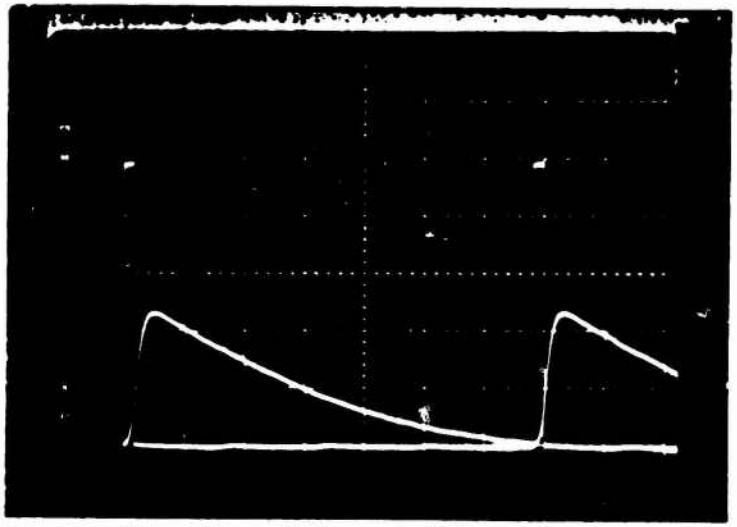

Detector 11. 1 ms Pulse, 1 V/cm Cal Source, 5 V/cm Signal, Band 2

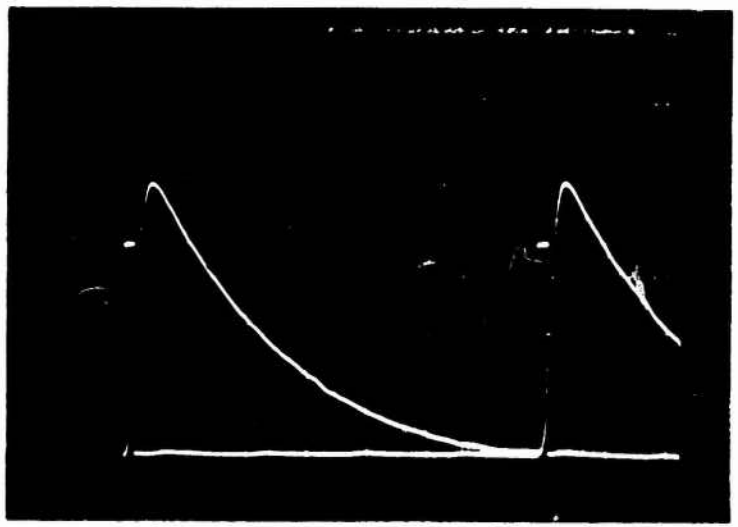

Detector 12. 1 ms Pulse, 3.6 V/cm Cal Source, 2 V/cm Signal, Band 3

Figure 37. (Continued)

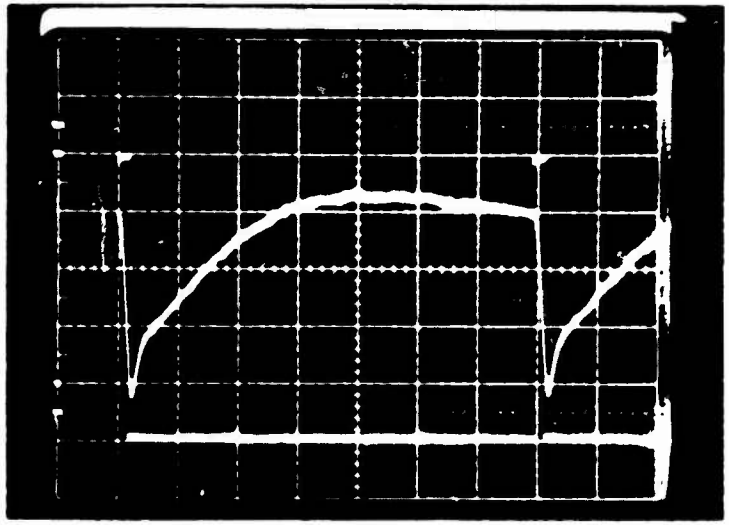

Detector 13. 1 ms Pulse, 1 V/cm Cal Source, 0.2 V/cm Signal, Band 1

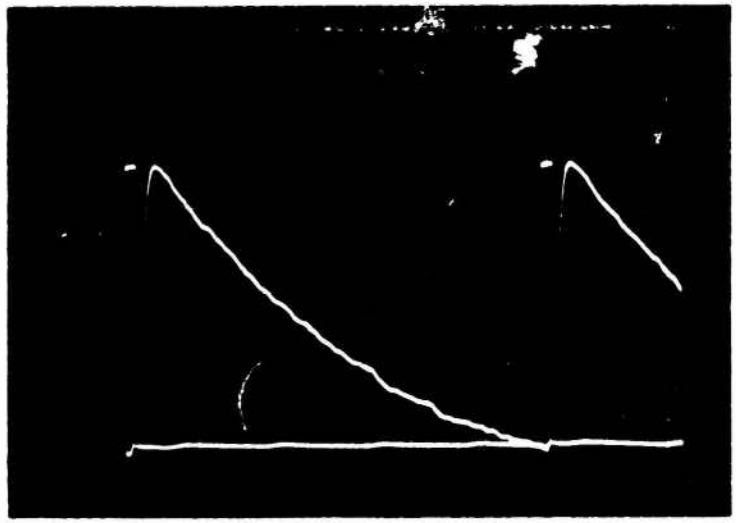

Detector 14. 1 ms Pulse, 1 V/cm Cal Source, 0.5 V/cm Signal, Band 2

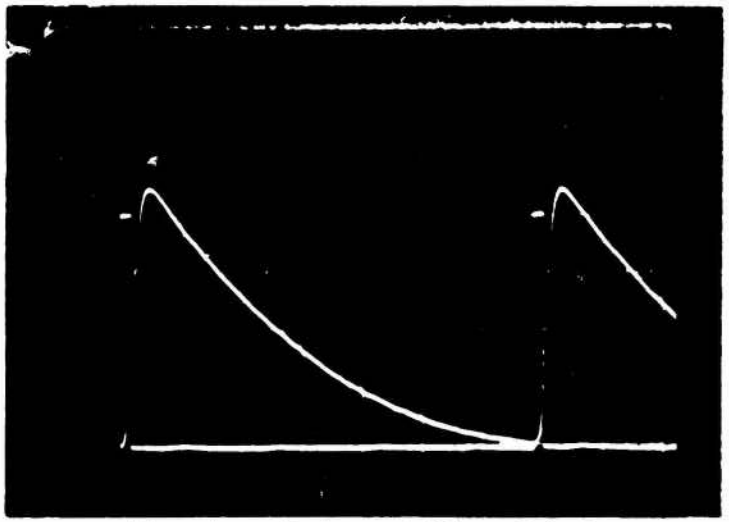

Detector 15. 1 ms Pulse, 4 V/cm Cal Source, 5 V/cm Signal, Band 3

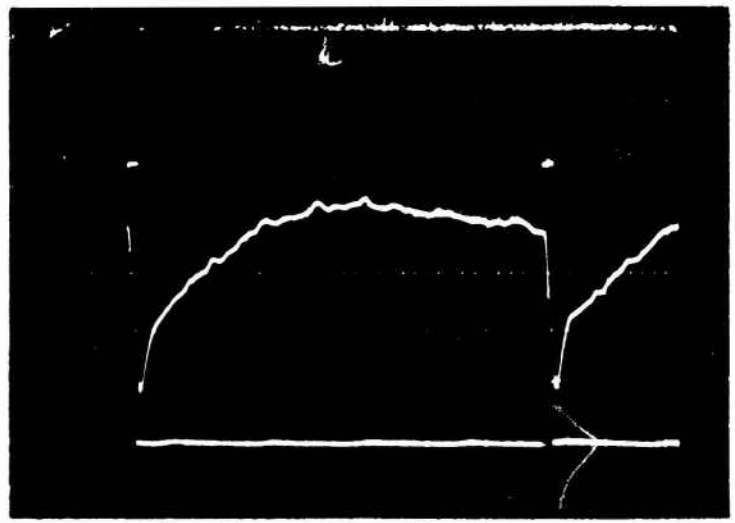

Detector 16. 1 ms Pulse, 1 V/cm Cal Source, 0.2 V/cm Signal, Band 1

Figure 37. (Continued)

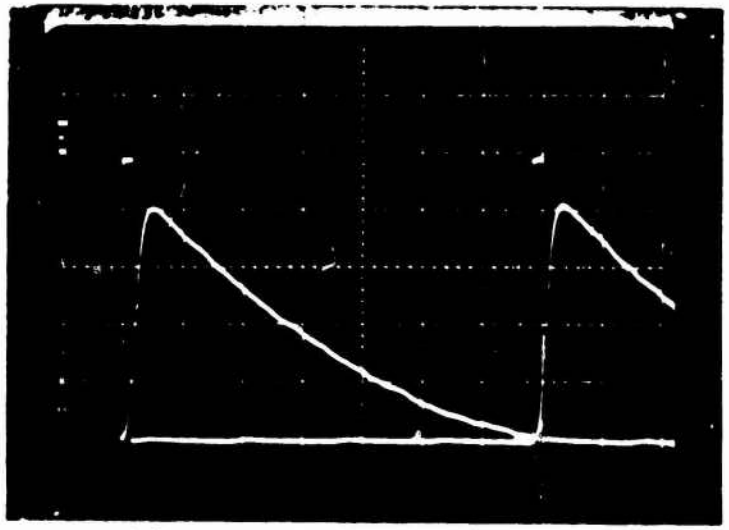

Detector 17. 1 ms Pulse, 1 V/cm Cal Source, 2 V/cm Signal, Band 2

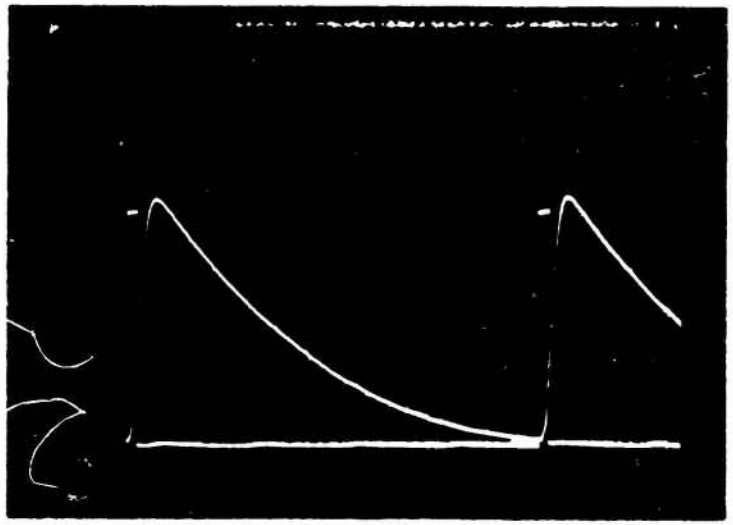

Detector 18. 1 ms Pulse, 4 V/cm Cal Source, 5 V/cm Signal, Band 3

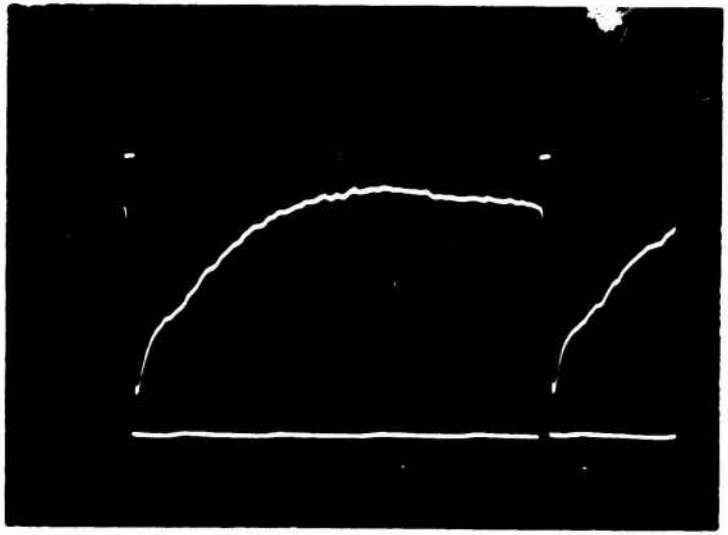

Detector 19. 1 ms Pulse, 1 V/cm Cal Source, 0.2 V/cm Signal, Band 1

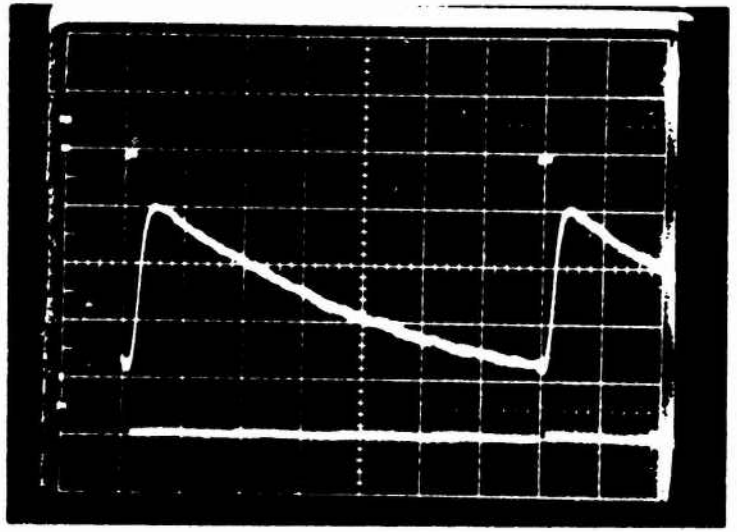

Detector 20. 1 ms Pulse, 1 V/cm Cal Source, 0.5 V/cm Signal, Band 2

Figure 37. (Continued)

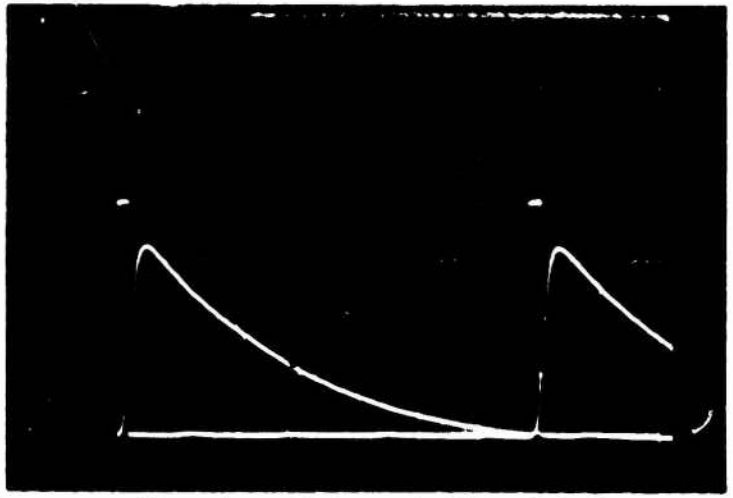

Detector 21. 1 ms Pulse, 4 V/cm Cal Source, 5 V/cm Signal, Band 3

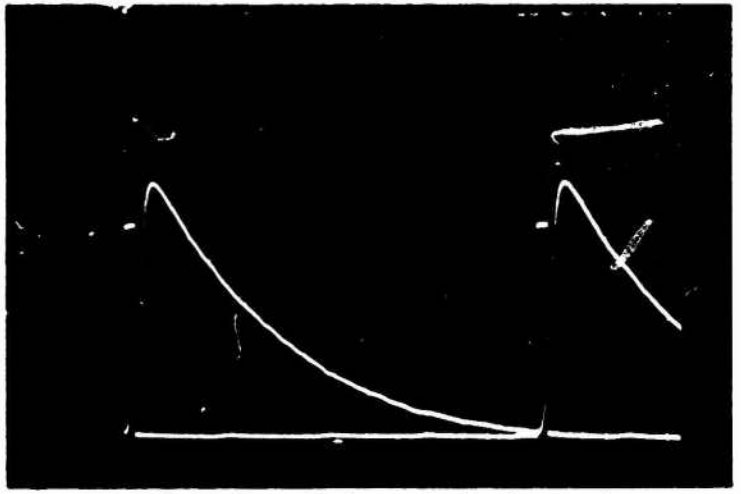

Detector 22. 1 ms Pulse, 3.6 V/cm Cal Source, 2 V/cm Signal, Band 3

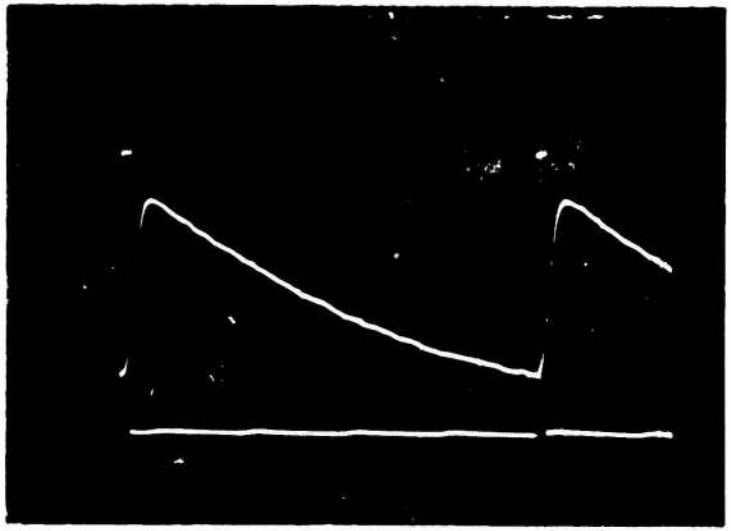

Detector 23. 1 ms Pulse, 1 V/cm Cal Source, 1 V/cm Signal, Band 2

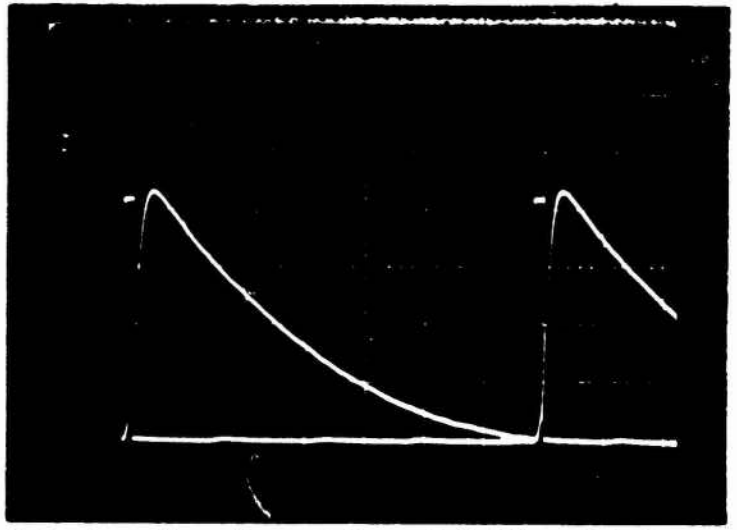

Detector 24. 1 ms Pulse, 4.2 V/cm Cal Source, 5 V/cm Signal, Band 3

Figure 37. (Continued)

5.2 CROSSTALK MEASUREMENTS

A test was run to determine electrical crosstalk by optically blocking all detectors but three (one per band) and exposing the detectors to chopped infrared radiation. The signals were measured on the exposed detectors and compared to the signals on the unexposed detectors. Figure 38 shows the percentage of signal pickup by unexposed detector channels and the measured signal for the exposed detectors.

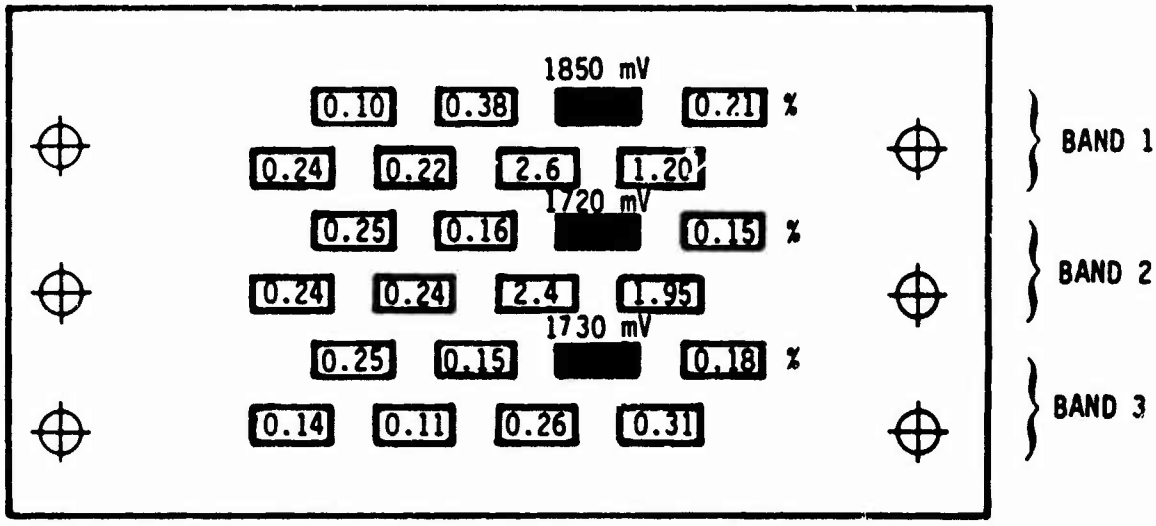

Figure 38. Crosstalk Test Results

5.3 FEEDBACK RESISTOR DATA

Figure 39 shows the resistance of the Eltec Resistor Model 112 as a function of temperature. These resistors inherently display the best characteristics for this range of resistance in the 4.2K to 10K area. The entire lot was screened by wiring the resistors to a dip tube and immersing them in cryogenic liquids. A Keithley Model 610C Electrometer was used and the current selections were chosen so the highest voltage output would be close to the 1V range.

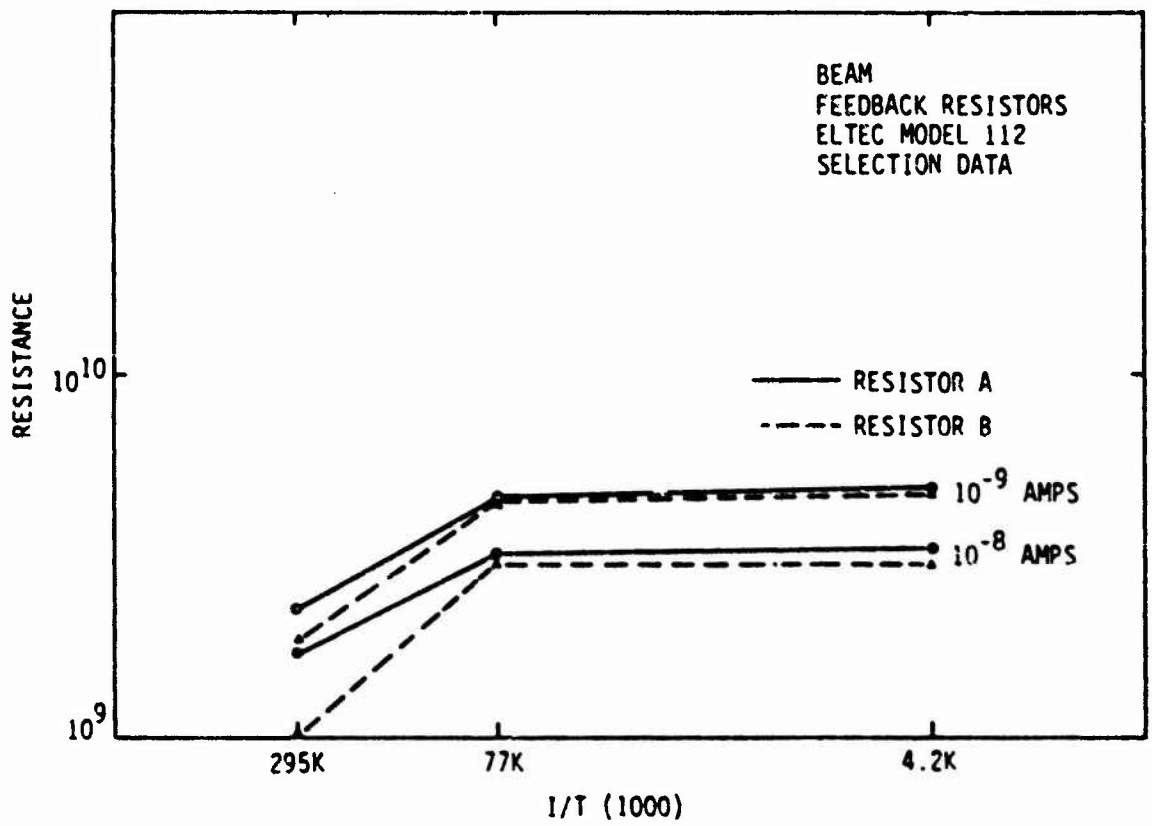

Figure 39. Eltec Resistor Resistance vs Temperature

APPENDIX A

SPECTRAL RESPONSE CURVES

RELATIVE RESPONSE FOR Si:Ga (Z027)

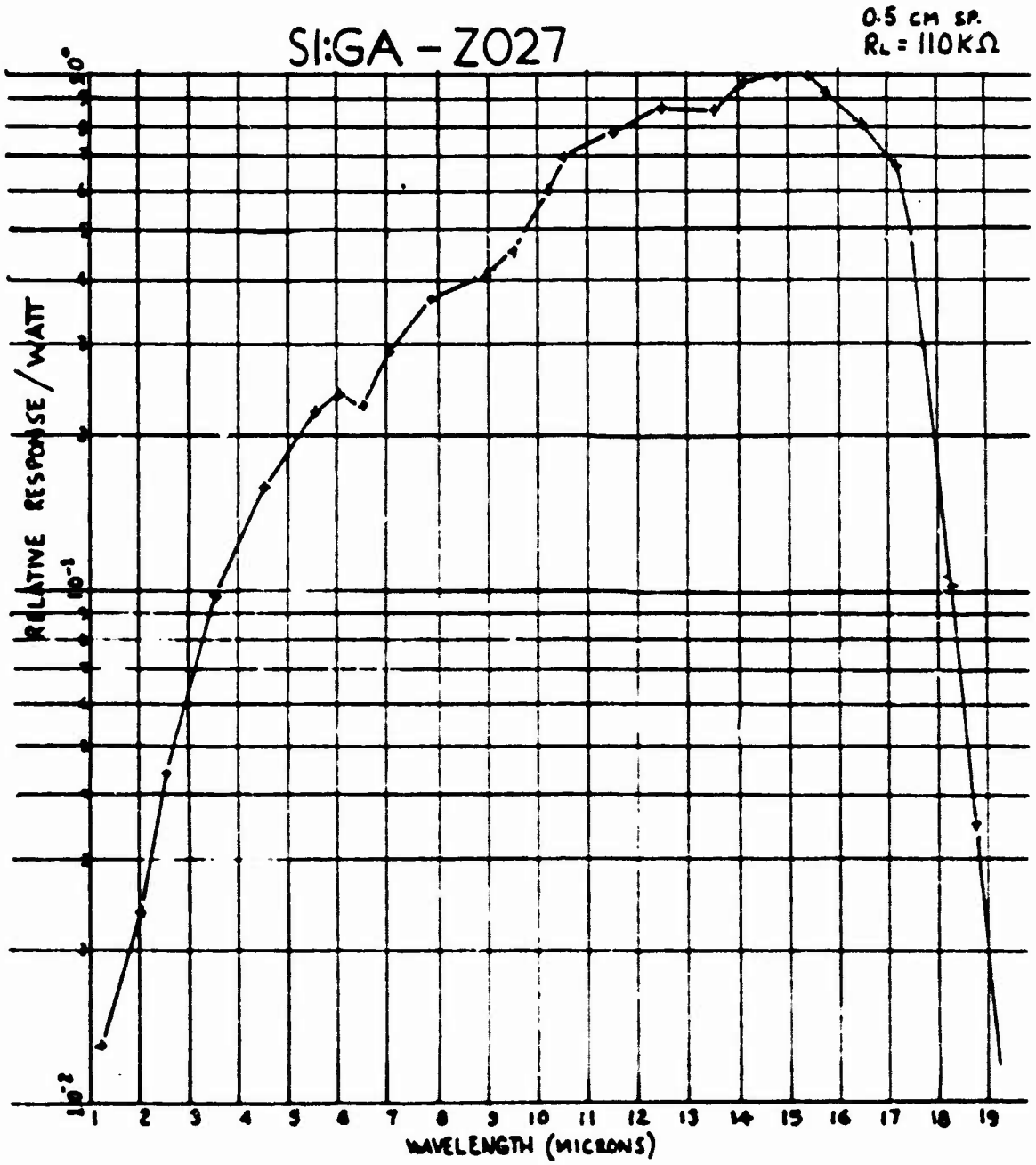

TRANSMISSION CURVE FOR BAND 1

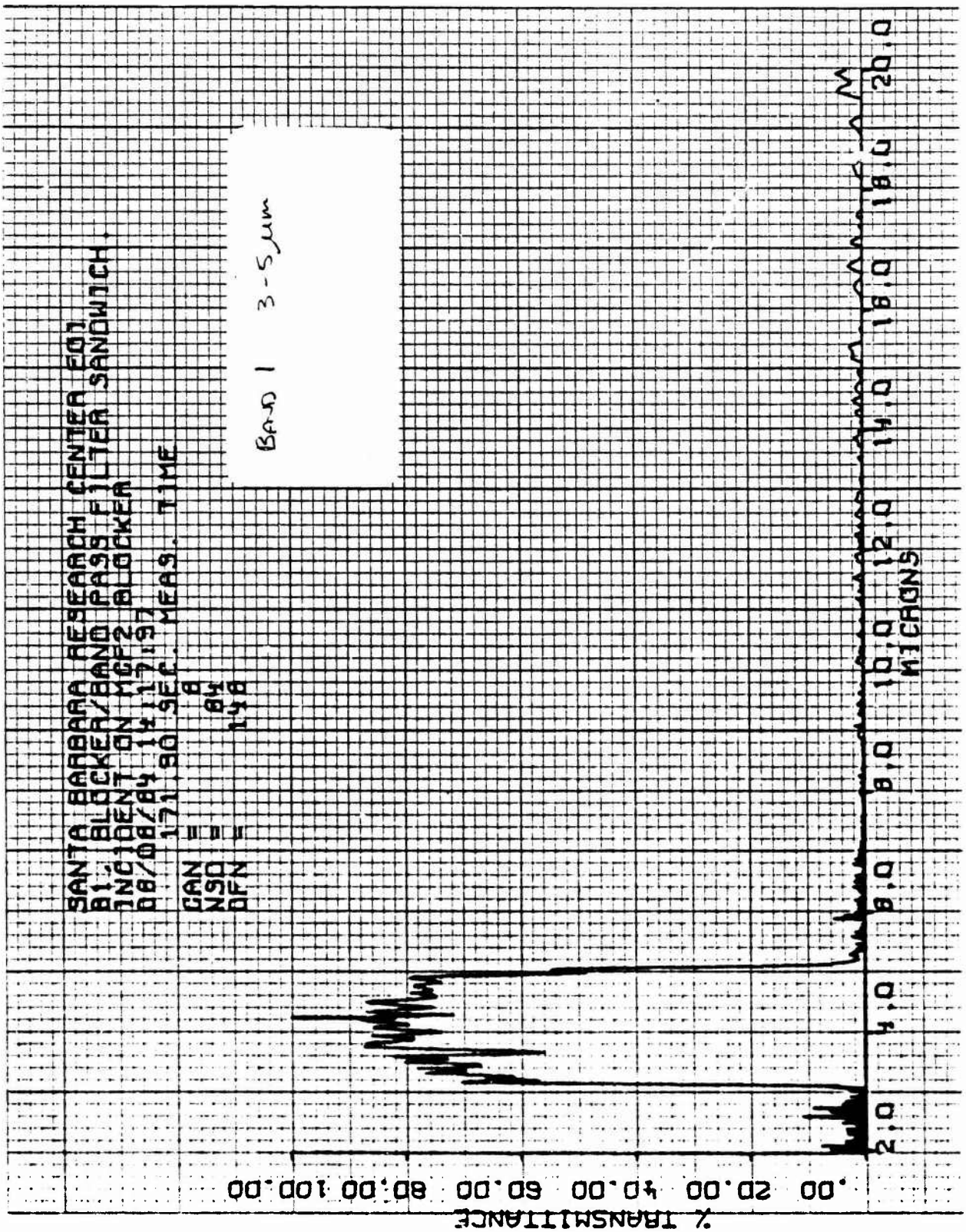

TRANSMISSION CURVE FOR BAND 2

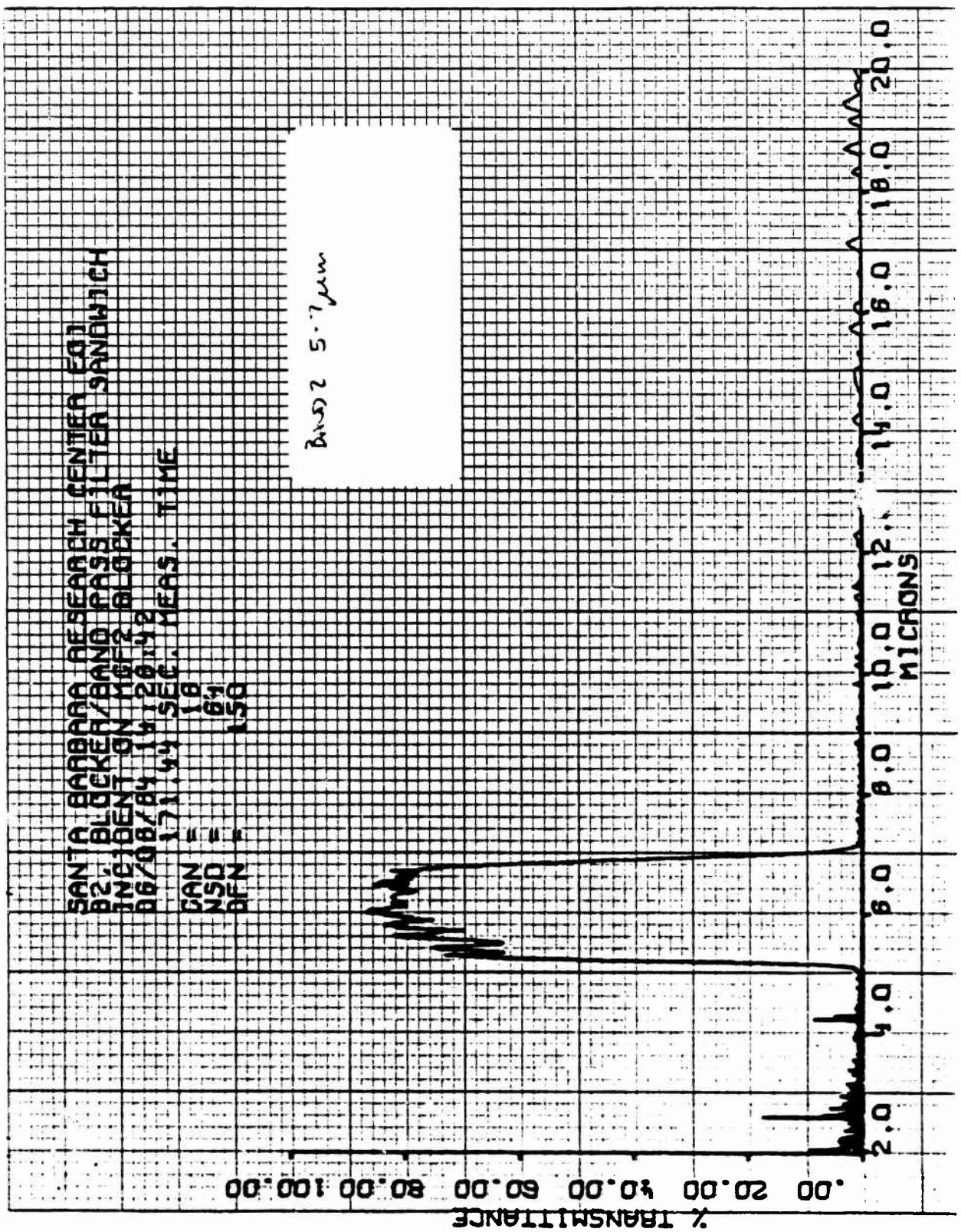

TRANSMISSION CURVE FOR BAND 3

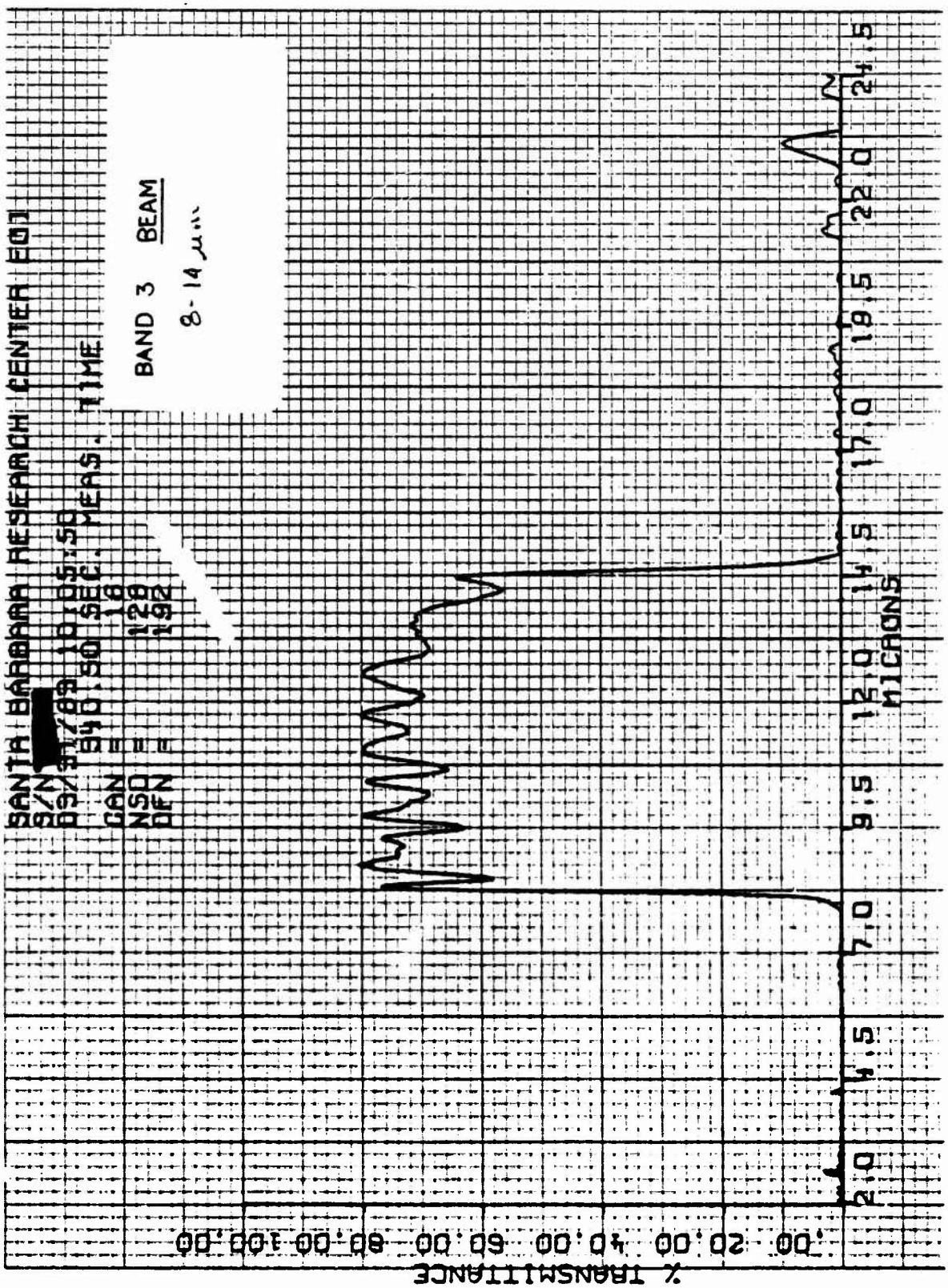

APPENDIX B

TEMPERATURE SENSOR CALIBRATION CURVES

BEAM FPA-BASE

CARBON RESISTANCE TEMPERATURE SENSOR CALIBRATION

TEMP. SENSOR 160K79

CALIBRATION POINTS - T = 77.35 27.16 4.21 KELVIN
R = 1.417 2.400 34.500 KOHM

FORMULA - LN(R) = LN(0.78771 KOHM) + (9.47965)*(T**(-0.63969))
= LN(A) + (B)*(T**(P))

TEMP (KELVIN)	R108 (KOHM)	DT/DR (DEG/KOHM)	TEMP (KELVIN)	R108 (KOHM)	DT/DR (DEG/KOHM)
2.00	345.810	-0.001	20.0	3.177	-7.0
2.50	153.931	-0.004	21.0	3.044	-7.9
3.00	86.124	-0.011	22.0	2.926	-8.9
3.50	55.421	-0.023	23.0	2.820	-9.9
4.00	39.123	-0.040	24.0	2.725	-11.0
4.50	29.467	-0.065	25.0	2.639	-12.2
5.00	23.271	-0.099	26.0	2.561	-13.4
5.50	19.047	-0.141	27.0	2.490	-14.7
6.00	16.030	-0.194	28.0	2.425	-16.0
6.50	13.791	-0.257	29.0	2.365	-17.4
7.00	12.079	-0.331	30.0	2.310	-18.8
7.50	10.736	-0.416			
8.00	9.660	-0.516	32.0	2.212	-21.8
8.50	8.761	-0.627	34.0	2.127	-25.1
9.00	8.053	-0.751	36.0	2.052	-28.6
9.50	7.441	-0.888	38.0	1.986	-32.3
10.00	6.921	-1.039	40.0	1.928	-36.2
10.50	6.474	-1.203	42.0	1.876	-40.3
11.00	6.086	-1.381	44.0	1.828	-44.6
11.50	5.747	-1.573	46.0	1.786	-49.1
12.00	5.448	-1.780	48.0	1.747	-53.8
12.50	5.183	-2.000	50.0	1.711	-58.8
13.00	4.947	-2.235			
13.50	4.734	-2.484	55.0	1.635	-72.0
14.00	4.543	-2.748	60.0	1.571	-86.3
14.50	4.370	-3.026	65.0	1.518	-101.9
15.00	4.212	-3.319	70.0	1.472	-118.6
15.50	4.066	-3.627	75.0	1.433	-136.5
16.00	3.936	-3.949	80.0	1.399	-155.5
16.50	3.816	-4.286	85.0	1.369	-175.5
17.00	3.702	-4.637	90.0	1.342	-196.6
17.50	3.598	-5.003	95.0	1.318	-218.8
18.00	3.502	-5.384	100.0	1.296	-242.0
18.50	3.412	-5.779			
19.00	3.329	-6.189	150.0	1.156	-527.2
19.50	3.251	-6.613	200.0	1.084	-901.5
20.00	3.177	-7.053	250.0	1.039	-1356.2
20.50	3.109	-7.506	300.0	1.008	-1885.5

PROGRAM DVIDC, REVISED 3 MARCH 197 (DMODE = 1)

CARBON RESISTANCE TEMPERATURE SENSOR CALIBRATION

BEAM-ICS

TEMP. SENSOR 121K79

CALIBRATION POINTS - T = 77.35 27.16 4.21 KELVIN
R = 1.386 2.430 34.500 KOHM

FORMULA - LN(R) = LN(0.77187 KOHM) + (9.57042)*(T**(-0.64259))
= LN(A) + (B)*(T**(P))

TEMP (KELVIN)	R108 (KOHM)	DT/DR (DEG/KOHM)	TEMP (KELVIN)	R108 (KOHM)	DT/DR (DEG/KOHM)
2.00	354.780	-0.001	20.0	3.117	-7.1
2.50	156.423	-0.004	21.0	2.986	-8.0
3.00	86.951	-0.011	22.0	2.869	-9.0
3.50	55.690	-0.022	23.0	2.765	-10.1
4.00	39.172	-0.040	24.0	2.671	-11.2
4.50	29.421	-0.065	25.0	2.587	-12.4
5.00	23.182	-0.098	26.0	2.510	-13.6
5.50	18.939	-0.141	27.0	2.440	-14.9
6.00	15.914	-0.193	28.0	2.376	-16.3
6.50	13.674	-0.257	29.0	2.317	-17.7
7.00	11.963	-0.332	30.0	2.263	-19.1
7.50	10.622	-0.419			
8.00	9.549	-0.518	32.0	2.166	-22.2
8.50	8.674	-0.630	34.0	2.082	-25.5
9.00	7.949	-0.755	36.0	2.009	-29.1
9.50	7.341	-0.894	38.0	1.945	-32.8
10.00	6.824	-1.046	40.0	1.887	-36.8
10.50	6.380	-1.212	42.0	1.836	-41.0
11.00	5.995	-1.392	44.0	1.789	-45.4
11.50	5.659	-1.587	46.0	1.748	-50.0
12.00	5.362	-1.796	48.0	1.709	-54.9
12.50	5.100	-2.019	50.0	1.675	-59.9
13.00	4.866	-2.257			
13.50	4.656	-2.510	55.0	1.599	-73.4
14.00	4.466	-2.778	60.0	1.537	-88.1
14.50	4.295	-3.060	65.0	1.485	-104.0
15.00	4.139	-3.357	70.0	1.440	-121.1
15.50	3.997	-3.669	75.0	1.402	-139.3
16.00	3.866	-3.996	80.0	1.368	-158.7
16.50	3.746	-4.338	85.0	1.339	-179.2
17.00	3.635	-4.695	90.0	1.312	-200.8
17.50	3.533	-5.067	95.0	1.289	-223.5
18.00	3.438	-5.454	100.0	1.267	-247.3
18.50	3.349	-5.855			
19.00	3.267	-6.272	150.0	1.131	-539.4
19.50	3.189	-6.704	200.0	1.060	-922.9
20.00	3.117	-7.150	250.0	1.016	-1389.3
20.50	3.049	-7.612	300.0	0.986	-1932.3

PROGRAM JV108, REVISED 3 MARCH 197 (JMODE = 1)